University of New Mexico
UNM Digital Repository

Physics & Astronomy ETDs | Electronic Theses and Dissertations

7-12-2014

A Study of Charge Transport: Correlated Energetic Disorder in Organic Semiconductors, and the Fragment Hamiltonian

Jonathan Allen

Follow this and additional works at: https://digitalrepository.unm.edu/phyc_etds

Recommended Citation
Allen, Jonathan. "A Study of Charge Transport: Correlated Energetic Disorder in Organic Semiconductors, and the Fragment Hamiltonian." (2014). https://digitalrepository.unm.edu/phyc_etds/3

This Dissertation is brought to you for free and open access by the Electronic Theses and Dissertations at UNM Digital Repository. It has been accepted for inclusion in Physics & Astronomy ETDs by an authorized administrator of UNM Digital Repository. For more information, please contact disc@unm.edu.

Jonathan R. Allen

Candidate

Physics and Astronomy

Department

This dissertation is approved, and it is acceptable in quality and form for publication:

Approved by the Dissertation Committee:

David H. Dunlap , Chairperson

Steve Valone

Susan R. Atlas

Paul Schwoebel

Yang Qin

A Study of Charge Transport: Correlated Energetic Disorder in Organic Semiconductors, and the Fragment Hamiltonian

by

Jonathan Robert Allen

B.S., University of Idaho, 2007

M.S., Physics, University of New Mexico 2011

DISSERTATION

Submitted in Partial Fulfillment of the
Requirements for the Degree of

Doctor of Philosophy,
Physics

The University of New Mexico

Albuquerque, New Mexico

May, 2014

©2013, Jonathan Robert Allen

Dedication

To Liz

Acknowledgements

I would like to express the utmost gratitude to my advisor Professor David Dunlap for his boundless insight and support during my work at the University of New Mexico. I learned from him more than I thought possible, and I am grateful for his presence over the last few years.

Many thanks to Professor Susan Atlas at UNM and Dr. Steve Valone at Los Alamos National Laboratory. Without their guidance and help, a large part of the work presented in this dissertation would not have been possible.

Thanks to Sebastian Röding at the University of Würzburg, who wrote the original version of the C++ code used for the simulations described in this thesis. His work and intellectual input were invaluable.

I would like to thank my professors at the Department of Physics and Astronomy at UNM, especially Profs. V. M. Kenkre, Sudhakar Prasad, Ivan Deutsch, Daniel Finley, Carl Caves, and Rouzbeh Allahverdi, for teaching fantastic courses.

Thank you to Mickey Odom and Dr. Jeff Saul for your support, and for teaching me so much about teaching.

My thanks go to all of my friends and family who supported me during my time in school, especially my parents and my wonderful wife.

Finally, I would like to acknowledge the thousands of individuals who have coded for the LaTeX project *pro bono publico*. It is due to their efforts that anyone may now generate a professionally typeset document.

This work was supported in part by the Defense Threat Reduction Agency, and the Department of Energy at Los Alamos National Laboratory.

A Study of Charge Transport: Correlated Energetic Disorder in Organic Semiconductors, and the Fragment Hamiltonian

by

Jonathan Robert Allen

B.S., University of Idaho, 2007
M.S., Physics, University of New Mexico 2011
Ph.D., Physics, University of New Mexico 2014

Abstract

This dissertation details work done on two different descriptions of charge transport. The first topic is energetic disorder in organic semiconductors, and its effect on charge transport. This is motivated primarily by solar cells, which can be broadly classified as either inorganic or organic. The inorganic class of solar cells is older, and more well-developed, with the most common type being constructed from crystalline silicon. The large silicon crystals required for these cells are expensive to manufacture, which gave rise to interest in photovoltaic cells made from much less costly organic polymers. These organic materials are also less efficient than their silicon counterparts, due to a large degree of spatial and energetic disorder. In this document, the sources and structure of energetic disorder in organic semiconductors are explored, with an emphasis on spatial correlations in energetic disorder. In order for an organic photovoltaic device to function, there must be photogeneration of an exciton (a bound electron-hole pair), exciton transport, exciton dissociation, and transport of the individual charges to their respective terminals. In the case of this thesis, the main focus is exciton dissociation. The effects of correlation on exciton

dissociation are examined through computer simulation, and compared to the theory and simulations of previous researchers. We conclude that energetic disorder in organic semiconductors is spatially correlated, and that this correlation improves the ability of excitons to dissociate.

The second topic of this dissertation is the Fragment Hamiltonian model. This is a model currently in development as a means of describing charge transport across a range of systems. Currently there are many different systems which exhibit various charge transport behaviors, which are described by several different models. The overarching goal of the Fragment Hamiltonian model is to construct a description of charge transport which accurately describes the behavior of multiple different materials (i.e. metallic conductors or ceramic insulators) in the appropriate limits. The Fragment Hamiltonian model is explored in the context of the tight-binding model, and properties such as the conductivity of several different systems are deduced.

Contents

List of Figures

1

Introduction

Nearly every piece of modern technology we interact with on a daily basis is electronic, or has electronic components. This has been made possible by the explosion in our understanding of electronic behavior at the micro- and nanoscale over the last half-century. Our knowledge is far from complete, if such a thing can even be said to exist. To fill in the gaps, tools are constantly being developed, be they ever more sophisticated analytical models, or continuously improving computer simulations.

This dissertation is composed of two parts. In the first, we will be examining disordered organic semiconductors and the charge transport behavior they exhibit. In the second part, a model of charge transfer named the Fragment Hamiltonian (FH) is developed.

The conductivity σ of a material is an important quantity for any physical application. Whether a substance is a conductor, a semiconductor, or a insulator is defined by whether or not it will carry an electrical current at low temperature and in the presence of a small perturbing electric field. The low temperature requirement (actually the limit that $T \to 0$ in ideal models) ensures that random thermal fluctuations are not responsible for the motion of electrons. The requirement of a small electric field (again, in ideal models actually an infinitesimal field strength dE) allows the distinction between the conductor, semiconductor, and insulator to be made. A conductor will typically carry a current which is proportional to the electric field

$$\vec{J} = \sigma \vec{E}, \tag{1.1}$$

an expression of Ohm's law. In an insulator, the conductivity $\sigma = 0$, and no current will appear for any applied field, at least in an ideal model. In real insulators a strong enough electric field will cause ionization in the material, resulting in what is called *dielectric breakdown*, and often the destruction of a component or device.

The definition of a semiconductor is less exact, and generally depends on how strong the electric field is to which it will be exposed [1]. Generally speaking, a semiconductor is an insulator for small values of the electric field. As the field strength is increased, there is a critical value for which a semiconductor will begin conducting a current. The energy one must input via the electric field before conduction occurs is called the *bandgap*.

Many semiconductors such as the ubiquitous silicon, used in computing and photovoltaic cells, are fashioned to have a very orderly microscopic structure. Some of the highest quality silicon solar cells, for example, are fabricated using a single large crystal [2]. This give electrons in the material a very high mobility μ, defined as

$$\mu = \frac{v_e}{E}, \tag{1.2}$$

the velocity v_e of an electron in an electric field of magnitude E. This high mobility allows for efficient solar cells.

The expense required to grow these large crystals has given rise to great interest in organic semiconductor technology. Devices made from organic polymers can be made at much smaller cost. The trade off, however, is that these organic materials are subject to much less control in their manufacture. This causes them to be disordered on the microscopic level. This disorder results in lower mobilities, and in the case of solar cells, consequently lower efficiencies. The exact nature and consequences of this disorder on charge transport are not well understood. In Chapter 2 an overview of solar cell technology and the underlying physics will be given. Chapter 3 gives a review of the diffusion mechanism by which charges move about in semiconductors, as well as a description of the Onsager model [3] of charge dissociation in a medium which forms the foundation of much of the modern understanding of charge behavior in organic solids. Chapter 4 details some of the preceding work which motivated the results presented in this dissertation. Chapter 5 is a discussion of the nature of disorder in organic semiconductors, including its structure and what causes it, as

well as what effects it is expected to have on charge transport. Chapter 6 completes the first part of this thesis by detailing the simulations performed by the author and collaborators, giving a comparison of the results to previous analytical, numerical, and simulative work, and discussing the overall significance of the results and the conclusions drawn from them.

Part 2 of this dissertation is an exploration of the Fragment Hamiltonian model. The FH formalism, being developed by Valone [4] at Los Alamos National Laboratory, attempts to describe a flexible, general model for charge transfer across a variety of systems. A hurdle in modeling complex systems is the fact that in most cases materials which exhibit different charge transport behaviors are described by different models, which are often not compatible. As a result, it is difficult to accurately describe, for example, the behavior at an interface of a conductor and an insulator.

In an attempt to overcome such hurdles, the FH model describes systems in terms of 'fragment' quantities and their charge states. Ideally, a fragment is defined such that the description of charge transfer in a system is simplified enough that the expectation values for observables of interest may be determined. This may mean that individual atoms become fragments, or that larger structures such as whole molecules or clusters of molecules are defined as fragments. Once this determination is made, the Fragment Hamiltonian may be expressed as

$$\hat{H}^{(f)} = \sum_{A} \hat{H}_A + \frac{1}{2} \sum_{A \neq B} \hat{V}_{AB}, \tag{1.3}$$

where the terms $\hat{H}_A$ represent the energy of a fragment A due to all the various relevant electronic contributions, and the terms $\hat{V}_{AB}$ represent the interactions between two fragments A and B.

Chapter 7 gives an overview of the tight-binding model and some other relevant formalism, in the context of which the FH model will subsequently be discussed. In Chapter 8 the Hubbard model is introduced. The Hubbard model is an extension of the tight-binding model which includes electron-electron interactions, and is used as a place of comparison with the FH model, which can be defined analogously to the Hubbard model and can be expected to exhibit similar behavior. Finally, in Chapter 9 the FH model is examined for the same system as the Hubbard model, as well as a larger system, and its behavior relative to the tight-binding and Hubbard models is

discussed.

Part I

Energetic Disorder in Organic Semiconductors

2

Some Background on Photovoltaic Cells

To motivate the discussion in the following few chapters, it is helpful for the reader to understand the basic operating principles of photovoltaic cells. These can be classified broadly into two types, organic and inorganic. Both types have the same basic function, in that the goal of both types of devices is to absorb photons which excite electrons that are subsequently gathered as electric current. The two categories of devices use quite different processes to achieve this result, however. Said processes will be discussed presently, and details can be found in numerous texts such as [5, 6].

2.1 Electron-Hole Pair Generation and Recombination

Electron-hole pairs can be produced in a material by any process which supplies enough energy to excite an electron out of its bound state in the valence band into the conduction band (see Chapter 7 for more details on band structure), forming a coulombically attracted pair of charges. Such a process could be a thermal excitation, with a strong phonon bumping the electron into an excited state. Another is impact ionization, with another particle in the material colliding to supply the energy. In photocells, however, the dominant process which achieves this is the absorption of

photons.

If a photon is incident on a material and carries energy equal to or larger than the band gap of the material, it can excite an electron. Otherwise, it is reflected or absorbed as heat. If the energy supplied is enough to promote an electron to the conduction band, but not sufficient for the electron and hole to overcome their mutual coulomb attraction and move away from one another, a temporary bound state called an exciton is formed. In inorganic semiconductors this binding energy tends to be smaller than the ambient thermal energy k_bT at room temperature, and the electron and hole behave more or less as free particles. In organic semiconductors the binding energy tends to be larger than k_bT at room temperature, resulting in mobile excitons [5], which will be discussed in more detail later.

These electron-hole excitations are inherently transient, and the charges will recombine via a number of different processes. The simplest way in which this happens is radiative recombination. An electron and hole will approach near one another, and the coulomb attraction will draw them together into neutrality, releasing a photon with energy equal to the kinetic energy given up by the particles. If an electron and hole which began together are recombined together, the process is referred to as geminate recombination. Otherwise, the process is called bulk recombination.

Other forms of recombination are non radiative, such as Auger recombination. Auger recombination is essentially the reverse of impact ionization, and there are two possible cases for this process. The first is that of a free electron imparting its energy upon a hole, which is subsequently dissipated into the lattice as phonons. The second possibility involves two electrons and one hole. The first electron moves through the system with some energy before colliding with the second electron and transferring that energy. The first electron, now slowed down, annihilates with a hole while the second electron dissipates the energy into the lattice via phonons. This sort of dissipative loss is unavoidable in practice, and largely responsible for the efficiency ceiling silicon solar cells are beginning to encounter [5].

Another form of recombination is due to impurities. Some impurities within the material have occupation energies which lie between the valence and conduction bands, capturing electrons or holes and successively dissipating their energy over several energy states. This makes recombination easier than in processes in which the energy is dissipated in a single transition, since the charges' energy can be dissipated

in a series of steps by a series of phonons.

Keeping in mind the descriptions of these processes, the diffusion length of an electron or hole, once generated, is the average distance which it can diffuse in a material before it suffers a recombination event (or events, as the case may be). This distance varies based on the substance in question, with diffusion lengths in disordered organic semiconductors being much shorter than those inside inorganic crystal semiconductors.

2.2 Inorganic Photocells

Inorganic photovoltaic cells are the more well-developed of the two categories of devices, and comprise the vast majority of solar cells currently in operation. They are typically fabricated from a light-absorbing silicon layer (the "active layer") sandwiched between two metallic terminals. This is known as a bilayer configuration, as in Figure 2.1. One terminal is a conductor such as aluminum, while the other terminal is most often Indium Tin Oxide (ITO), which is transparent to allow light into the cell.

The silicon layer is arranged into a P-N junction (see [1], pp. 590-605), with two zones being "doped" to contain a larger or smaller number of charge carriers as necessary. The process of doping replaces some of the silicon atoms with a guest material possessing the desired electronic properties. To produce the N-zone, a dopant such as phosphorous is used, which possesses one more electron in its valence shell than silicon, resulting in a surplus of bound electrons. The P-zone is often doped with boron, which has one fewer electrons than silicon, resulting in a surplus of bound holes. The reader should bear in mind that materials are charge neutral, but possess different chemical potentials as a result of doping. When the two zones are brought together, electrons from the N-zone migrate to the holes in the P-zone near the interface as a result of the difference in the chemical potential between the two zones. As charges migrate, the charge imbalance produces a net electric potential difference across the interface. Charges cease migrating when the equilibrium condition

$$\phi_n - \phi_p = \mu_p - \mu_n \tag{2.1}$$

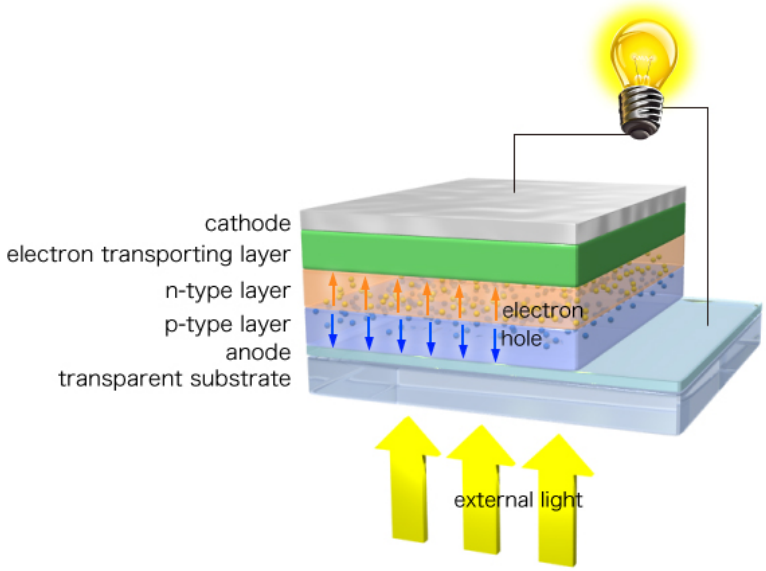

Figure 2.1: Electrons are excited in the p-type zone, where they diffuse to the space-charge region at the interface of the two zones. Those which successfully diffuse without recombining are then swept across the interface to the positive terminal, contributing to the current (Image courtesy of the Center for Future Chemistry, Kyushu University).

is reached, where the ϕ's are the electric potentials and the μ's are the chemical potentials. This results in a rather substantial electric field in the region very near to the interface, as high as $10^6 \frac{V}{m}$ at a range of 10-300nm from the interface [1, 5]. The extent of this so-called space charge region is much smaller than either the penetration length of relevant wavelengths of light or the diffusion length of the charge carriers in a silicon cell, however. The field therefore drives charges strongly only near the interface, and weakly elsewhere in the device.

To operate, the device is connected into a circuit and illuminated. In the case of solar cells, the light corresponds to the solar spectrum. The frequencies of light incident on a particular material play a large part in determining how much energy can be collected. Different materials absorb different wavelengths more readily. Inorganic semiconductors such as silicon absorb across the entire visible spectrum and into the infrared. A silicon cell has a bandgap of approximately 1.1eV [7], corresponding to the near-infrared part of the solar spectrum. Electrons will be excited most effectively by photons at or just above this energy, so the inorganic crystals' broad absorptivity contributes greatly to their effectiveness in photocells.

Once an electron is excited into the conduction band, it will diffuse through the medium. Electrons in such uniform silicon crystals, where scattering is low, have rather large mobility $\mu = \frac{v_{drift}}{E}$, the drift velocity per unit electric field. In a silicon crystal the value of μ is on the order of $10^3 \frac{cm^2}{Vs}$. Therefore, even though the electric field is weak outside the narrow zone near the junction and the charge motion is primarily diffusive, they still traverse the cell with reasonable efficiency. If a charge does not undergo a recombination process at some point in its journey, upon reaching the space charge region near the junction interface it will be quickly swept across by the electric field and onward to its respective terminal to be collected and contribute to the current, as in Figure 2.2.

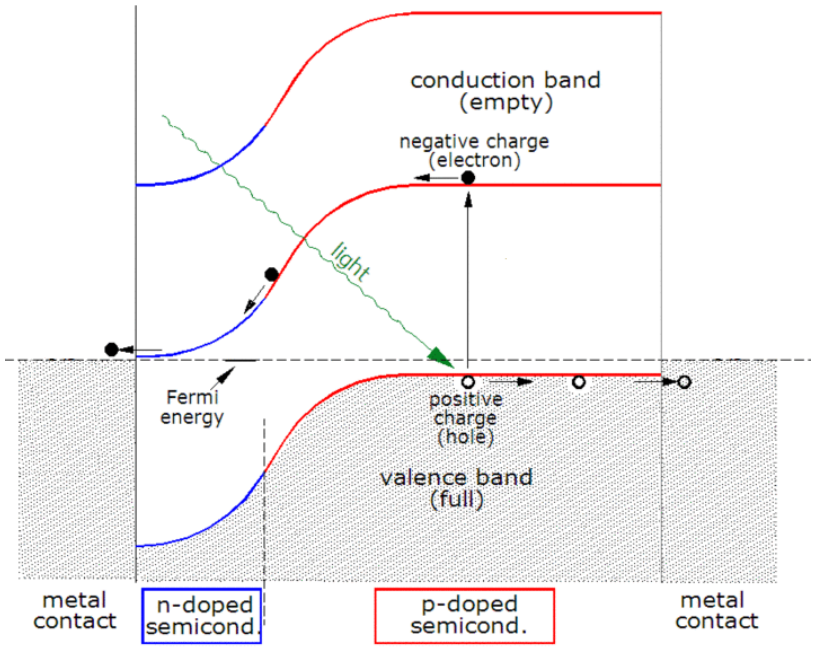

Figure 2.2: An energy diagram of an excited charge traversing an inorganic solar cell. (Wikimedia Commons)

One important consideration which must be made is that of the dimensions of the device. If the device is too thin, light passes through it without interacting. If the device is too thick, dissipative recombination effects take away charge carriers before they can be collected at the terminals, robbing some of the useful current. Additionally, if the device is too thick, light cannot penetrate the entire depth of the cell, resulting in wastefully dark, inert regions. Given the absorptivity of the silicon compounds employed, typical specifications for a silicon solar cell put the light

absorbing P-zone at approximately 300μm and the N-zone at roughly 1μm [5].

2.3 Organic Semiconductors and Energetic Disorder

At this point, we turn our attention to photovoltaics made from organic semiconductors. There are variety of organic materials whose electronic properties have been investigated over the years. These range from organic perfect crystals such as naphthalene, anthracene, and tetracene [8], to long-chain conjugated polymers such as polyacetylene [9], to conjugated small molecules such as copper phthalocyanine [10]. When saying that a molecule is conjugated it is meant that there is a region where the atomic p-orbitals overlap as in Figure 2.3 to form a pi-bond. This results in a

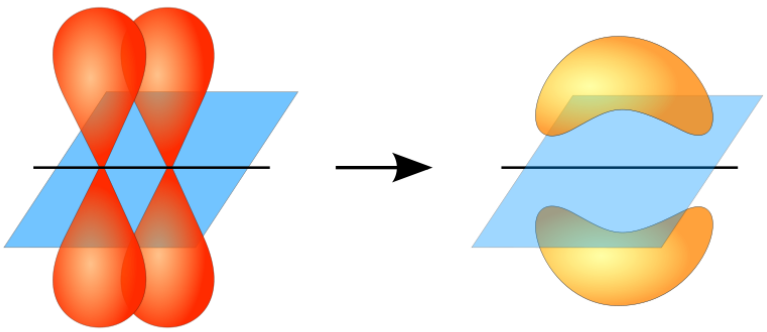

Figure 2.3: p-orbitals overlapping to form a pi-bond. (Wikimedia Commons)

delocalized orbital which spans the entire molecule (however large or small it may be). If this pi-bonded region is doped to remove a few electrons, the electron mobility in the region becomes very high, and their motion is locally band-like.

The largest motivating factor in modern organic photocell research is economy of manufacture. Producing large organic crystals is more expensive and time consuming than creating thin films whose morphology is much less controlled, and therefore much more disordered. Such cells are often fabricated by evaporating the material and vapor depositing it onto an appropriate substrate. Another method is to centrifugally spin

coat the material onto the device as a liquid solution. In either case the result is a disordered solid with small conjugation lengths, usually spanning no more than a few molecules. In addition, the polymer chains have twists, kinks, packing, and various defects which affect the size and shape of the orbitals, and the degree to which they overlap [11]. As a result, the electrons become localized to single molecules or small clusters of molecules. Due to this localization, the charges cannot exhibit band motion over the whole medium, but rather exhibit so called "hopping" motion, as in Figure 2.4. This localization means that the eigenstates are better approximated

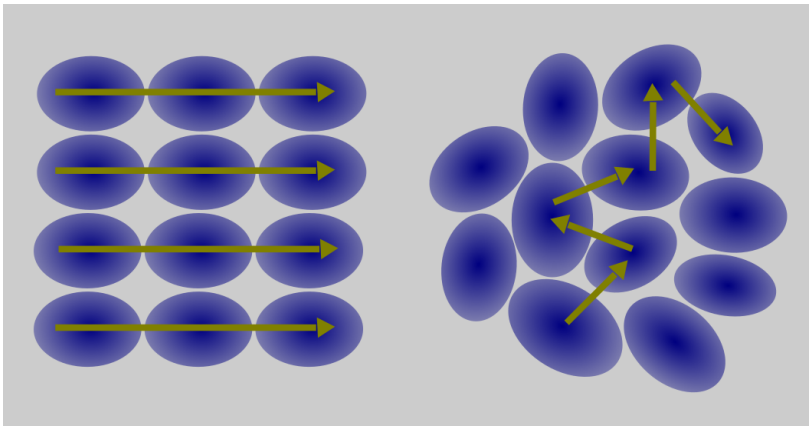

Figure 2.4: Band Motion in a crystal (left) versus hopping motion in a disordered polymer (right).

by localized orbitals in a site basis, rather than Bloch states which describe band motion (see Chapter 7). The participating orbitals at each site are called the Highest Occupied Molecular Orbital (HOMO) and the Lowest Unoccupied Molecular Orbital (LUMO). The disorder in the system translates into disorder in the energies at each site. These differences in site energies mean the electrons spend the majority of their time residing on a site, and have a probability to intermittently hop, as illustrated in Figure 2.5.

There exist finishing procedures which mitigate the disorder, such as annealing. This process amounts to cooking the material to allow it to organize into clusters of crystal structures which are less disordered. However, the annealing process itself is somewhat random, and only serves to mitigate the disorder [7]. The disorder in such systems is difficult (if not impossible) to avoid, and makes local charge transport much harder to predict than in ordered systems.

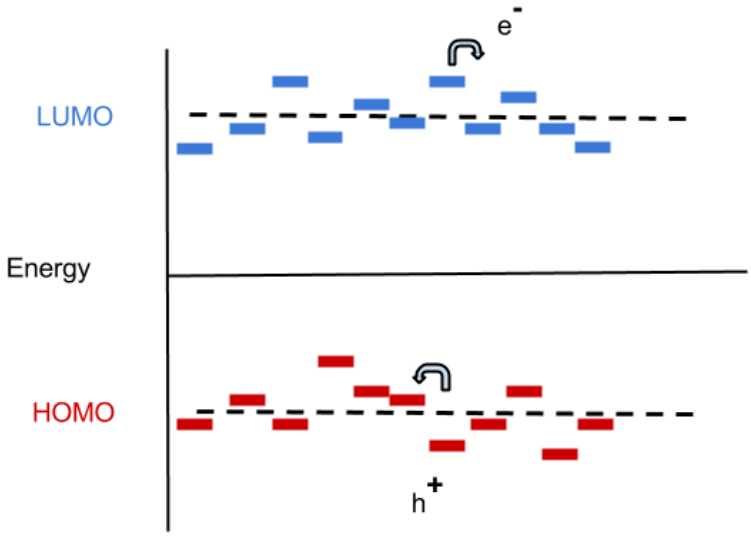

Figure 2.5: The energetic disorder between the occupation levels causes hopping transport.

2.4 Organic Photocells

Having discussed energetic disorder and how it sets organic semiconductors apart from inorganic, the operation of organic photovoltaic cells will be discussed in more detail. Reference [7] is a review article from the University of Würzburg which contains details of the current state of the technology.

Organic solar cells are similar in construction to their inorganic counterparts, but differ in several important ways. One difference is in the way the active material interacts with light. The organic polymers in question have a much higher light absorptivity, which means a much thinner layer of material is needed to capture photons. Typical device thicknesses are on the order of 100-300 nm, as opposed to $\sim 300\ \mu$m for an inorganic cell. Unfortunately, The part of the available spectrum which can be absorbed is generally narrower than in silicon devices. While inorganic devices may absorb across the entire visible spectrum and well into the infrared, the organic polymers typically used only absorb in the visible spectrum [7]. This leaves a portion of the solar spectrum, namely infrared, unused.

The mechanisms of charge transport are markedly different in organic cells, as well. The terminals are made from the same, or similar, materials as in a silicon device, but

the choice of materials is much more important to the successful operation of the cell. In a silicon cell, charge carriers depend on largely on their high mobility ($\sim 10^3 \frac{cm^2}{Vs}$) to diffuse across the majority of the active layer. In an organic cell, however, μ is on the order of $10^{-2} \frac{cm^2}{Vs}$. The lower the mobility, the more time a charge spends in transit, and the higher the probability is that it will experience a recombination event. This reduces the current produced. The low mobility in organics means that a significant electric field must be present across the entire device to drive the charges. This is where the choice of metals for the terminals becomes important. The amount of energy required to remove an electron to some point far away with zero energy corresponds to the Fermi level E_f of the metal. The work function W of a metal is defined as the energy required to bring the electron back to the surface of the metal where there exists an electrostatic potential Φ,

$$W \equiv -e\Phi - E_f. \tag{2.2}$$

When two metals with different work functions are brought into close proximity, the energy difference produces a net electrostatic potential difference between them. The thinness of organic photocells means that the terminals are close enough to one another that this can produce a substantial electric field across the device. For example, consider two common metals which are used as terminals, aluminum and ITO. Aluminum has a work function between 4-4.5 eV, while ITO can have a work function as high as 5.3 eV [12]. This can produce a field across the entire device on the order of $10^4 - 10^5 \frac{V}{m}$. This field helps compensate for the low mobility in organic semiconductors, and increases the speed with which the charges are transported.

As mentioned earlier, the exciton binding energies in organic polymers are larger than those in silicon, preventing the electron and hole from dissociating as easily. Instead, they tend to form mobile, bound excitons. Some of the earliest organic photovoltaic cells were constructed with a single layer of material. As far back as 1958, the photovoltaic effect was reported in a cell based on magnesium phthalocyanine by Kearns and Calvin [13]. These designs relied largely on thermal excitations to dissociate the excitons generated in the active layer (everything between the terminals, in this case), and since the Coulomb binding energy of a typical exciton in such a system is on the order of 0.5 eV, which is much larger than the thermal energy at room temperature (0.025eV), exciton dissociation was very inefficient. Something

more was needed to disengage the electron and hole from one another.

The next iteration in organic solar cells, presented by Tang [10] in 1986, was a bilayer cell analogous to the inorganic cells described earlier. In this configuration two materials are used. One is a polymer donor material with a low electronegativity, and the second a highly electronegative fullerene acceptor. Electronegativity can be defined in various ways (some definitions have units, and some not), and it measures the tendency of an atom or molecule to attract electrons [14]. An overview of electronegativity can found in Appendix A. Excitons are generated from absorbed photons primarily in the donor material due to its lower relative electronegativity. As an exciton migrates to the interface, the acceptor provides a lower energy state for the electron to occupy than in the donor, and pulls the electron across the interface, dissociating the exciton. This configuration improved efficiency by a large factor, but the total efficiency was still quite low, around 1% under the solar spectrum. The problem lay in the fact that exciton diffusion lengths in the organic materials used were not large enough for many excitons to reach the interface. Exciton diffusion length is defined as the average distance an exciton travels before it undergoes a recombination event, and can be very short due to disorder in organic materials. Diffusion lengths have been reported for various materials in experiment to be in the range of 3-30 nm [7]. Given that the devices are larger than 100 nm, the excitons could not travel far enough to reach the interface reliably, illustrated in Figure 2.6.

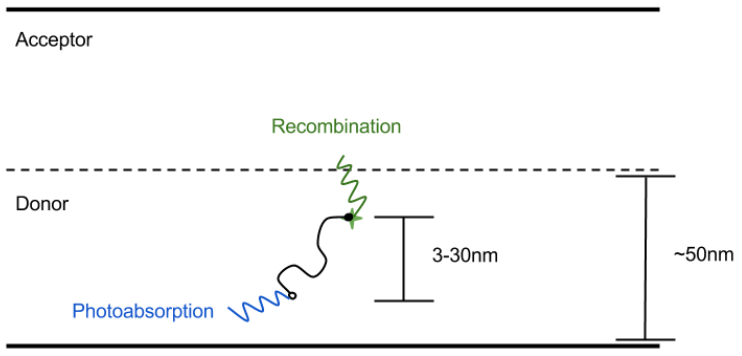

Figure 2.6: The exciton diffusion length falls short of reaching the interface in an organic bilayer device.

Modern organic solar cells have introduced methods to minimize the distance any

given exciton must travel to reach an interface. The most important way in which this is accomplished is with what is known as the bulk heterojunction configuration. This method was presented in a 1995 paper by Yu et al. [15] In this arrangement the donor and acceptor materials are mixed in solution in such a way that they have random phase separation throughout, as in figure 2.7. By random phase separation,

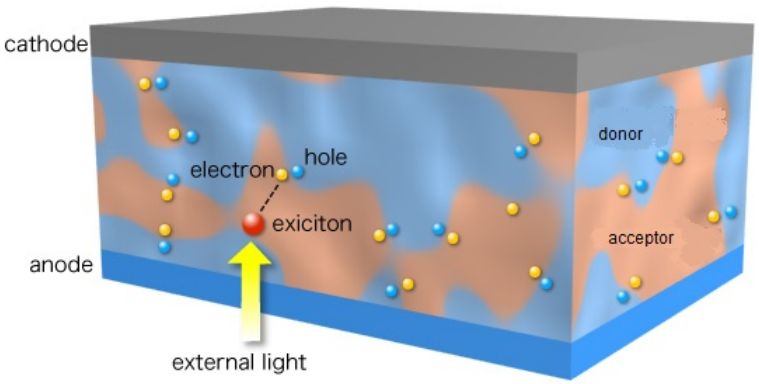

Figure 2.7: A schematic for an organic bulk heterojunction solar cell (Image courtesy of the Center for Future Chemistry, Kyushu University).

it is meant that the two materials are not completely mixed, but that there are small pockets of each material intertwining one another. In this way the distance between interfaces is decreased, increasing the chance that an exciton will reach one within its lifetime, and increasing the efficiency of these devices.

This was a big step forward, as once an exciton reaches an interface and dissociates, geminate recombination is very unlikely. Numerous issues still remain, however. Many of the excitons still fall short of reaching an interface, for example. Another problem is that due to the random nature of the mixing in the active layer, sometimes a charge will end up in an "island" of material which has no interface with a terminal. Such charges have no way to reach a terminal, cannot contribute to the current, and will eventually recombine. Thus, in spite of dramatic improvements in the past few decades, organic solar cells are still far behind their silicon counterparts in terms of efficiency. As of the writing of this document, highly optimized bulk heterojunction polymer solar cells have been reported with solar spectrum power conversion effi-

ciencies on the order of 10%. While a vast improvement, this is still well below the efficiencies of inorganic cells, which can reach efficiencies above 30% [16].

In order to further improve the performance of organic solar cells, and organic optoelectronic devices in general, a better understanding of the processes which occur is needed. In order for such a device to function, there must be photoabsorption, exciton transport, exciton dissociation, and charge transport. In the case of this thesis, the main focus is exciton dissociation.

3

Fundamentals of Charge Diffusion

As mentioned earlier, one of the most fundamental considerations in an optoelectronic device is the motion of electrons and holes. As such, it is important to have an understanding of the basic mechanisms governing how charges behave before one can deal with elaborate systems such as solar cells. To that end, the following chapter will attempt to lay a groundwork for understanding diffusion in anticipation of the discussion of charge dissociation to follow later.

3.1 The Diffusion Equation

In 1855, Adolph Fick derived the equation which describes the diffusive flux $\vec{J}$ of particles which have concentration f in a continuous medium [17]. Fick's first law is phenomenological, and states

$$\vec{J} = -D\vec{\nabla}f, \tag{3.1}$$

where $\vec{J}$ is the particle flux through some unit area, the diffusion coefficient D determines how the concentration f changes in time as a function of the concentration gradient. $\vec{J}$ has units of $\frac{quantity}{area \cdot time}$, and D has units of $\frac{area}{time}$. Now consider the continuity equation in the case of steady state

$$\frac{\partial f}{\partial t} = -\vec{\nabla} \cdot \vec{J}. \tag{3.2}$$

Inserting (3.1) into (3.2), we arrive at Fick's second law, also commonly referred to as the diffusion equation

$$\frac{\partial f}{\partial t} = D\nabla^2 f. \tag{3.3}$$

This equation describes the change in the concentration of particles as a function of time due to diffusion.

Another way in which the concentration of particles may change is via drift, i.e. particle motion due to some force. In the next section, the Smoluchowski equation will be described, which generalizes the diffusion equation to include drift terms.

3.2 The Smoluchowski Equation for a Pair of Diffusing Charges

A relevant example of diffusion in the presence of drift is the case of two opposite charges undergoing Brownian motion in a fluid. The formalism was developed, founded on Fick's work, by a few different people near the beginning of the twentieth century, most notably Einstein and Smoluchowski [18, 19]. The two charges in question may represent an electron and an ion diffusing in a fluid such as an electrolyte solution, which was a problem of interest at the time. This model of diffusion in a continuous medium is inadequate to describe charge motion in more complex systems such as disordered solids, but it is a useful and venerable foundation upon which to build a theory.

Consider now two opposite charges diffusing near one another through space. Let the positive charge be located at position $\vec{r}_1$, and the negative charge at position $\vec{r}_2$. The two particles also experience one another's coulomb potential U, with

$$U_1 = \frac{+e}{\epsilon|\vec{r}_1 - \vec{r}_2|} \quad , \quad U_2 = \frac{-e}{\epsilon|\vec{r}_1 - \vec{r}_2|}, \tag{3.4}$$

where ϵ is the dielectric constant. Incorporating the effect of the Coulomb potentials, the distribution function $f(r_1, r_2, t)$ describing the locations of the particles as a function of time then obeys [19]

$$\frac{\partial f}{\partial t} = D_1\vec{\nabla}_1 \cdot \vec{\nabla}_1 f + D_2\vec{\nabla}_2 \cdot \vec{\nabla}_2 f - \mu_1\vec{\nabla}_1 \cdot (-\vec{\nabla}_1 U_1)f - \mu_2\vec{\nabla}_2 \cdot (-\vec{\nabla}_2 U_2)f, \tag{3.5}$$

where $-\vec{\nabla}U$ is the force on a charge. The mobilities μ_1 and μ_2 give the drift velocity of a charge per electric field $\left(\frac{\vec{v}}{|\vec{E}|}\right)$. They are represented by

$$\mu_1 = \frac{+eD_1}{k_bT} \quad , \quad \mu_2 = \frac{-eD_2}{k_bT}. \tag{3.6}$$

At this point, it should be noted that only the relative motion of the charges is important, and so will be extracted. With that in mind, define the relative coordinate $\vec{r}$ and the center-of-mass (CM) coordinate $\vec{R}$ as

$$\begin{aligned} \vec{r} &= \vec{r_1} - \vec{r_2} \\ \vec{R} &= \frac{m_1\vec{r_1} + m_2\vec{r_2}}{m_1 + m_2} = a\vec{r_1} + b\vec{r_2}, \end{aligned} \tag{3.7}$$

where the m's are the masses of the particles, and a and b are defined simply for brevity. Letting the operator $\vec{\nabla}_\alpha$ be the gradient with respect to the coordinate $\alpha = \vec{r_1}, \vec{r_2}, \vec{R}, \vec{r}$, one finds from the definitions in (3.7)

$$\begin{aligned} \vec{\nabla}_{r_1} &= a\vec{\nabla}_R - \vec{\nabla}_r \\ \vec{\nabla}_{r_2} &= b\vec{\nabla}_R + \vec{\nabla}_r. \end{aligned} \tag{3.8}$$

Equation (3.5) then becomes

$$\begin{aligned} \frac{\partial f}{\partial t} &= D_1(a\vec{\nabla}_R - \vec{\nabla}_r)\cdot((a\vec{\nabla}_R - \vec{\nabla}_r)f) + D_2(b\vec{\nabla}_R + \vec{\nabla}_r)\cdot((b\vec{\nabla}_R + \vec{\nabla}_r)f) \\ &+\mu_1(a\vec{\nabla}_R - \vec{\nabla}_r)\cdot((a\vec{\nabla}_R - \vec{\nabla}_r)U_1)f + \mu_2(b\vec{\nabla}_R + \vec{\nabla}_r)\cdot((b\vec{\nabla}_R + \vec{\nabla}_r)U_2)f \\ &= \left((a^2D_1 + b^2D_2)\nabla_R^2 + (D_1 + D_2)\nabla_r^2 + 2(bD_2 - aD_1)\vec{\nabla}_R\cdot\vec{\nabla}_r\right)f \\ &+\frac{e}{k_bT}\left((a^2D_1 + b^2D_2)\nabla_R^2U_1 + (D_1 + D_2)\nabla_r^2U_1 + 2(bD_2 - aD_1)\vec{\nabla}_R\cdot\vec{\nabla}_rU_1\right)f, \end{aligned} \tag{3.9}$$

noting that $U_1 = -U_2$.

In the interest of eliminating the cross terms $\vec{\nabla}_R\cdot\vec{\nabla}_r$, consider the diffusion coefficients. For particles undergoing Brownian motion in some fluid, it is reasonable to assert on physical grounds that the diffusivity is inversely proportional to the mass of the particle. However, in the most general case of diffusion, this is not necessarily true. Consider the time-independent Schrödinger equation, which has an analogous

form to the diffusion equation

$$(E - V(\vec{r}))\Psi(\vec{r}) = \frac{-\hbar^2}{2m}\vec{\nabla}^2\Psi(\vec{r}). \tag{3.10}$$

When one separates $\Psi(\vec{r})$ into relative and center-of-mass coordinates, one arrives at the same transformation as in (3.7). Since $\frac{-\hbar^2}{2m}$ is analogous to D, it stands that the center-of-mass coordinate R goes as

$$\vec{R}_{cm} = \frac{\frac{1}{D_1}\vec{r}_1 + \frac{1}{D_2}\vec{r}_2}{\frac{1}{D_1} + \frac{1}{D_2}}. \tag{3.11}$$

Therefore, one is justified in saying

$$D_1 \propto \frac{1}{m_1} \quad , \quad D_2 \propto \frac{1}{m_2} \quad \Rightarrow \quad \frac{D_1}{D_2} = \frac{m_2}{m_1}. \tag{3.12}$$

Recall from equation (3.7) the following

$$\begin{aligned} a &= \frac{m_1}{m_1 + m_2} = \frac{1}{1 + \frac{D_1}{D_2}} \\ b &= \frac{m_2}{m_1 + m_2} = \frac{1}{1 + \frac{D_2}{D_1}}. \end{aligned} \tag{3.13}$$

This implies that

$$aD_1 = \frac{1}{\frac{1}{D_1} + \frac{1}{D_2}} = bD_2. \tag{3.14}$$

Thus, all of the cross terms of the form $2(bD_2 - aD_1)\vec{\nabla}_R \cdot \vec{\nabla}_r$ vanish. Equation (3.9) then reduces to

$$\begin{aligned} \frac{\partial f}{\partial t} = \Big(&(a^2 D_1 + b^2 D_2)\nabla_R^2 + (D_1 + D_2)\nabla_r^2 \\ &+ \frac{e}{k_b T}((a^2 D_1 + b^2 D_2)\nabla_R^2 U_1 + (D_1 + D_2)\nabla_r^2 U_1)\Big) f. \end{aligned} \tag{3.15}$$

Performing a standard separation of variables, assume that f has the seperable form

$f = f(\vec{r})f(\vec{R})$. Plugging this into equation (3.15), we get

$$\begin{aligned}
&\frac{\partial f(\vec{r})}{\partial t} - (D_1 + D_2)\nabla_r^2 f(\vec{r}) - \frac{e}{k_b T}(D_1 + D_2)\nabla_r^2 U_1 = C f(\vec{r}) \\
&= \frac{\partial f(\vec{r})}{\partial t} - \vec{\nabla}_r \cdot \left((D_1 + D_2)\vec{\nabla}_r f(\vec{r}) + \frac{e}{k_b T}(D_1 + D_2) f(\vec{r})\vec{\nabla}_r U_1 \right) \\
&\rightarrow \frac{\partial f(\vec{r})}{\partial t} - \vec{\nabla}_r \cdot \vec{J} = C f(\vec{r}),
\end{aligned} \tag{3.16}$$

where $\vec{J}$ is the particle current. Since $\frac{\partial f(\vec{r})}{\partial t} = 0$ in steady state, the continuity equation (3.2) dictates that $C = 0$. Redefining

$$\vec{\nabla}_r = \vec{\nabla} \quad , \quad D_1 + D_2 = D \tag{3.17}$$

for brevity, we get

$$\frac{\partial f}{\partial t} = D\vec{\nabla} \cdot (\vec{\nabla} + \frac{e}{k_b T}\vec{\nabla} U_1) f. \tag{3.18}$$

This equation has various names in various disciplines, such as the convection-diffusion equation or the drift-diffusion equation, but in this context it will be referred to as the Smoluchowski equation [20].

The Smoluchowski equation is often used to determine chemical reaction rates [21]. As electrons and ions diffuse around each other, they can recombine if they approach closely enough, constituting a chemical reaction. Understanding this sort of interaction is also necessary if one is to understand charge behavior in more sophisticated systems, such as solar cells. To that end, the next section develops the concept of geminate recombination, defined as the recombination of an electron with the parent ion or hole from which it originated.

3.3 Onsager's Charge Recombination Theory

Prototypical work on charge recombination can be traced back to the beginning of the twentieth century. In his famous treatise "Radioactivity", Rutherford posited the phenomenon of impact ionization [22], which would inform the work of many scientists to follow. During the 1920's and 1930's, the effects of ionizing cosmic rays upon the air were being studied by numerous scientists in an attempt to explain the seemingly spontaneous ionization observed in gases within closed vessels [23–26]. The amount

of spontaneous ionization observed was agreed to be too great to be accounted for by ambient radioactive sources in the ground, air, and other surrounding materials. Thus, cosmic radiation became suspect [24].

One of the relationships being investigated was that between the amount of ionization and pressure. The ionization was measured inside metal pressure vessels at pressures sometimes over 100 atmospheres and altitudes as high as that at the top of Pike's Peak (14,000 ft.) [26]. The measured ionization was found not to decrease linearly with pressure, but to saturate to a limiting value near 140 atmospheres. One hypothesis which was proposed said that at high pressures a geminate recombination event becomes more likely, as the higher density causes an ejected electron to lose its kinetic energy to collisions before it can escape the coulomb attraction of the ion from whence it came [27, 28]. This discussion marked some of the earliest treatment of charge recombination.

In 1938, Lars Onsager wrote a famous paper titled "Initial Recombination of Ions" [3], in which he analyzed the phenomenon of an excited electron undergoing immediate recombination with its parent ion. Decades later, this paper became a cornerstone to the subject of charge recombination in materials, especially organic semiconductors. One of the important things Onsager addressed was the presence of an electric field. Compton and company predicted that a very large field would be required to have an appreciable affect on the ionization [29], and therefore one need not consider an external applied field. Compton arrived at this conclusion as follows: consider an electron and ion which have been excited apart from each other with initial distance r. On average, as each charge diffuses it will move a distance λ before it scatters. By definition, λ is the mean free path. The new separation of the second ion relative to the initial position of the other ion will then be

$$r + \delta = \sqrt{r^2 + \lambda^2}, \tag{3.19}$$

as in Figure 3.1. Therefore, assuming $\lambda^2 \ll r^2$ the probable separation of the particles after each scatters for the first time is

$$r + \delta_1 + \delta_2 = 2\sqrt{r^2 + \lambda^2} - r \approx r\left(1 + \frac{\lambda^2}{r^2}\right), \tag{3.20}$$

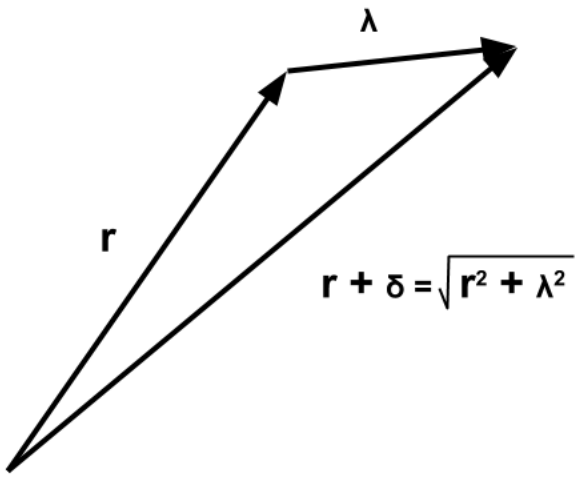

Figure 3.1: The two cases of a.) Stationary flow from a source at the origin, and b.) Diffusion from an initial separation r_0 and initial angle θ to the electric field.

which means the total change in separation is

$$\delta_r = \frac{\lambda^2}{r}. \tag{3.21}$$

The speed at which the ions diffuse is

$$\frac{\delta_r}{\tau} = \frac{\lambda^2}{\tau r}, \tag{3.22}$$

for an average time between scattering events τ. Meanwhile, the amount that the ions would be drawn together given an acceleration a due to the coulomb force in an interval τ is $\frac{1}{2}a\tau^2$. The rate of approach due to the coulomb force is then

$$\frac{\delta_{coulomb}}{\tau} = \frac{e^2\tau}{mr^2}. \tag{3.23}$$

The condition that the ions escape one another is then

$$\frac{\lambda^2}{\tau r} > \frac{e^2\tau}{mr^2}, \tag{3.24}$$

which Compton expressed as

$$r > r_0 \quad , \quad r_0 \equiv \frac{e^2\tau^2}{m\lambda^2}. \tag{3.25}$$

Expressing the scattering time as $\tau = \frac{\lambda}{v}$, with v given by

$$\frac{1}{2}mv^2 = \frac{3}{2}k_bT, \tag{3.26}$$

one gets

$$r_0 = \frac{e^2}{3k_bT}. \tag{3.27}$$

At room temperature, the electric field due to an electron at a distance r_0 is roughly $4 \times 10^4 \frac{V}{cm}$. This caused Compton to conclude that a large field would be required to have an appreciable effect, and an external field was thus initially neglected as a consideration. Experimental observation [30], Onsager submitted, indicated that not to be the case, and that a weaker field than that predicted by Compton would have an appreciable effect. The following is Onsager's analysis of the situation, in the context of weak electrolytes (i.e. those having a low concentration of ions) in a liquid. While it is true that Compton's work was in the context of a gas, an electrolyte solution is qualitatively very similar. It should therefore at least provide context for a qualitative explanation of the experimentally observed effects of an external field.

The first part of the analysis comes from an earlier paper written in 1934 [31], wherein Onsager approximately solved the diffusion equation in order to find the field dependence of the dissociation coefficient, which represents the fraction of the solution which is ionized. Parts of the analysis in [31] would become the basis for the result presented in his later paper, [3].

Consider a solution containing the time dependent densities $n_1, n_2, ..., n_s$ of ions of types $1, 2, ..., s$. The Coulomb interaction will cause the concentrations of ions at different locations to depend on the presence of other ions nearby. With that in mind, define the following quantity,

$$n_{ij} \equiv n_{ij}(\vec{r_2} - \vec{r_1}), \tag{3.28}$$

as the time average concentration of j-ions in a volume element dV_2 located at $\vec{r_2}$ given an i-ion in the volume element dV_1 located at $\vec{r_1}$. The distribution function

that gives the chance of simultaneously finding an i-ion in dV_1 and a j-ion in dV_2 can then be defined as

$$f_{ij}(\vec{r_2} - \vec{r_1}) = n_i n_{ij}(\vec{r_2} - \vec{r_1}). \tag{3.29}$$

To demarcate a bubble of interaction, define the quantity

$$Q = \frac{q_1 q_2}{2\epsilon k_b T}$$

as the "effective range" of the ions, namely the distance at which the coulomb interaction is comparable to the thermal energy. ϵ is the dielectric constant of the material, k_b is Boltzmann's constant, and T is temperature. The total concentration of interacting pairs of ions can be expressed as

$$\nu_{ij} = n_i \int_a^Q n_{ij}(\vec{r}) 4\pi r^2 dr, \tag{3.30}$$

where a is some small radius of nearest approach between the ions.

Since these charges are diffusing in a fluid, Onsager set about describing the system using the Smoluchowski equation described earlier. He expressed this as

$$\frac{\partial f}{\partial t} = k_b T(\omega_1 + \omega_2)\vec{\nabla} \cdot (e^{-\frac{U}{k_b T}} \vec{\nabla} f e^{\frac{U}{k_b T}}) = 0. \tag{3.31}$$

Onsager assumes the boundary conditions of a source at the origin and a sink at infinity (i.e. $\lim r \to \infty f(r) = 0$) so that the system is in steady state ($\frac{\partial f}{\partial t} = 0$). The ω's are diffusion coefficients per $k_b T$ ($\omega = \frac{D}{k_b T}$) so that $q\omega = \mu$, the mobility of an ion. Equation (3.31) tells us

$$\vec{\nabla} \cdot (\vec{\nabla} f - \frac{1}{k_b T} f \vec{\nabla} U) = 0. \tag{3.32}$$

The potential U represents the sum of the interactions with all the other ions in the solution and the external field. This makes the problem very difficult to solve. As a result, an approximation must be made, since a many-body interaction between ions is intractable. Therefore, since it has been assumed that the concentration of ions is low, let the potential experienced by the two ions simply include their mutual

coulomb interaction. The potential U then becomes

$$U = -qEr\cos\theta - \frac{q^2}{\epsilon r} = -k_b T(2Br\cos\theta + \frac{2Q}{r}), \tag{3.33}$$

where $B = \frac{qE}{2k_bT}$ (for convenience later), E is the magnitude of the applied field, and q is the elementary charge. This relation is still not exactly solvable, but for the boundary condition

$$\lim_{r\to\infty} f(r) = 0 \tag{3.34}$$

it can be expressed in the form of a definite integral [31]

$$f(r,\theta) = \frac{1}{r}e^{Br(\cos\theta-1)+\frac{2Q}{r}} \int_{s=0}^{s=2Q} J_0\left((-8Bs)^{\frac{1}{2}}\cos\frac{\theta}{2}\right) e^{-\frac{s}{r}} ds. \tag{3.35}$$

J_0 is the zeroth order Bessel function of the first kind. This relation acts as the starting point for the more famous result Onsager published in 1938 [3]. The result regards the probability ϕ that two charges will escape one another, defined as moving a very large (effectively infinite) distance apart. In order to define ϕ, one first defines the pair survival probability,

$$F(t) = \int f(\vec{r},t)d^3\vec{r}. \tag{3.36}$$

This represents the chance that a charge pair has not recombined at some time t. The quantity of more interest, however, is the probability ϕ that an initially bound electron-hole pair will escape one another entirely [32]. The probability ϕ is simply defined as the long time limit of $F(t)$,

$$\phi = \lim_{t\to\infty} F(t). \tag{3.37}$$

Some adjustments needed to be made to the analysis at this point to describe the phenomenon of initial recombination. Equation (3.32) was derived in [31] for the case of stationary flow from a source at the origin with a sink at $r = \infty$. The problem of initial recombination, however, assumes some instantaneous separation r_0 between the electron and hole to start, i.e. $f = f(r, r_0, ; t)$. Since some impulse is imparted upon them by incident radiation, driving them a short distance apart before they relax, the charges are not initially arbitrarily close. Therefore in his subsequent

paper [3], Onsager takes the source to lie at some point (r_0, θ), with initial angle θ to the electric field, and the origin and infinity to both be sinks, as in Figure 3.2.

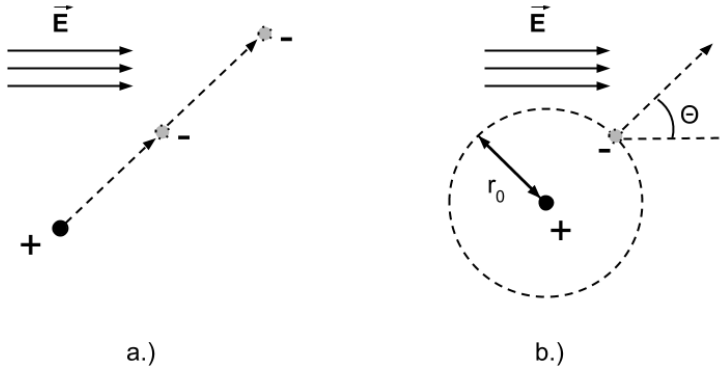

Figure 3.2: The two cases of a.) Stationary flow from a source at the origin, and b.) Diffusion from an initial separation r_0 and initial angle θ to the electric field.

At this point equation (3.32) is in terms of $\vec{r}$. What we want is the escape probability ϕ in terms of the initial separation r_0. In order to get such an expression, some manipulation of equation (3.32) is in order. Its Laplace transform is

$$\vec{\nabla} \cdot (\vec{\nabla}\tilde{f} - \frac{1}{k_b T}\tilde{f}\vec{\nabla}U) - s\tilde{f} = 0, \tag{3.38}$$

with

$$\tilde{f}(r, r_0, ; s) = \int_0^\infty f(r, r_0, ; t)e^{-st}dt. \tag{3.39}$$

Introducing

$$u(r, r_0; s) = \tilde{f}(r, r_0; s)e^{\frac{U}{k_b T}}, \tag{3.40}$$

equation (3.38) becomes

$$\vec{\nabla} \cdot (e^{-\frac{U}{k_b T}}\vec{\nabla}u) - se^{-\frac{U}{k_b T}}u = 0, \tag{3.41}$$

which is now self adjoint. This means that one can apply the reciprocity relation [33]

$$u(r, r_0, ; s) = u(r_0, r, ; s), \tag{3.42}$$

which gives

$$\vec{\nabla}_{r_0}(e^{-\frac{U(r_0)}{k_b T}}\vec{\nabla}_{r_0}u) - se^{-\frac{U(r_0)}{k_b T}}u = 0. \tag{3.43}$$

Plugging equation (3.40) back into equation (3.43) yields

$$\vec{\nabla}^2_{r_0}\tilde{f} - \frac{1}{k_bT}\vec{\nabla}_{r_0}U(r_0)\cdot\vec{\nabla}_{r_0}\tilde{f} - s\tilde{f} = 0. \tag{3.44}$$

Taking the inverse Laplace transform, one arrives at

$$\vec{\nabla}^2_{r_0}f - \frac{1}{k_bT}\vec{\nabla}_{r_0}U(r_0)\cdot\vec{\nabla}_{r_0}f = 0. \tag{3.45}$$

Finally, integrating over r and taking the long time limit as per equations (3.36) and (3.37), the expression governing the escape probability ϕ is

$$\vec{\nabla}^2_{r_0}\phi - \frac{1}{k_bT}\vec{\nabla}_{r_0}U(r_0)\cdot\vec{\nabla}_{r_0}\phi = 0, \tag{3.46}$$

which Onsager writes as

$$\vec{\nabla}_{r_0}\cdot(e^{-\frac{U(r_0)}{k_bT}}\nabla_{r_0}\phi) = 0. \tag{3.47}$$

If ϕ is taken to be a function of the initial distance r_0 and the initial angle θ with respect to the "downstream" direction of the electric field, the boundary conditions on ϕ are

$$\begin{aligned}\phi(0,\theta) &= 0\\ \phi(\infty,\theta) &= 1,\end{aligned} \tag{3.48}$$

In the case of zero electric field ($B = 0$), equations (3.47) and (3.48) are satisfied simply by the reciprocal of the Boltzmann factor times k_bT,

$$\phi = k_bTe^{\frac{U(r_0)}{k_bT}} = k_bTe^{-\frac{2Q}{r_0}}, \tag{3.49}$$

since in that case

$$\lim_{r_0\to 0}\vec{\nabla}_{r_0}\cdot(e^{-\frac{U(r_0)}{k_bT}}\nabla(k_bTe^{\frac{U(r_0)}{k_bT}})) = 0 \tag{3.50}$$

and

$$\lim_{r_0\to\infty}\vec{\nabla}_{r_0}\cdot(e^{-\frac{U(r_0)}{k_bT}}\nabla(k_bTe^{\frac{U(r_0)}{k_bT}})) = \lim_{r_0\to\infty}\nabla^2U(r_0) = \delta(r_0). \tag{3.51}$$

It turns out that the more difficult case of a nonzero field was actually solved in [31]. Recall the expression for $f(r,\theta)$ in equation (3.35). It so happens that dividing the right hand side by the Boltzmann factor satisfies the boundary conditions (3.48) for

ϕ.

$$\phi(r,\theta) = e^{Br(\cos\theta - 1)} \int_{s=\frac{2Q}{r}}^{s=\infty} J_0\left((-8Bs)^{\frac{1}{2}} \cos\frac{\theta}{2}\right) e^{-s} ds \tag{3.52}$$

To see the *relative* effect of the field, one divides equation (3.52) by equation (3.49). This effect is greatest for small values of the initial separation r_0, in which case

$$e^{\frac{2Q}{r_0}} \phi(r_0,\theta) \to J_0\left(4(-BQ)^{\frac{1}{2}} \cos\frac{\theta}{2}\right). \tag{3.53}$$

Approximating (3.53) as a power series in the dimensionless field strength B, one gets

$$e^{\frac{2Q}{r_0}} \phi(r_0,\theta) = 1 + 2BQ(1+\cos\theta) + O(B^2). \tag{3.54}$$

At this point, it is reasonable to assume a uniformly random distribution of initial angles, and an ensemble average over $\cos\theta$ gives zero. The current of ions escaping recombination relative to the zero field case can then be approximated as

$$\frac{I(E)}{I(0)} = \frac{\phi(E)}{\phi(0)} \approx 1 + 2BQ. \tag{3.55}$$

For $\epsilon = 1$ and $T = 300$ Onsager gets

$$2BQ = 1.07 \times 10^{-4} |E|.$$

For the above value of $2BQ$ and a field strength of $10^4 \frac{V}{cm}$, $\frac{I(E)}{I(0)} \approx 2$. This is a significant increase, at a field strength lower than that predicted by Compton et al. This result was rather famous in the extensive study of electrolytes at its time, but languished for many years after the Second World War until the advent of organic semiconductors. It became important in the last few decades in the context of organic photovoltaic devices, as most operate in this field regime ($10^4 \frac{V}{cm}$) [7]. In 1983, Charles Braun extended this model to consider charge transfer states in donor-acceptor systems [34].

The problem which Braun addressed was the unrealistically large apparent initial separation of excited charges in some semiconductors ([34] and references therein). When using the Onsager model to estimate the initial separation, the number of charges which were observed to dissociate implied an initial separation of $2-3$ nm. This is a rather large distance, much larger than is reasonable given the energy imparted to the excitation, which should only produce an initial separation of roughly

1 nm. To account for this increased dissociation, Braun points out that the initial excited state, referred to as the first charge transfer state (CT_1), has some nontrivial lifetime ($\sim 10^{-8}$ s). This prevents the exciton from instantly recombining as it would in the original Onsager model. As the charges linger in CT_1, they may partially dissociate and fall back into CT_1 many times, which improves the probability of ultimate dissociation to agree more closely with experiment. With this extension the Onsager result became something of a benchmark for results in exciton transport.

One of the major drawbacks of the Braun-Onsager model is that it does not account for spatially varying energetic disorder which is present in virtually all organic semiconductors. This disorder causes local changes in the behavior of the charges. For example, the presences of small crystallite clusters causes charges to have high mobility while in the crystals, but low mobility between clusters [35]. In the absence of an analytic theory in the face of disorder, much of the work done on charge transport in organic semiconductors is experimental and computational. In the following chapter, some of this work will be discussed.

4

Motivating Work on Energetic Disorder

4.1 Rates for Hopping Transport

This chapter will begin to explore charge transport in disordered semiconductors. It is immediately apparent that there are some major differences in the description of charge motion in a disordered solid when compared to a fluid such as the electrolyte solutions studied by Onsager. One of the most important differences is that charges do not experience continuous diffusion through the medium. In disordered organic semiconductors excited charges tend to spend the majority of their time occupying an atom or molecule. The valence electron orbitals of these occupation sites will overlap those of nearby sites to varying degrees, and occasionally the excited charges will tunnel, or "hop" to a nearby site. In this fashion they will undergo a random walk through the material under the influence of ambient electrostatic fields. The mobility of a charge in a disordered semiconductor depends on the rate at which it makes hops from site to site. There are a few different formalisms to describe these hopping rates, two of which will be discussed presently.

4.1.1 The Miller-Abrahams Hopping Rate

In 1960, Miller and Abrahams published a paper titled, "Impurity Conduction at Low Concentrations" [36]. The system being described corresponds to a doped semiconductor, with some concentration of ionized impurity sites. They perform a quantum mechanical analysis to derive the transition rates onto and off of these impurities. One assumption made, as one might infer from the title of the paper, is that the concentration of impurity sites is low. This means the individual impurities are far from one another, so that electrons interacting with an impurity are not interfered with by excited electrons elsewhere in the system. A second approximation is that of low temperature (on the order of a few kelvin). Finally, the electron-phonon coupling of the dopant sites is estimated according to the deformation potential approximation, in which the site energies are changed by an amount $E_1\eta$, where η is the relative change in the local lattice spacing.

Evaluating the overlap of the site matrix elements under these approximations, Miller and Abrahams arrived at the expression for the hopping rate ν_{ij} from site i to site j,

$$\nu_{ij} = \zeta E_1^2 |\Delta| R^{\frac{3}{2}} e^{-\frac{2R}{a_1}} \begin{cases} n & \Delta > 0 \\ n+1 & \Delta < 0 \end{cases} \tag{4.1}$$

The coefficient ζ is

$$\zeta = \frac{e^2}{6\rho_0 s^5 \hbar^4 \epsilon a((a_1/b_1)^2 - 1)}, \tag{4.2}$$

where e is the elementary charge, ρ_0 is the density of the medium, s is the speed of sound, and ϵ is the dielectric constant. Δ represents the energy difference between the sites, $E_j - E_i$. R is the distance between the sites, and a_1 and b_1 are the transverse and longitudinal radii of the local (approximately) hydrogen-like wavefunctions, respectively, which have the form,

$$\Psi_{Hyd} = \frac{1}{\sqrt{\pi a_1^2 b_1}} e^{-\sqrt{(x^2+y^2)/a_1^2 + z^2/b_1^2}}. \tag{4.3}$$

The value of a_1 is,

$$a_1 = \sqrt{\frac{\hbar^2 E_{obs}}{2m}}, \tag{4.4}$$

where E_{obs} is the experimentally observed ionization energy for the donor ground

state.

The factor of n is the Bose-Einstein distribution for phonons which are coupled to the electrons of interest, so the distribution of phonons carrying the correct energy to induce hopping is

$$n = \frac{1}{e^{\frac{\Delta}{k_b T}} - 1}. \tag{4.5}$$

Since this system is being considered at low temperature, $e^{\frac{\Delta}{k_b T}} \gg 1$, so that

$$n = \frac{1}{e^{\frac{\Delta}{k_b T}} - 1} \approx \frac{1}{e^{\frac{\Delta}{k_b T}}} = e^{-\frac{\Delta}{k_b T}}. \tag{4.6}$$

In the case of $n + 1$,

$$n + 1 = \frac{e^{\frac{\Delta}{k_b T}}}{e^{\frac{\Delta}{k_b T}} - 1} \approx \frac{e^{\frac{\Delta}{k_b T}}}{e^{\frac{\Delta}{k_b T}}} = 1. \tag{4.7}$$

The Miller-Abrahams hopping rate is typically rendered

$$\nu_{ij} = \begin{cases} \nu_0 e^{-\frac{2R}{a_1}} e^{-\frac{\Delta}{k_b T}} & \Delta > 0 \\ \nu_0 e^{-\frac{2R}{a_1}} & \Delta < 0 \end{cases} \tag{4.8}$$

4.1.2 The Marcus Hopping Rate

Another formulation of the transition rate was developed by Rudolph Marcus, and can be found in a paper of his from 1965 [37]. Originally formulated for the case of ions reacting in a solution, it was later extended to describe hopping in solids. In either case, the picture is that of a pair of ions transferring electrons across a dielectric background.

One of the central ideas Marcus had in mind while constructing this model of charge hopping was that of a "reorganization energy", represented by γ. This term arises from the idea that the surrounding medium is polarizable, and that there is some energy cost associated with changing the local polarization. The Marcus hopping rate is typically expressed as

$$\nu_{ij} = \nu_0 e^{-\frac{(\Delta+\gamma)^2}{4\gamma k_b T}}. \tag{4.9}$$

The prefactor ν_0 is an attempt frequency, similar to that in the Miller-Abrahams rate, or in any other rate theory equation. Δ is the same as in equation (4.8), which

Marcus expresses as the free energy in a vacuum of the reaction in question. The reorganization term γ is a function of the electron orbital distortion of the environment, and is typically determined experimentally.

The decision about which hopping rate to use in a model has been subject to much debate, as it is difficult to determine which description is the better for a given system. The Marcus rate can be problematic, as it is Gaussian in Δ when $\Delta \gg \gamma$, which is a valid regime, for example in a solid with low polarizability. Consider expanding the exponent in equation 4.9

$$\nu_{ij} = \nu_0 e^{-\frac{(\Delta+\gamma)^2}{4\gamma k_b T}} = \nu_0 e^{-\frac{\Delta^2}{4\gamma k_b T} - \frac{\Delta}{2k_b T} - \frac{\gamma}{4k_b T}}. \tag{4.10}$$

In a system with very low polarizability, i.e. a very small γ, the first term in the expansion will cause the hopping rate to become very small. A too-small hopping rate may not accurately describe the hopping dynamics of the system, as the hopping rate in a very nonpolarizable material may be weakly dependent on the reorganization energy.

The Miller-Abrahams rate is not without its own problems, however. The assumption of low temperature is certainly not valid for modeling semiconductors at room temperature. The assumption of low concentration is also not necessarily valid for all systems which the Miller-Abrahams rate is used to model. In spite of these drawbacks, the Miller-Abrahams rate is a decent approximation, and is used extensively for a wide range of parameters.

4.2 Bässler's Pair Dissociation in Energetically Random Hopping Systems

Much of the author's work presented in the next chapter on energetically disordered hopping systems was predicated on the work of H. Bässler et al. [38–46]. This work focused on the geminate recombination of coulombically interacting electron-hole pairs diffusing within an energetically random hopping system, and the effect that energetic disorder has on the dissociation rate of the charge pairs. This system was explored by Albrecht and Bässler through Monte Carlo computer simulations.

This chapter will focus on those detailed in [41].

It is generally agreed that in organic semiconductors there exist a few intermediate excitonic charge transfer (CT) states [7, 34]. Many organic solids such as crystalline polydiacetylenes [41] have a low dielectric constant. As a result, the coulombic binding energies of these CT excitons are high, and the initial separations are small.

Experiments indicate that excited charges in non-crystalline conjugated polymers such as polyphenylene vinylenes (PPVs) have a lower coulomb binding energy. Therefore they may relax to relatively large "thermalization lengths", defined as the distance at which the electron's excess kinetic energy has been dissipated into the lattice. The charges then equilibrate, forming an exciton with the electron and hole bound across 2-3 nm [41]. Albrecht and Bässler conducted simulations regarding this large exciton as the initial state. The charges were then allowed to diffuse, and the rate of recombination was recorded.

In these simulations [41], the system is represented as a cubic lattice in which each site possesses an occupation energy for an electron or hole to reside on it. In this case, the occupation energies are drawn from a Gaussian distribution, as in Figure 4.1. In reality the disorder of the occupation energy is due to contributions from

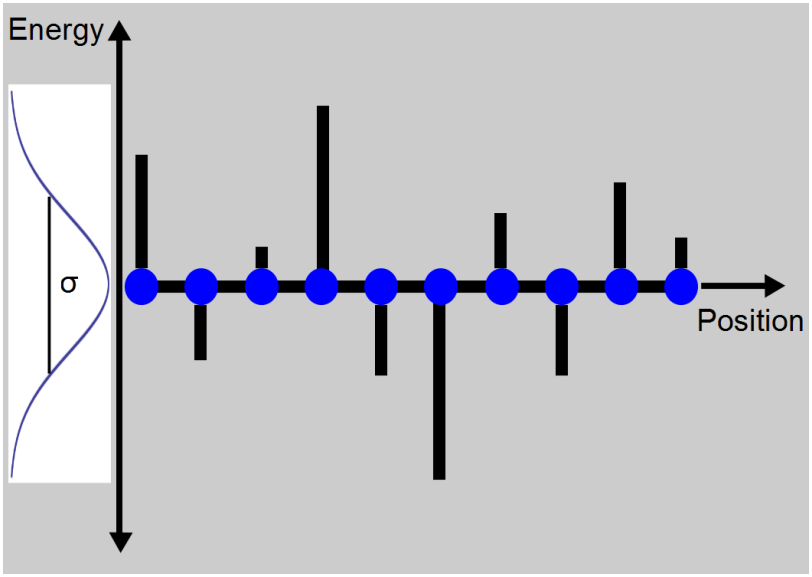

Figure 4.1: Gaussian occupation energies in 1D.

various sources. The differences in electronegativity, an atom or molecule's tendency to bind electrons (or conversely, to repel holes), are one such contribution. Another

factor is the charge-dipole interaction. There are a number of fixed dipole moments distributed throughout the material, and for a charge located on a site anywhere in the system the energy from this contribution is

$$U_i = \sum_{j \neq i} \vec{p_j} \cdot \vec{E_i}, \tag{4.11}$$

where $\vec{p_j}$ is the dipole moment at site j and $\vec{E_i}$ is the field due to the charge at site i. These myriad contributions are difficult to completely account for, however. The choice of the so-called "Gaussian Disorder Model" was prompted by the fact that spectroscopy indicates that electronic density of states (DOS) of organic semiconductors tends to have a Gaussian profile, with variances reaching $\sigma = 0.1$eV, which is approximately $4k_bT$ at room temperature [40, 41].

A natural question to ask is "How can these simulations be performed on a uniform cubic lattice if organic semiconductors are spatially disordered, as well as energetically? Shouldn't a complete simulation include effects of positional disorder?" Spatial disorder has certainly been treated by several different investigators, for example [39, 47–49].

Energetic and spatial disorder may each dominate under different circumstances. Most hopping rates are some variation on the form $e^{-2\alpha R}e^{-\frac{\Delta}{k_bT}}$. It may be the case that two sites which have a large, favorable downhill energy mismatch do not have strongly overlapping wavefunctions, as in Figure 4.2. In this case, the $e^{-\frac{2R}{a}}$ term may be very small and prevent an otherwise probable hop, to the point of causing temperature independence. It may also happen that two sites are close to one another, and overlap strongly, as in Figure 4.3. In this event, $e^{-\frac{2R}{a}} \approx 1$, and the hopping is governed entirely by Δ and the temperature. A whole range of configurations is possible. In 1969, Mott published a model describing conduction in non-crystalline materials which is known as Mott Variable Range Hopping [47]. He defined the range between two sites to be

$$\mathcal{R} = 2\alpha R + \frac{\Delta}{k_bT}. \tag{4.12}$$

The rates ν to hop between two sites

$$\nu \propto e^{-\mathcal{R}} \tag{4.13}$$

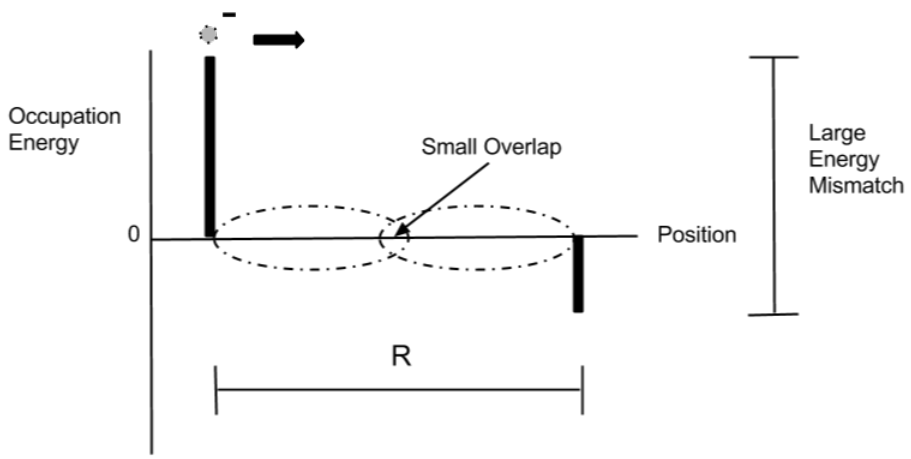

Figure 4.2: Two hopping sites with a large energy mismatch and a small wavefunction overlap.

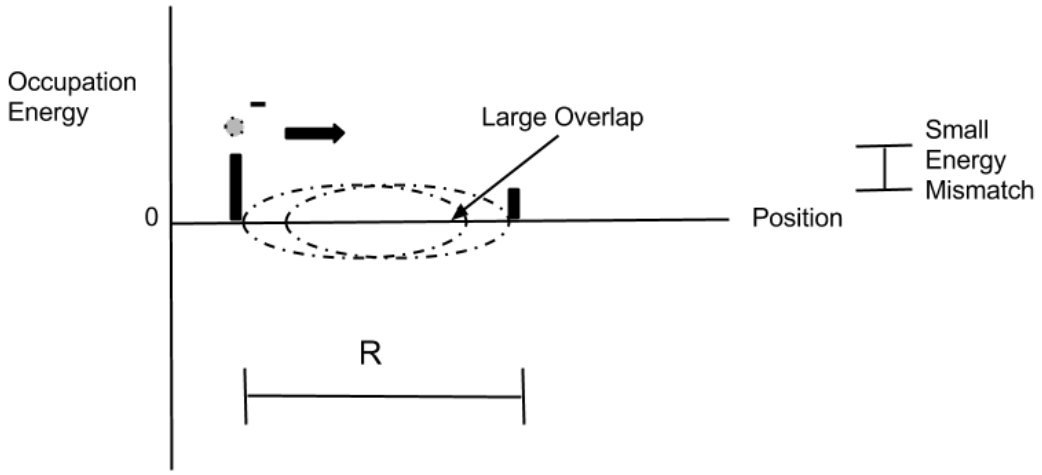

Figure 4.3: Two hopping sites with a small energy mismatch and a large wavefunction overlap.

are highest for the smallest values of the four-dimensional coordinate $\mathcal{R}$ which describes the different configurations of sites.

In the systems being treated presently there are some factors which mitigate spatial disorder. One is the fact that the temperature is usually taken to be near room temperature, $T = 300K$. This causes hopping to tend toward nearest spatial neighbors. In addition, the packing of molecules in a relevant polymer tend to be restrictive enough that the spatial variation is not large. Thus it is valid to focus on the effects of energetic disorder over spatial disorder.

Albrecht and Bässler's simulations were performed using the Monte Carlo method [41], in which an ensemble average of a random process is taken from many iterations. Each iteration was initialized with a cubic lattice with a spacing between sites of $a = 8$ Å. The sites were populated with a Gaussian random distribution of energies of variance $0.05eV \leq \sigma \leq 0.15eV$. A uniform electric field was superimposed over the entire lattice. A hole was located at the center of the lattice, and an electron placed three lattice sites in the downfield direction to represent a thermalized charge transfer state as described earlier. The electron was then allowed to diffuse about the grid, hopping according to the Miller-Abrahams rate. This process is visualized

in Figure 4.4. The conditions for ending an iteration of the simulation were either

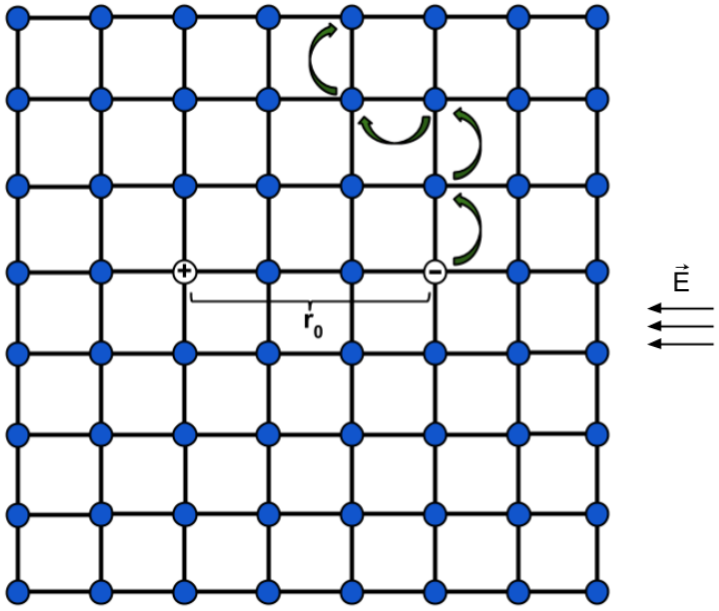

Figure 4.4: A diagram representing charges hopping on a model lattice. The charges are initially placed a distance r_0 apart with the electron placed "downstream" in the direction of the electric field, and then allowed to diffuse according to the Miller-Abrahams hopping rate. In the simulations of Albrecht and Bässler, only the electron is allowed to migrate, as in the Onsager model.

that the electron and hole occupy the same site (recombination), or that the electron traveled $100a$ from the hole, stated to be five times the coulombic capture radius at $295K$ and $a = 8$ Å. The coulombic capture radius R_c corresponds to the separation between the charges at which the coulomb potential energy is equal to the ambient thermal energy,

$$\frac{e^2}{\epsilon R_c} = k_b T \quad \rightarrow \quad R_c = \frac{e^2}{\epsilon k_b T}. \tag{4.14}$$

2000 iterations were made per data point.

4.2.1 Energetic Disorder in Bässler's Simulations

Before discussing the conclusions at which Bässler et al. arrived, an aside regarding some of the reasoning underlying these simulations is given. The question remains,

why would one expect such energetic disorder to change the probability of an exciton dissociating? One answer is that such energetic disorder may provide a barrier to recombination. Organic photovoltaic devices generally absorb light primarily in the visible spectrum, where photon energies are typically $1 - 3$ eV [7]. As a result, excited charges are initially relatively "hot", letting them achieve appreciable separation before they thermalize into the charge transfer state discussed earlier. In an energetically flat system there is little to resist the charges' mutual coulomb attraction, causing them to be drawn back together. In an energetically disordered system, however, there is an opportunity for the two charges to be excited across an energetic barrier, which would inhibit recombination, as in Figure 4.5. As a result, one might

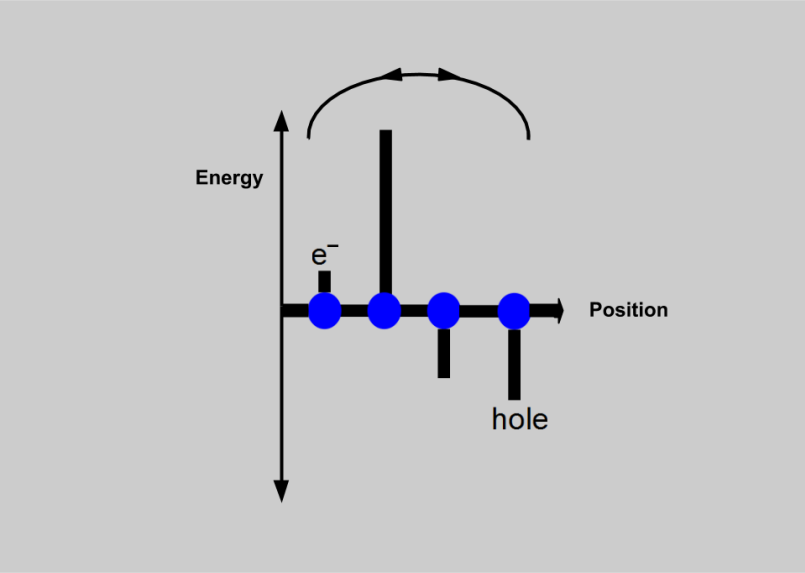

Figure 4.5: Energetic disorder preventing recombination.

expect that a certain amount of disorder would improve the probability of a charge pair escaping one another and dissociating, and improve the overall photocurrent. Energetic disorder may actually lower the mobility of the charges, but increase the total number of pairs which dissociate.

4.2.2 ϕ versus T

One of the relationships these simulations explore is the effect of temperature on the escape probability ϕ in an energetically disordered system. Albrecht and Bässler's

findings on this front are presented in Figure 4.6. As one can see, the presence of

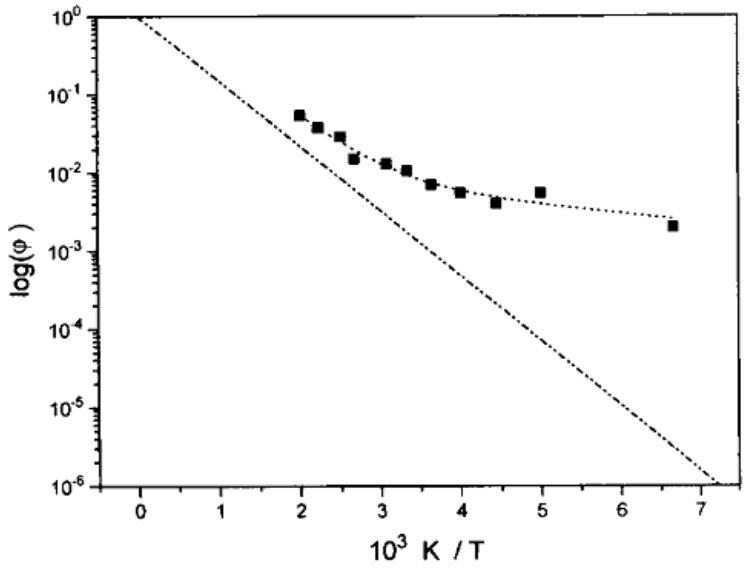

Figure 4.6: An Arrheneius plot of Albrecht and Bässler's result for ϕ versus $\frac{1}{T}$. Initial charge separation $r_0 = 3a = 24$Å, field of $10^4 \frac{V}{cm}$, temperature $T = 250K$, and dielectric constant $\epsilon = 3.55$. The dashed line is the prediction of the three-dimensional Onsager theory.

energetic disorder in the simulation improves the chances for charge pair to dissociate relative to the Onsager theory. The trend of the data for large T is toward converging with the Onsager result, which is reasonable. At very large T, the thermal energy of the charges is well above the strength of the disorder, i.e. $e^{\frac{\Delta}{k_b T}} \approx 1$ for all values of Δ. As a result, the disorder cannot appreciably change the hopping dynamics in this regime.

According to Figure 4.6, the energetic disorder has the greatest effect at low temperatures. For small values of T, the thermal energy of the charges is now comparable to or smaller than the strength of the disorder. This means that hopping configurations such as the one described in Figure 4.5 would be much more effective at keeping the charges separated.

4.2.3 ϕ versus σ

The behavior of most interest in the context of this thesis is that of the escape probability ϕ versus the strength of the disorder, which is characterized by the width σ of the Gaussian disorder profile. Albrecht and Bässler's results are displayed in Figure 4.7. For a fixed temperature, the dissociation yield appears to increases exponentially

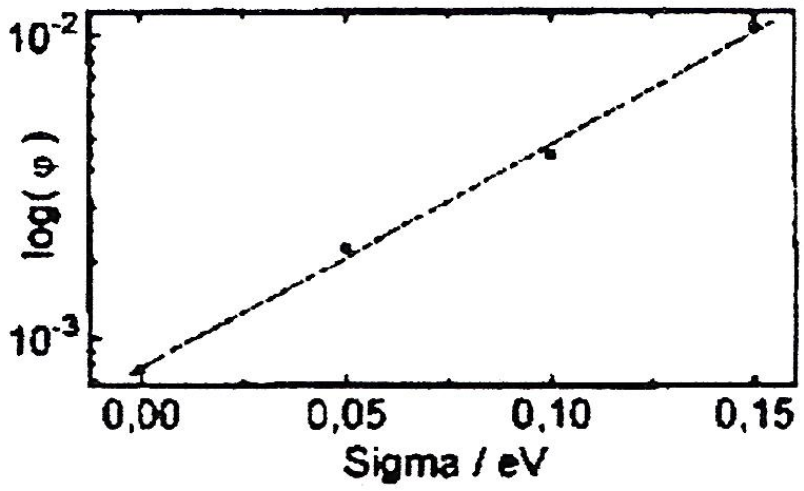

Figure 4.7: Bässler's result for ϕ versus σ. Initial charge separation $r_0 = 3a = 24$Å, field of $10^4 \frac{V}{cm}$, temperature $T = 250K$, and dielectric constant $\epsilon = 3.55$. The data point for $\sigma = 0$ is the value predicted by the Onsager theory.

with the strength of the disorder. While this is a rather important result, it is founded on three data points, presumably due to computational limitations at the time (1995). The data point for $\sigma = 0$ is taken from the theoretical Onsager result rather than simulation. The validity of such an assumption may be questionable in the context of these simulations. For example, in [50] Scher and Rackovsky present an analytical description of geminate recombination on a lattice, and conclude that while their results are qualitatively the same as Onsager's, they are quantitatively different. Reference [50] studies an ordered lattice, but one would not expect that the presence of disorder in the simulations would improve the agreement of the result with Onsager's theory. This difference in behavior between the lattice and continuum is also supported by the author's work which follows.

5

Correlated Energetic Disorder

The preceding chapters have been laying the foundation for the idea of correlated energetic disorder in solids. The organic semiconductors which are useful for opto-electronic applications are largely amorphous or polycrystalline [7], so the presence of disorder is a given. As we have already discussed, one of the more popular descriptions of this disorder is the Gaussian Disorder Model, introduced by Bässler [38]. It is inferred from spectroscopic results that the electronic DOS is Gaussian in shape, and many simulations similar to those described in the previous chapter [41] implement this as a completely Gaussian random distribution of the occupation energies of hopping sites. However, having a Gaussian DOS and having energies pulled from a Gaussian random distribution are not necessarily the same thing.

There is no reason, a priori, to believe that the energetic disorder at any given point in an organic polymer is determined completely randomly, without regard for the local structure. Several papers have explored this idea, including [51–57]. These papers are concerned largely with explaining observed mobilities in disordered polymers. Papers [53–55] discuss a possible source of correlation, namely the charge-dipole interaction, which is strongly indicated as the dominant source of spatial energetic correlation [54].

5.1 Dipole Correlation

One of the ideas central to understanding energetic correlation is discussed by Novikov and Vannikov in [53], and that is the concept of dipole field contributions to the energy landscape. There are myriad fullerene compounds, organic polymers, and dopants used in the construction of optoelectronic devices. The individual materials possess fixed molecular dipole moments ranging from very weak to very strong, usually in the range of 1-8 Debyes [58]. These dipole moments can also change based on factors such as molecular orientation and packing, but the bottom line is that, in their bulk forms, these materials contain various fixed dipole moments throughout. The field produced by such a collection of dipoles makes up the dominant contribution to the energy landscape a charge will see when it traverses the material.

Consider now a charge undergoing hopping motion on a lattice such as the one used in the simulation described in the previous chapter. The potential that it experiences at some site i on the lattice can be described by

$$U_i = \sum_{j \neq i} \vec{p}_j \cdot \vec{E}_i, \tag{5.1}$$

where $\vec{p}_j$ is the dipole moment at site j and $\vec{E}_i$ is the field due to the charge at site i. As the charge hops to an adjacent site, the angle it makes with any given dipole in the lattice only changes a small amount. As a result, net field the charge sees due to the dipole contributions from the entire lattice also only changes a small amount, as pictured in Figure 5.1. This implies that the site energies are correlated, and that the energy landscape of the material should have smoother gradients than those in a system characterized by perfectly random energetic disorder. Figures 5.2 and 5.3 illustrate the contrast between a random distribution of occupation energies and spatially correlated energies.

5.2 Consequences of Correlation

Having established that it is perfectly reasonable to expect that the energetic disorder within an organic polymer should be correlated, the next topic to address is that of

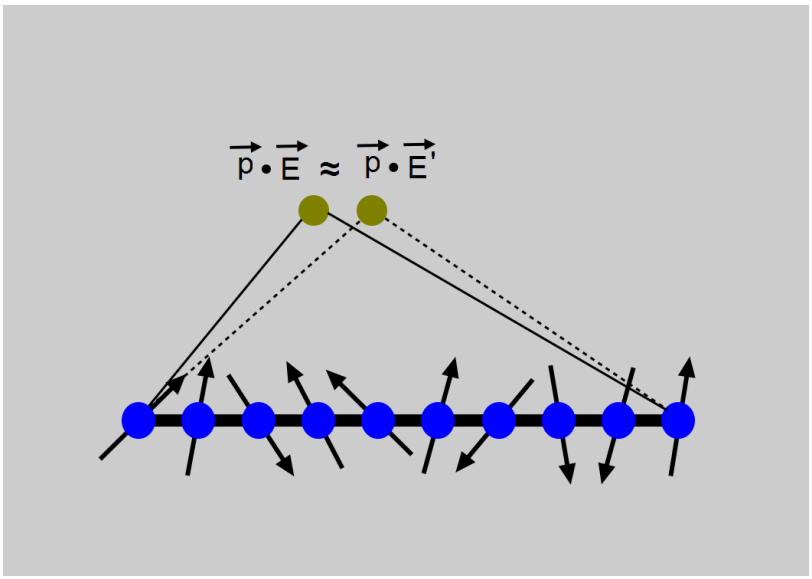

Figure 5.1: An illustration of the charge-dipole interaction as a charge moves across a lattice.

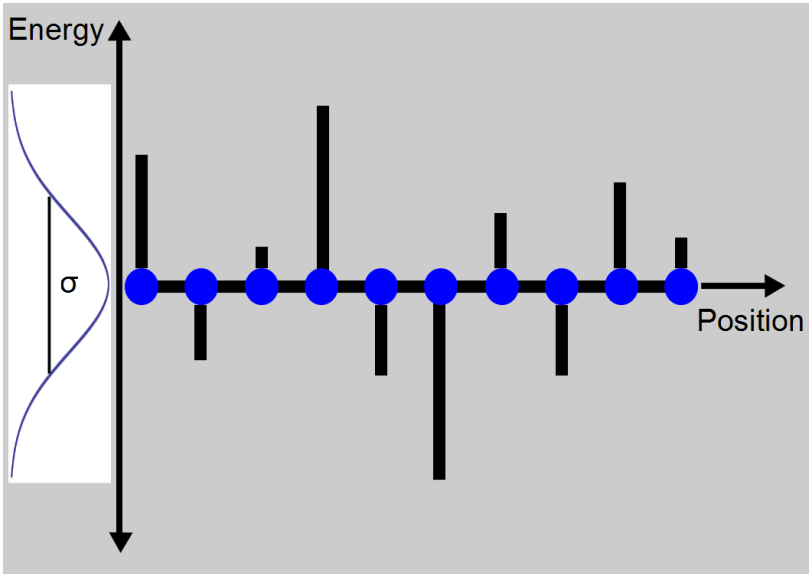

Figure 5.2: A 1D example of Gaussian site energy distribution. The energies indicated by the bars are drawn independently from a Gaussian distribution of width σ.

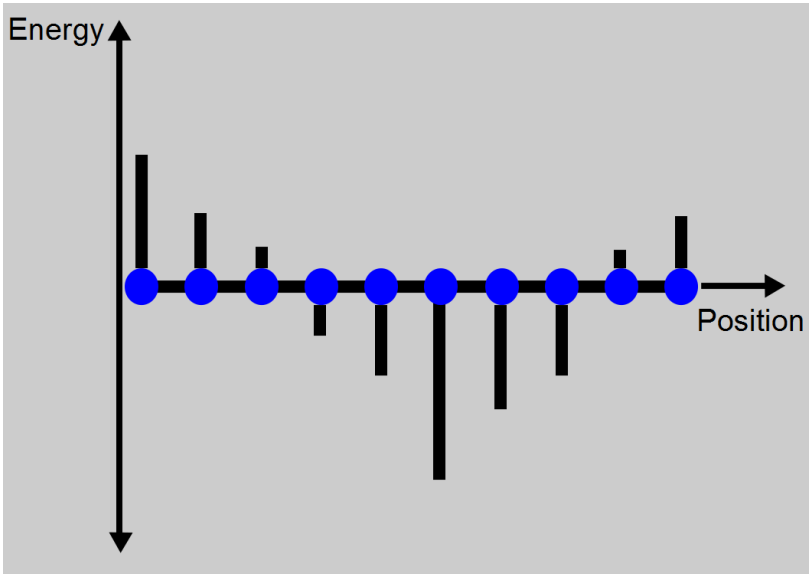

Figure 5.3: An example of what correlated site energy distribution would be expected to look like. This is merely illustrative, and not data.

the effects correlation will have on the charge transport.

5.2.1 Charge Trapping

One of the more obvious effects of correlation is a reduction of charge trapping. When referring to a "trap", it is meant the presence of a site (or a cluster of sites) which has very low energy relative to its surroundings. Such regions can cause carrier localization, a phenomenon in which the charges are stuck in a location for an extended period of time. In contrast to many simulations where only a single pair of charges are considered, in a real device there are $\sim 10^{15} \frac{electrons}{cm^3}$ traveling through the system. In the presence of an electric field, the electrons have some average drift velocity in one direction. In that case, that there are $\sim 10^{15} \frac{holes}{cm^3}$ moving in the opposite direction. The longer a charge remains trapped, the higher the probability becomes that it will encounter a hole, and be lost to one of the various bulk recombination mechanisms described in Chapter 2. Correlation in the disorder means, however, that the presence of isolated sites with deep energies which act as traps is reduced [56]. If a site has a low occupation energy, the correlation dictates that the sites nearby will have similar energies, making the trap less severe.

It is conceivable that the strength and density of traps in an organic polymer

could be manipulated by modifying the correlation. This might be accomplished by strategically doping the host material with some highly polar substance in a clever fashion.

5.2.2 Field-Dependent Mobility

The Poole-Frenkel law, originating from 1938, states that for a charge in a semiconducting solid

$$\mu(E) \propto e^{\gamma\sqrt{E}}, \tag{5.2}$$

where μ is the mobility of the charge, E is an applied electric field, and $\gamma \propto \frac{1}{k_b T}$. This behavior was first observed an organic semiconductor by Pai in 1970 [59], and has been found to be ubiquitous among many organic solids. In 1995 Gartstein and Conwell published a paper detailing Monte Carlo simulations of a molecular system with correlated disorder [60]. Their results gave a field dependent mobility which resembles the behavior of equation (5.2). This was later corroborated analytically by Dunlap, Kenkre, and Parris [56].

The results of [60] and [56] were important, as they shed light on a question which had lacked a satisfactory answer for more than two decades. Simulations had been done using the Gaussian Disorder Model in the parameter regimes which had been probed by experiment, but these show a behavior which resembles $\mu \propto e^{E}$ rather than the observed $\mu \propto e^{\sqrt{E}}$ behavior [56].

Bulk mobility is frequently used as a figure of merit when studying energetic disorder. Much work has been done analytically, numerically, and in simulation [61–69] for various quantities of merit (field-dependent mobility, power conversion efficiency, geminate recombination rates, etc.), but mobility is a natural choice. After all, the speed of a charge with mobility μ is $v = \mu E$, which means $\mu = \frac{\sigma}{e}$, the conductivity per unit charge. When characterizing a semiconductor, conductivity is often a priority.

In the last few years, Groves et al. conducted extensive simulations relating to organic photovoltaic devices [64, 65, 68, 69]. These simulations were rather sophisticated, designed to encompass many features of an actual device. A comprehensive simulation does allow one to study several quantities of merit at once, but the space of tunable parameters may be large. This may make it difficult to isolate the factor

or combination of factors which cause a particular behavior.

A 2010 paper by Groves et al. [69] examines the effect of charge trapping on the performance of polymer solar cells. Both Gaussian disorder and correlated disorder, using the approach of Gartstein and Conwell [60], were simulated in the report. The correlated disorder was found to reduce trapping, and give a slightly larger mobility than the uncorrelated. However, correlating the disorder was found to substantially improve the power conversion efficiency over uncorrelated disorder by a factor of 2.5 and 3.1 for simulated bilayer and blended heterojunction devices, respectively. These improvements were indicated to have little to do with the differences in bulk mobility between correlated and uncorrelated disorder, but were instead a result of spatial configuration of the disorder. This indicates that a better understanding of the local properties within a material is important to a better understanding of charge transport.

5.2.3 Charge Separation

Another, perhaps less obvious, effect of spatial correlation is that of driving an electron-hole pair apart from one another spatially. To help explain this, consider Figure 5.4. These plots are example cross-sections of correlated Gaussian energy landscapes. The method used to correlate the disorder follows Gartstein and Conwell [60]. These landscapes were achieved in this case by first generating a lattice of site energies drawn from a Gaussian random distribution, as in the previous chapter. Then for each site an average of all the energies of the surrounding sites was taken, out to some predetermined distance referred to as the correlation radius, R_c. On a cubic lattice this was taken such that the zone being averaged was a cube of size R_c^3 rather than a sphere for computational simplicity. The energy of each site was then reassigned to be this average, i.e. for an uncorrelated energy landscape with energies E_i at sites i, the correlated energy at each site is

$$E_{cor}^{i} = \frac{\sum_{j \in R_c} E_j}{R_c^3}. \tag{5.3}$$

This produces a "smoothing" effect on the energy landscape. As the reader can see, the correlation radius does not have to become very large at all before extended zones (i.e. comprised of several or more adjacent sites) of high and low energy begin

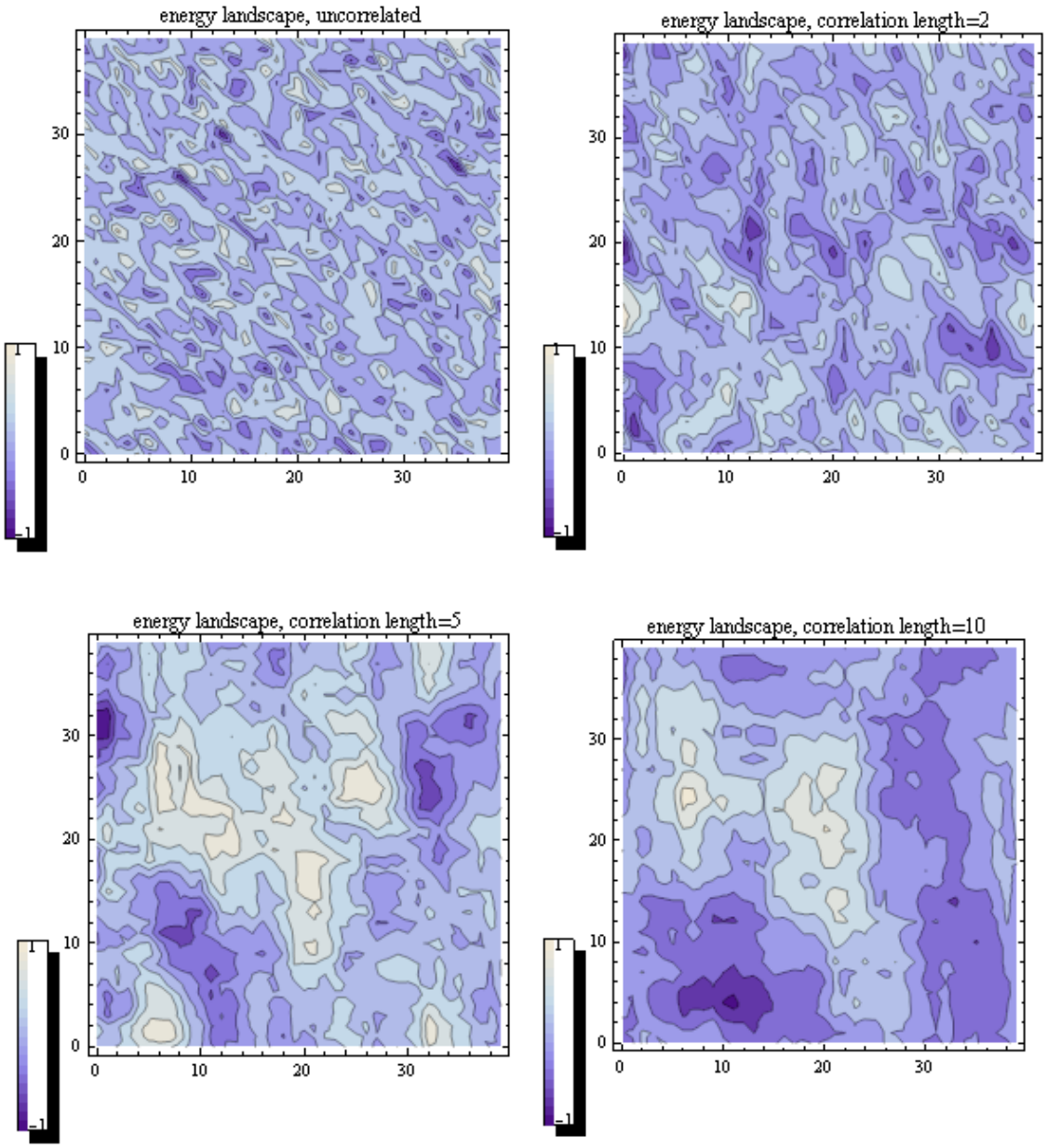

Figure 5.4: A selection of 2D cross-sectional samples of correlated energy landscapes. The uncorrelated case (top left) is simply Gaussian disorder, and the energy gradients are very sharp. For a correlation radius $R_c = 2a$ (top right), zones of similar energy are already beginning to appear. At $R_c = 5a$ (bottom left), energetic hills and valleys which extend across large fractions of the landscape have appeared. Finally, at $R_c = 10a$ (bottom right), the energy landscape is partitioned into just a few large zones of high and low energy.

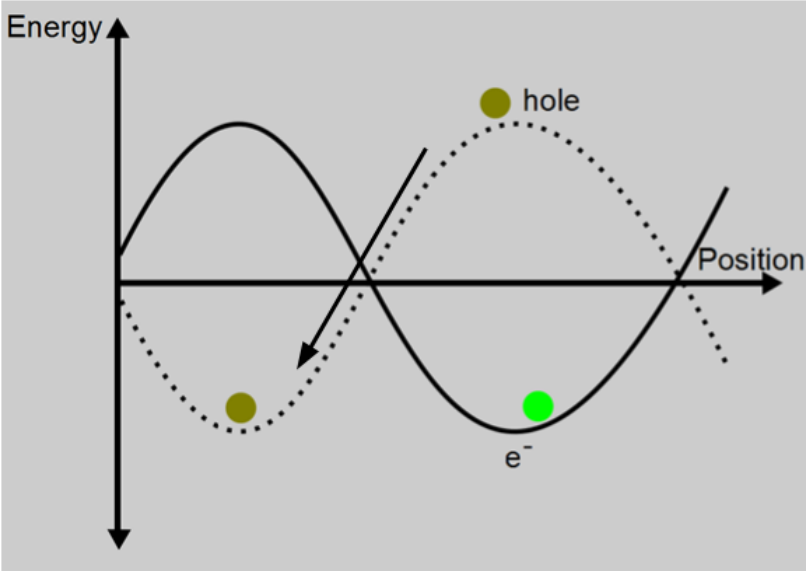

Figure 5.5: An illustration of opposite charges experiencing opposite energy landscapes. For an electron and hole initially near one another in what is a potential minimum for the electron, the hole sees a potential maximum instead.

to appear. These energetic "hills" and "valleys" result in a charge carrier avoiding certain locations on the lattice while preferring others. A profound effect appears when *both* the positive and negative charges are considered simultaneously. Due to their opposite charge, the occupation energy for a particular site will differ between the electron and hole by a sign. Then, for example, if both charges are initially near one another in what is a potential minimum for the electron, the hole will see a potential maximum instead. This results in the negative charge tending to be drawn to locations which the positive charge avoids, and vice versa, as illustrated in Figure 5.5. This tendency to be drawn apart spatially should result in the electron and hole dissociating with higher probability than in the perfectly random case. In this way energetic correlation may provide a mechanism which is useful for improving charge transport in disordered organic materials.

6

Simulating Geminate Recombination

To study correlated energetic disorder, computer simulations were employed. The simulations were programmed in C++, and performed on various personal computers, using the Monte Carlo method. I would like to acknowledge Sebastian Röding, an exchange student from the University of Würzburg for the prototype program design.

In this chapter, several phases of simulation will be detailed after the general specifications of the program are presented. The first phase of simulations were performed on a lattice with no disorder present, so that a reference can be made to the Onsager calculation. Next, geminate recombination (recombination of an electron and hole which originated together) was simulated on a lattice using the Gaussian Disorder Model, similar to those of Albrecht and Bässler described in 4.2. The author's results are then compared and contrasted. Finally, simulations were done in a system with spatially correlated energetic disorder, so that the effects of correlation may be examined.

6.1 Simulation Specifications

The system was simulated on a simple cubic lattice, with spacing $a = 8$Å. The energy landscapes were generated as three-dimensional lattices of size $40 \times 40 \times 40$ sites. In order to allow the charges to move beyond the boundaries of said lattice, the simulations were done on an arbitrarily large lattice formed by tessellating these

$40 \times 40 \times 40$ lattices. It was recognized that this would introduce some artificial long-range order, but this was deemed acceptable due to the fact that in most cases the condition for the charges to escape one another required them to be separated by no more than $\sim 100a$, and would therefore generally result in their traversing no more than two sub-lattices.

Various system sizes and choices of boundary conditions appear throughout the literature. Schönherr et al. performed simulations of exciton diffusion under the Gaussian Disorder Model on a lattice $29 \times 29 \times 29$ sites in extent. Gartstein and Conwell performed hopping mobility simulations on a lattice of size $1000 \times 40 \times 40$, with a field in the x-direction. Both Groves et al. [68] and Bässler [40] chose lattices of size $70 \times 70 \times 70$ with periodic boundary conditions. For lattice spacings of $0.8 - 1.0$nm, 70 lattice sites approaches the size of an organic device (~ 100nm), and so there is not much reason to simulate very large systems. The lattice size for the author's simulations was chosen on the grounds that it was the largest that was computationally tenable, as for the later simulations involving dipole fields, the computational effort scales as N^6, where N is the number of lattice sites. This is due to the fact that to simulate a physical dipole field, every site on the lattice was populated with a randomly oriented fixed dipole. The energy on each site was then calculated from the contributions of the dipoles on the other $N^3 - 1$ sites. Thus, $\sim N^3 \times N^3 = N^6$ operations are required.

Let an iteration of the simulation be defined as a single pair of charges being allowed to hop until the termination conditions are met (recombination or escape). A single data point is then the average of many iterations. For hopping on a lattice with no disorder, a round of simulation (30 data points, with $\sim 10^4$ iterations) took a few minutes. In the case of Gaussian disorder, the charges took very many more hops ($\sim 2^6$ per iteration), and a round of simulation ($10 - 15$ data points, with $\sim 10^4$ iterations) took a few hours. For artificially correlated disorder and dipole disorder, many operations were required to generate each lattice, as mentioned above. This greatly increased the the CPU time required, and a round of simulation ($10 - 15$ data points, with $\sim 2 \times 10^4$ iterations) took as much as two days.

For a given iteration, each lattice site j was assigned an occupation energy E_{0j} based on the type and strength of the disorder. Several different varieties of energetic disorder were studied. First, simulations were done using the Gaussian Disorder

Model to provide a baseline for comparison with Albrecht and Bässler. Following that, a set of simulations were performed using the method of imposed correlation corresponding to equation (5.3). Finally, a set of simulations were done to demonstrate a physical source of correlation, incorporating the charge-dipole interaction produced by superimposing randomly oriented fixed dipoles at every lattice site.

The simulations were performed on one energy configuration a predetermined number of times before the site energies were re-randomized. The ensemble was thus comprised of many small 'batches'. The majority of the processing time was taken by constructing the lattices, and this served to reduce the computational load compared to generating a new energy landscape every single iteration. The charges were oriented randomly on a sphere of radius r_0 at the center of the lattice, as opposed to Albrecht and Bässler's simulations, in which the charges were started at a fixed location. Randomizing the starting location means that the particles effectively see a different disorder field for each trajectory, as pointed out by Gartstein and Conwell [51]. This allowed more data points to be gathered by taking advantage of processor time already spent to generate a lattice. The total number of iterations differed depending on the computational complexity of the configuration being simulated, but every data point consists of no fewer than 2000 iterations.

A uniform electric field of magnitude E in the x direction was imposed on the lattice to represent the field that arises due to the built-in potential of a device. The positive charge was located at the center of the lattice, and the negative charge was placed randomly on a spherical shell of radius $3a$ about the positive charge. Both charges were then allowed to hop to nearest neighbors only, according to the Miller-Abrahams rate defined in equation (4.8), with $\nu_0 = e^{-\frac{2R}{a}} = 1$, as in Figure 6.1. Taking all the contributions into account, the energy difference Δ_{ij} for hopping from site i to site j is

$$\Delta_{ij} = (E_{0j} - E_{0i}) - q\vec{E} \cdot \vec{a}_{ij} + (\frac{q^2}{\epsilon r_i} - \frac{q^2}{\epsilon r_j}), \tag{6.1}$$

where $\vec{a}_{ij}$ is the vector from site i to an adjacent site j, and r_j is the distance from the charge in question on site j to the other charge, so that $\frac{q^2}{\epsilon r_j}$ is the energy due to the Coulomb potential felt by a charge on site j due to its complementary charge. Normalizing the hopping rate R_{ij} from site i to site j by the sum of the rates for all

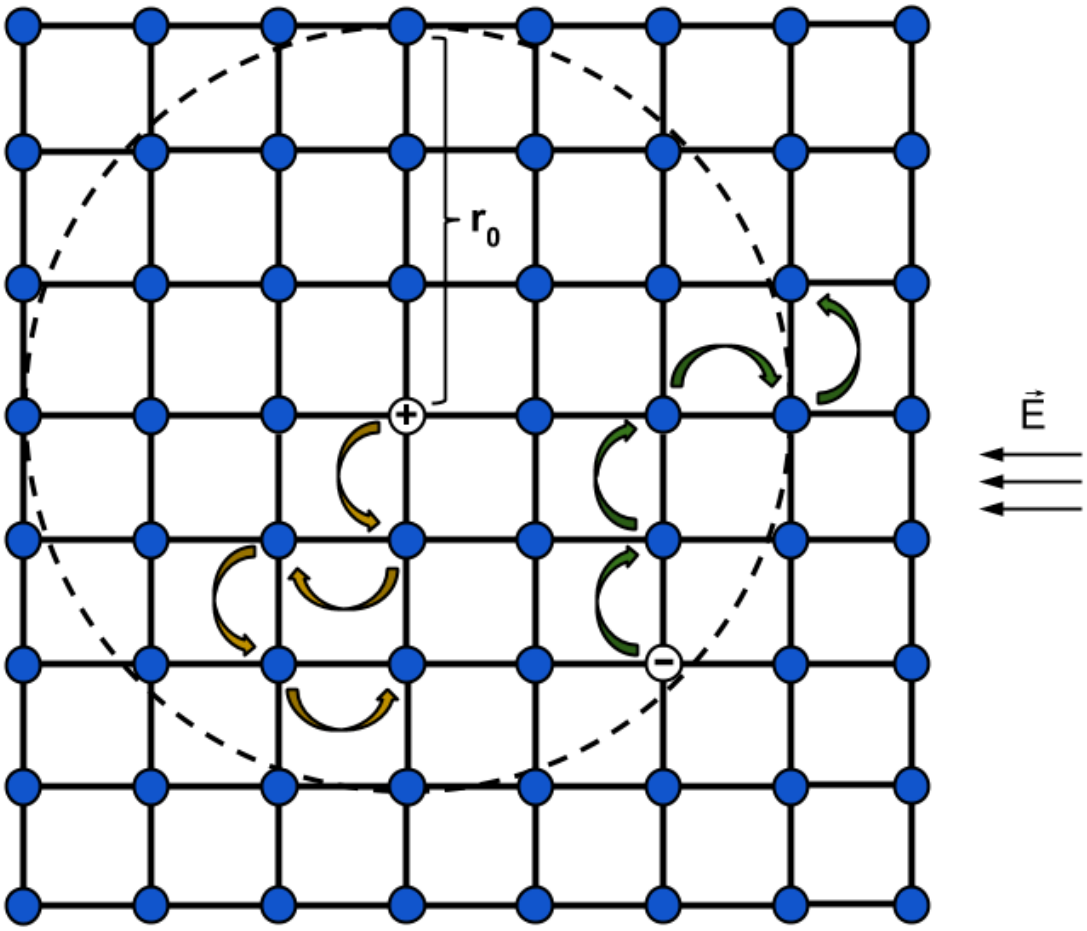

Figure 6.1: A diagram representing charges hopping on a model lattice. The charges are initially placed a distance r_0 apart with the electron placed on a spherical shell about the hole, and then allowed to diffuse according to the Miller-Abrahams hopping rate. In the present simulations, both charges are allowed to hop.

adjacent sites gives the probability to hop from site i to site j, i.e.

$$P_{i\to j} = \frac{R_{ij}}{\sum_k R_{ik}}, \tag{6.2}$$

where k spans all adjacent sites. To choose which charge hopped in which direction at each step, a random number p (normalized to one) is chosen from a uniform probability distribution. The probability for charge $m = 1$ or 2 to hop in a direction $l = \pm x, \pm y, \pm z$ is denoted $P_{m,l}$. An array P is populated with the probabilities $P_{m,l}$, and is normalized so that $\sum_{m,l} P_{m,l} = 1$, viz.,

$$|P_{1,+x}| \ldots |P_{1,-z}|P_{2,+x}| \ldots |P_{2,-z}|, \tag{6.3}$$

where each cell has width $P_{m,l}$. The value of p falls into one of these cells, simultaneously choosing which particle hops, and which direction it takes.

An iteration of the simulation would be terminated upon meeting one of two criteria. The first criterion was that of both charges occupying the same site, interpreted as recombination. The second condition was that of escape, when the charges traveled sufficiently far apart from one another. The range for this was determined in one of two ways, via either the coulomb radius, as in Albrecht and Bässler's simulations, or the Poole-Frenkel radius, a new additional criterion. The coulomb radius corresponds to the distance at which the coulomb energy of the two charges is equal to the thermal energy k_bT of the environment, i.e.

$$\frac{q^2}{\epsilon r_c} = k_bT \quad \rightarrow \quad r_c = \frac{q^2}{\epsilon k_bT}. \tag{6.4}$$

The Poole-Frenkel radius [70] is field dependent, calculated in the following manner: the energy of the mobile charge is

$$U = -\frac{q^2}{\epsilon r} - q\vec{E}\cdot\vec{r}. \tag{6.5}$$

To put a lower bound on the Poole-Frenkel radius, let the charges lie on a line parallel to the field, so that $\vec{E}\cdot\vec{r} = Er$. Doing this also serves to put a lower bound on the Poole-Frenkel radius. Next, find the saddle point, by setting the derivative of the

potential energy surface to zero,

$$\frac{dU}{dr} = \frac{q^2}{\epsilon r^2} - qE = 0. \tag{6.6}$$

Solving for r gives the Poole-Frenkel radius

$$r_{pf} = \sqrt{\frac{q}{\epsilon E}}. \tag{6.7}$$

This distance is a watershed for the charges. At less than this distance, the attractive interaction between the particles dominates, and they tend to approach one another. At greater than this distance, the external field takes over, and the charges tend to be swept apart. This criterion was used in the high-field regime, since merely comparing the coulomb attraction to the system's thermal energy is not an accurate indicator of how bound the particles are at high field ($E > 10^5 \frac{V}{cm}$).

Which radius was used depended on the field strength for a particular simulation. The two conditions were compared, and whichever radius was smaller was used. The escape condition was then set to be five times the appropriate radius to minimize error in declaring the charges dissociated, and in an attempt to maintain contact with Albrecht and Bässler's simulations.

6.2 Results: Comparison with the Onsager Calculation

As a benchmark for our computer simulations, we will begin with a comparison to the Onsager result [3]. For these comparisons, the positive charge was fixed at the center of the lattice, and the other charge was allowed to hop, in accordance with the conditions used by Onsager. Results for the case of an ordered lattice are presented in Figure 6.2. As the reader can see, dissociation yield on an ordered lattice has the same shape as the Onsager continuum result, but different values. The lattice case produces a higher yield at lower field strengths, and also does not saturate to 100% for very high values of the field.

The reason for the difference between the simulation and the continuum case

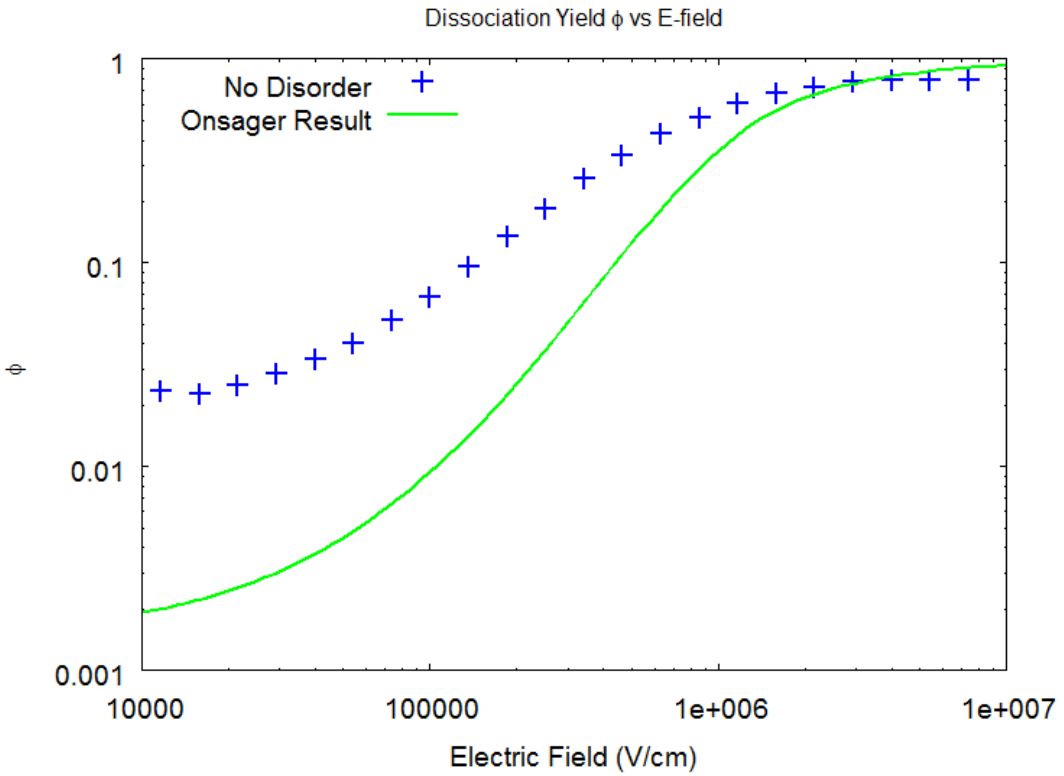

Figure 6.2: The dissociation yield ϕ as a function of field magnitude for an ordered lattice and for the Onsager theory. The Miller-Abrahams hopping rate is used on a lattice with spacing $a = 8$Å. The initial condition for both curves is $r_0 = 3a = 24$Å.

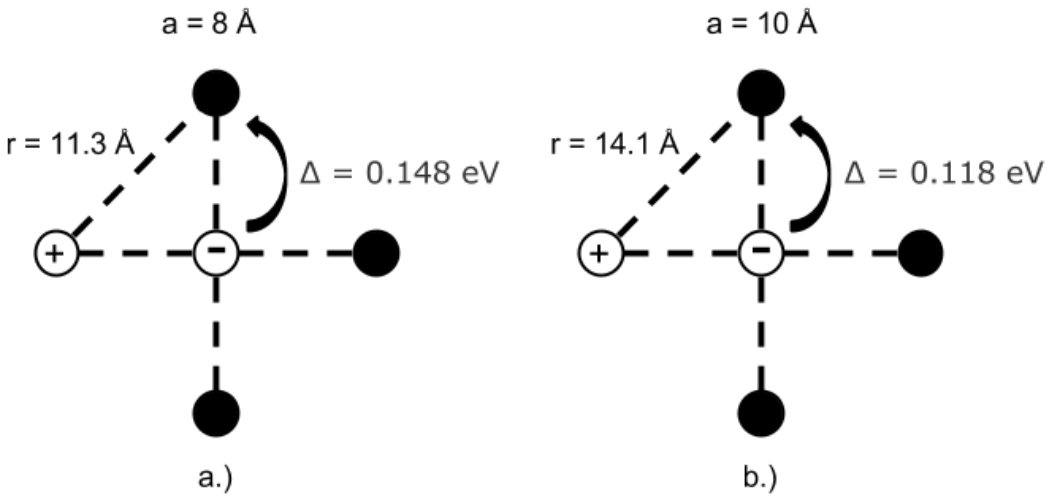

Figure 6.3: A simplified illustration of the effect of varying the lattice spacing. Case a.) represents an inter-site distance of 8Å as used in simulation, while case b.) represents a larger spacing of 10Å.

studied by Onsager is not completely clear. The most obvious difference between the two cases is that the Onsager result is determined by diffusion in the continuum, whereas the hopping charges are restricted to a discrete lattice. It seems likely that the nature of the Miller-Abrahams hopping rate is responsible for some of the deviation of the simulation from the Onsager theory. To clarify, consider the effect of varying the lattice constant in the zero disorder, zero field, room temperature case ($|\vec{E}| = 0, T = 300K$). Figure 6.3 gives a picture of what occurs. Merely varying the inter-site distance between the two cases changes the energy of the coulomb interaction, causing the value of Δ to be markedly different and altering the hopping rates. The probability to recombine on the first hop was calculated to be $P = 0.989$ for case a, and $P = 0.966$ for case b. Thus, parameters which are not present in the Onsager theory will have effects which cause the simulations on a discrete lattice to deviate from the continuum theory. However, taking the limit of a very small lattice spacing while keeping the initial separation distance constant causes the results for the discrete system to converge toward the solution in the Onsager theory, as in Figure 6.4 (cf. Figure 6.2). As the reader can see, shrinking the lattice constant does indeed result in dissociation yields more near to the Onsager result.

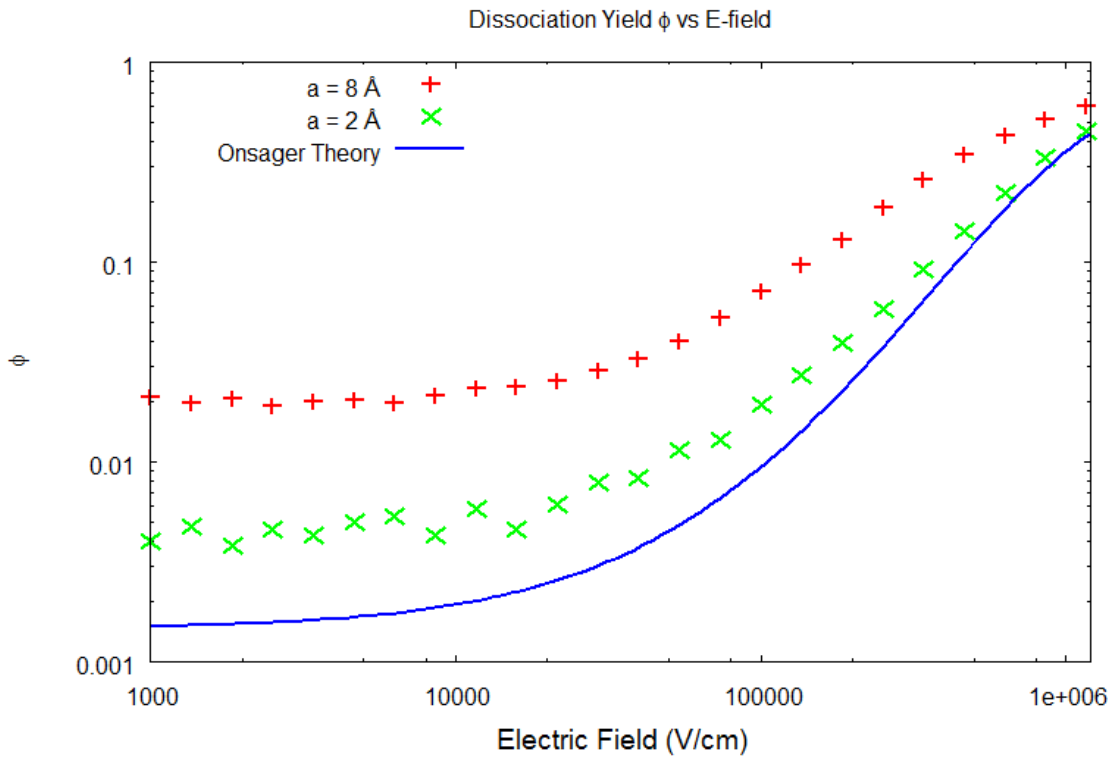

Figure 6.4: The dissociation yield ϕ as a function of field magnitude for an ordered lattice at $a = 8$Å, an ordered lattice at $a = 2$Å, and for the Onsager theory. This is to confirm that the results for the discrete case converge to the Onsager analytic result in the continuum. $T = 300K$ and $r_0 = 24$Å in all cases.

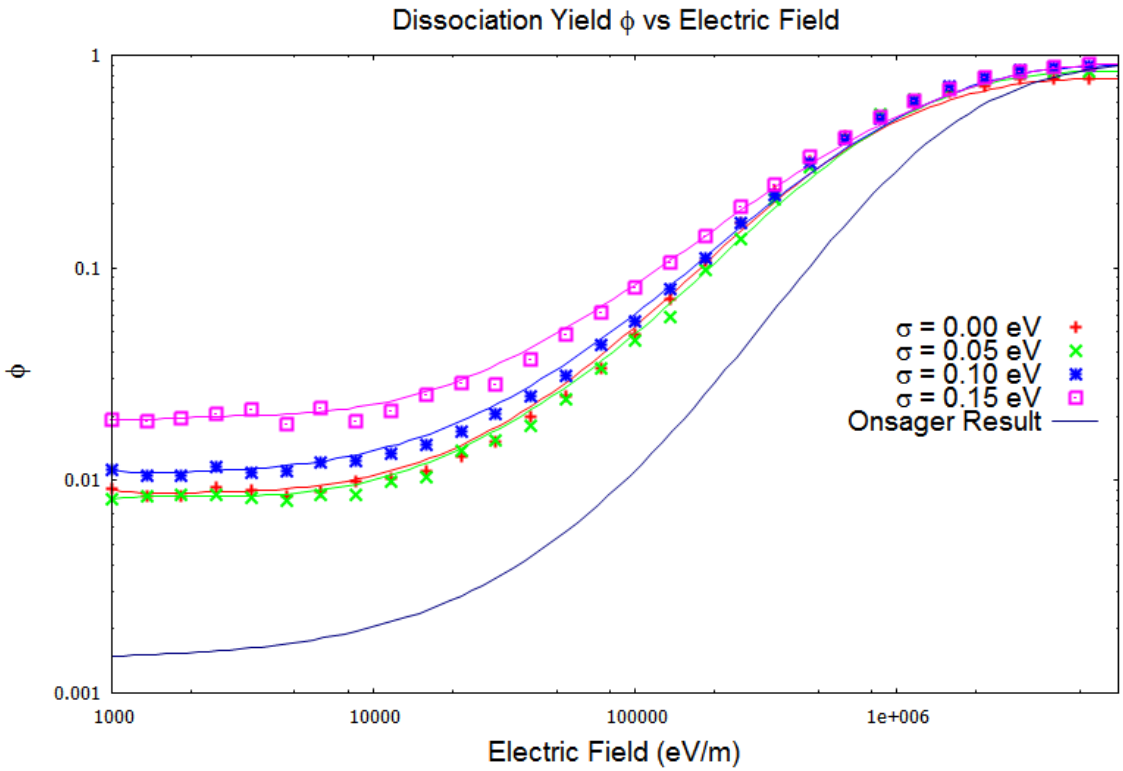

Figure 6.5: The dissociation yield ϕ as a function of field magnitude for several values of the disorder parameter σ at $T = 300K$.

6.3 Dissociation with Uncorrelated Gaussian Disorder

Having confirmed that our numerical approach agrees with the continuum approach (Onsager) for the case of no disorder, let us now turn our attention to the effects of disorder on the quantum yield. This stage of simulations was an effort to compile results for charge hopping using the Gaussian Disorder Model. These results could then be compared with previous results, namely those of Albrecht and Bässler [41]. For this set of simulations, the positive charge was fixed at the center of the lattice while the negative charge was allowed to roam, to maintain contact with reference [41]. Figure 6.5 shows the field dependence of ϕ for several different values of σ. Increasing σ generally causes an increase in the dissociation yield for a given field strength. Note however that a small amount of disorder ($\sigma = 0.05$ eV) actually decreases the value of ϕ slightly relative to the case of no disorder. This agrees with

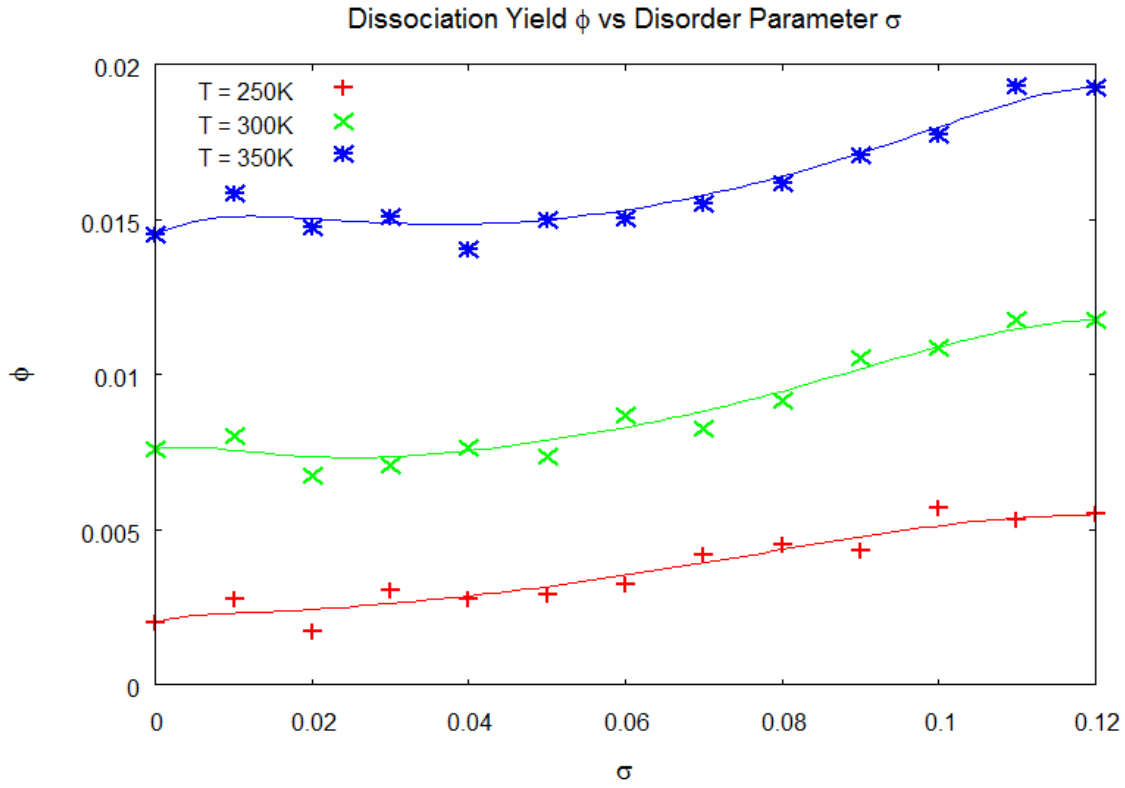

Figure 6.6: The dissociation yield ϕ as a function of the disorder parameter σ at $T = 250K$, $T = 300K$, and $T = 350K$. In all cases $|\vec{E}| = 10^4 \frac{V}{cm}$ and $r_0 = 24$Å.

Figure 6.6, which plots the value of ϕ versus the disorder strength σ. ϕ dips slightly before beginning to increase in each curve, for reasons not currently understood. A large number of iterations were averaged to produce each data point, giving a rather narrow error. The process being simulated can be described as a Bernoulli coin flip with a weighted probability

$$\begin{array}{ll} p & \text{, Dissociation} \\ 1-p & \text{, Recombination.} \end{array} \tag{6.8}$$

The variance of such a process is $p(1-p)$, and the standard error is thus $\frac{p(1-p)}{\sqrt{N}}$, where N is the number of iterations. We will approximate p by the value of the data point. The number of iterations is at least 2000, so for $\phi = 0.01$, an error estimate is $\frac{0.01(1-0.01)}{\sqrt{2\times10^3}} \approx 3 \times 10^{-3}$, or about 3%. Therefore, this oscillation appears to fall slightly outside of the noise, but its source is unknown.

It appears that for uncorrelated disorder, referring in particular to Figure 6.5,

a rather large value of σ is required to significantly improve the dissociation rate. Significant increases in ϕ do not begin to appear until values of σ approach 0.15eV, which is well above the values of the disorder width usually found in experiment (< 0.1eV) [7]. This seems to indicate that uncorrelated disorder cannot have a large effect on ϕ.

The relationship between ϕ and σ in Figure 6.6 appears to be roughly linear, rather than the exponential relationship indicated by Albrecht and Bässler. In [41] they point out that an asymptotic form of the dissociation yield is

$$\lim_{E \to 0} \phi = e^{r_c/r_0}, \tag{6.9}$$

recalling r_c to be the coulombic capture radius. They then assert that an increase in σ corresponds formally to a decrease of the ratio r_c/r_0. We believe them to be mistaken. It has already been shown that it is very unlikely that the data point for $\sigma = 0$ in Figure 4.7 is correct, as the dissociation yield on a lattice differs from the Onsager result. This leaves three data points, from which a conclusion is difficult to justify. Furthermore, consider the ratio r_c/r_0; since r_0 is an independent parameter, lowering r_c is the only way to shrink the ratio. A lowering of r_c corresponds to a lowering of the coulombic binding energy. This cannot be due to energetic disorder as it is implemented. To lower the coulombic binding energy, one would have to screen the charges from one another, and introducing disorder into the site occupation energies does no such thing. Thus, it is difficult to see how energetic disorder would have an effect on the ratio r_c/r_0 and lead to and exponential relationship between ϕ and σ.

Figure 6.6 does corroborate Bässler's conclusions that disorder improves the dissociation yield, and that this effect is more pronounced at low temperatures. By this it is meant that, if the reader compares the curves in Figure 6.6, the data set for the lower temperature sees a larger gain in ϕ relative to the higher temperatures. The value of ϕ in the curve at the lowest temperature for maximum σ is roughly triple the value for no disorder ($\frac{\phi(\sigma=0.12)}{\phi(\sigma=0)} \approx 3$). The curve for the highest temperature, on the other hand only sees a gain of roughly 30% ($\frac{\phi(\sigma=0.12)}{\phi(\sigma=0)} \approx 1.3$). One might expect this, since as the temperature of the system increases, the relative strength of the disorder decreases, pictured in Figure 6.7. An electron with more thermal energy does not see as large of an energetic barrier when hopping to a site with a large occupation energy as does an electron at a lower temperature.

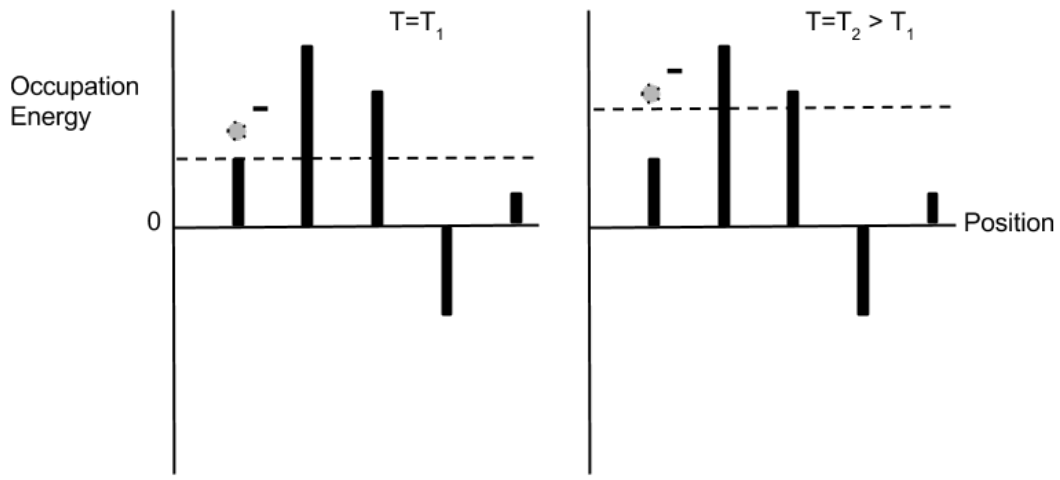

Figure 6.7: As the temperature increases, the energy required to hop between adjacent sites is reduced.

Between these results and those cited previously, it is clear that energetic disorder reduces the occurrence of geminate recombination. Still remaining are the questions of whether this energetic disorder is being properly modeled, and what a more appropriate model may be in the case that it is not. The following sections are concerned with the notion that energetic disorder must be correlated, and how correlation occurs.

6.4 Correlated Energetic Disorder I

After constructing a reference point from the simulations on Gaussian random energy landscapes, the next step was to introduce correlated energetic disorder. How does one go about correlating disorder? Several methods may be found in the literature, a few examples of which will be presented in this section, followed by a description of the methods used by the author, and the reasoning behind those choices.

In a paper by Abramavicius and Valkunas [57], energetic correlation between two sites was modeled by an exponential pair correlation function. Specifically, in 1D (which generalizes directly to higher dimensions) for sites l and m with energies E_l and E_m,

$$\langle E_l E_m \rangle = \sigma^2 e^{-\frac{|x_l - x_m|}{R_c}}, \tag{6.10}$$

where $\langle ... \rangle$ denotes a statistical average, σ^2 is a variance, $|x_l - x_m|$ is the distance between the two sites, and R_c is the correlation radius. The site energies can always be expressed in terms of their Fourier transforms,

$$E_l = \sigma \sum_k a_k e^{2i\pi kx/N}, \tag{6.11}$$

where N is the number of sites and k is the Fourier index. It can be shown that the Fourier coefficients satisfy

$$|a_k| = \sqrt{I_k}, \tag{6.12}$$

I_k being the amplitude of the power spectrum.

This is one approach to expressing the energetic correlation, but it is not physically appropriate to describe what is understood to be the dominant source of correlation [53, 54], namely the charge-dipole interaction. The exponential correlation described in [57] decays strongly with distance, and is a weaker correlation than that induced by a system of dipoles. The correlation described by Novikov and Vannikov in [53] is more long ranged, decaying proportional to $\frac{1}{r}$ in 3D, rather than exponentially. In addition this correlation retains a Gaussian character in 3D. We are interested in simulating a physical system of dipoles, therefore the exponential correlation will not be used.

For reasons which were also mentioned in section 5.2.3, this phase of simulation departs further from the typical procedure employed when simulating charge diffusion on a disordered lattice [41, 44, 51, 57]. Usually, the positive charge is fixed at the center of the lattice while the negative charge is allowed to roam, corresponding with Onsager's formalism. For this simulation, however, both charges will be free to hop. This is because fixing one charge would defeat one of the major benefits of correlation described in 5.2.3. Since the site occupation energy each charge experiences differs by a sign, each of the charges sees an energy landscape which is inverted compared to the other. This results in areas of the lattice which are high energy for the electron to be low energy for the hole, and vice versa. As the two charges seek out their respective low energy regions, they become spatially separated. If both charges were not allowed to diffuse this effect would not appear, at least not completely.

In this phase of simulations, the correlation method used was that described in section 5.2.3. First, the lattice was populated with random energies drawn from a

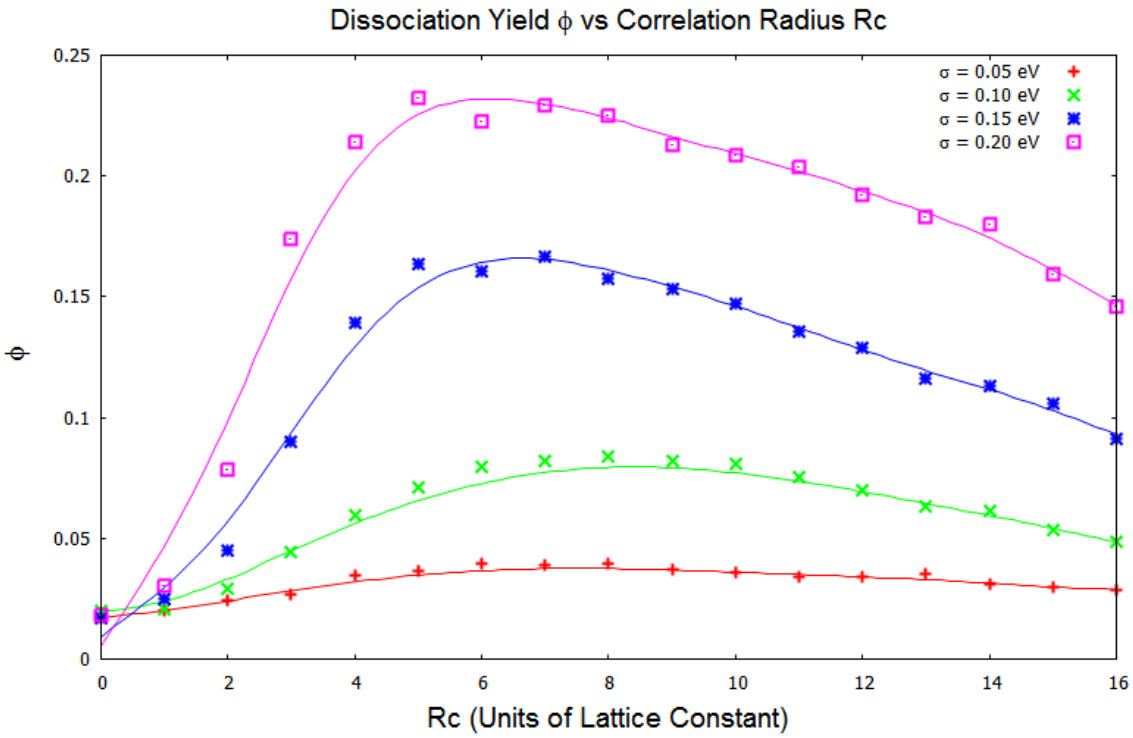

Figure 6.8: The dissociation yield as a function of the correlation length, parametrized by several values of σ, with $T = 300K$ and $|\vec{E}| = 10^4 \frac{V}{m}$. As the correlation radius is increased, the overall dissociation yields go up. However, in the limit of $R_c \to \infty$ these curves all tend asymptotically to the same value, as this limit corresponds to an energetically flat landscape, independent of σ.

Gaussian distribution. Then, each site was then reassigned an energy equal to the average of the energies of all the sites around it out to the radius R_c, called the correlation radius. This produces a "smoothing" effect proportional to the size of R_c. Several examples of correlated energy landscapes for various values of R_c are found in Figure 5.4.

The reason for using this simplified correlation method at this stage, as opposed to a more physical correlative procedure, was to establish some of the qualitative behavior of the system. For example, having the correlation radius as a tunable parameter (which it is not in [53]) allows one to examine the behavior of the system as a function of the strength of the correlation. This allows for the investigation of the effects of correlation across different length scales.

Figure 6.8 is a plot of ϕ versus R_c for several values of σ. There are a few features to note. First, as a function of R_c the dissociation yield peaks at some value of the

correlation radius, and then begins to taper down as R_c continues to increase. For small values of R_c, ϕ will have approximately the same values as the uncorrelated case. When R_c becomes very large, every point in the lattice is being correlated with many other sites. As the samples over which an average is being taken become large (i.e. R_c is large), the energy of each site approaches the mean value of the random distribution which originally populated the sites, per the Central Limit Theorem. In this case the original distribution was Gaussian, with a mean of zero. Thus, when R_c becomes very large, the correlated energies of all the sites on the lattice tend asymptotically to zero. Simply stated, when R_c is so large that every site becomes the average of all the sites in the system, the energy landscape becomes flat.

It should be noted that there is a process competing with the asymptotic flattening of the energy landscape, however. After the averaging procedure was performed during the correlation step, the energies were scaled up by a factor of $\sqrt{N}$, where $N = (2R_c)^3$ is the number of sites within the correlation radius. This is once again due to the Central Limit Theorem, wherein the variance of the distribution of samples, σ_s, is equal to

$$\sigma_s = \frac{\sigma}{\sqrt{N}}. \tag{6.13}$$

This was done to make sure that the variance of the correlated landscape remained the same as the uncorrelated one from which it was derived.

Another interesting behavior is the magnification of the effect of the disorder which occurs when correlation is introduced. As mentioned previously while discussing Figure 6.6, increasing the strength of the disorder σ leads to an increase in the dissociation yield ϕ. In the case of correlated disorder, the trend becomes magnified. In Figure 6.9, the relationship between ϕ and σ is very linear, with a much steeper slope than in the uncorrelated case. This concurs with the idea presented in 5.2.3 of correlated disorder causing the pair of charges to be driven apart. Larger values of σ manifest as deeper valleys and taller hills in the correlated energetic landscape. Consider a valley in the energy map. As this valley becomes deeper, it presents a stronger attractive center to its corresponding charge, while simultaneously becoming a more repulsive to the opposite charge. This causes the effect of the disorder to be magnified relative to the uncorrelated case, in which there are no distinct attractive or repulsive regions.

While artificial, this method of correlation was nonetheless very useful for gather-

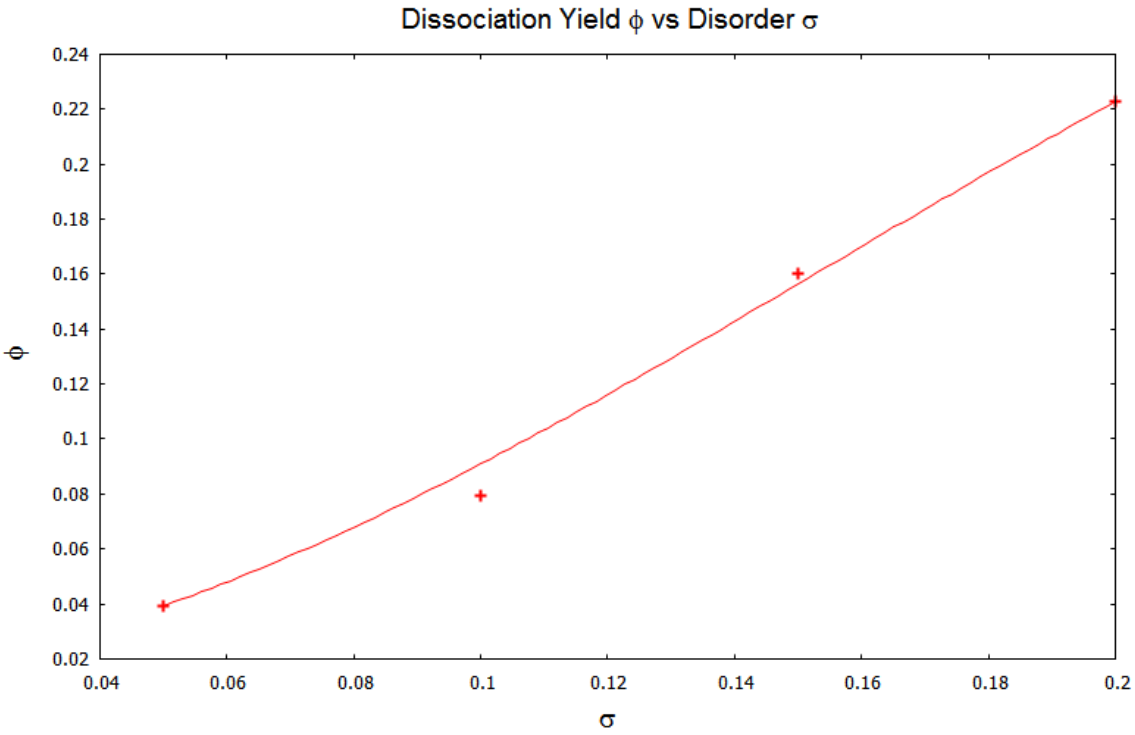

Figure 6.9: The dissociation yield as a function of σ at $T = 300K$ and $|\vec{E}| = 10^4 \frac{V}{cm}$. In this case, data was taken on a correlated energy landscape, with $R_c = 6a$, roughly where the peak values of ϕ occur in Figure 6.8. Compare to the upper curve in Figure 6.6, which represents the uncorrelated case for otherwise identical parameters.

ing information about the qualitative effects of energetic disorder. It has been clearly demonstrated that correlation enhances the effect the disorder has on dissociating the two charges. It has also been demonstrated that there exists some optimal correlation range for the purpose of separating the pair of charges.

Unfortunately, in actual physical systems the ability to manipulate the correlation is still quite limited, as it arises from interactions which are intrinsic to the material being studied. Precisely manipulating the correlation would require controlling structures at the molecular scale, which is not economical at the moment. Thus, the correlation length is not an accessible feature in current disordered organic semiconductor technology. In the next section a more physical model of correlation will be examined.

6.5 Correlated Energetic Disorder II

In the final stage of simulations, a physical system of fixed dipoles was mimicked. To achieve this, each lattice site was assigned a fixed, randomly oriented dipole. These dipoles were given moments ranging between 0 and 5 Debyes, and the moments of all the dipoles on a given lattice were the same, only the orientation was randomized. Once the dipoles were placed, the contribution to the occupation energy of each site due to the charge-dipole interaction from this field of dipoles was calculated. Due to the long computation time required for such a process, the size of the lattice was reduced to $20 \times 20 \times 20$. A few test results were compared to the original lattice size of $N = 40$, and no significant difference was found. An example of the dipolar energy landscape is presented in Figure 6.10, alongside a sample of a landscape which was correlated synthetically, as in section 6.4.

As the reader can see, the two samples appear to have a very similar structure. In the case of dipole disorder, there is no correlation radius R_c available as a tunable parameter, and as a result the spatial extent of the energetic hills and valleys is essentially fixed. Changing the strength of the dipole moments corresponds to tuning the width σ of the Gaussian distributions used to generate disorder in the previous phases of simulation. Increasing the dipole strength causes stronger disorder, which is to say it results in higher hills and deeper valleys in the energy landscape, but this effect is not apparent on a 2D cross-section of the energy. A comparison of the

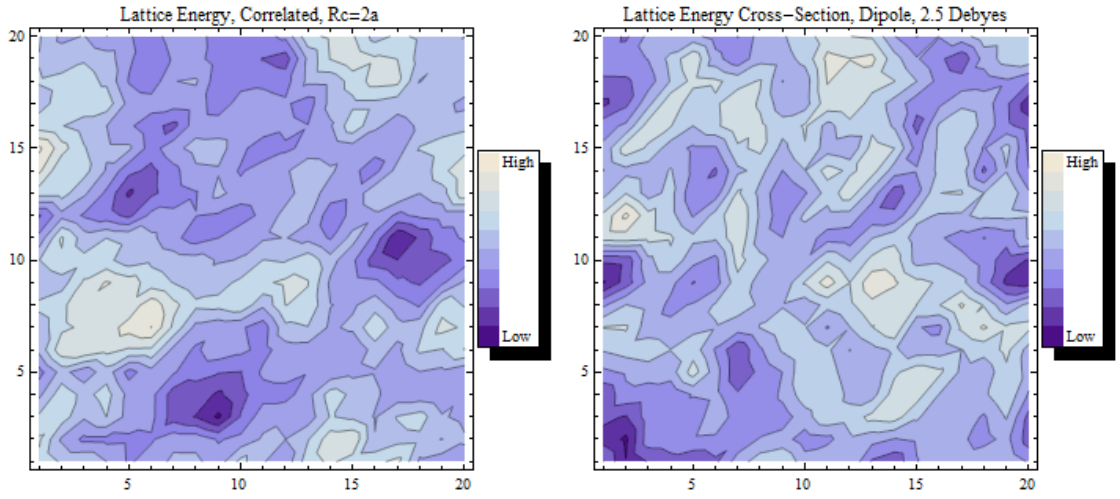

Figure 6.10: The plot on the left is a cross-section of an artificially correlated landscape with $R_c = 2a$. On the right is a plot of an energy landscape generated by summing the charge-dipole interaction across a field of randomly oriented dipoles with moments of strength 2.5 Debyes. In both cases, the variance of the disorder is $\sigma \approx 0.1$ eV. Qualitatively, the artificially correlated disorder seems to have sightly broader hills and valleys, but both plots have very similar character.

dissociation yield for dipole disorder versus artificially correlated disorder with a fixed correlation radius is plotted in Figure 6.11. As the variance for the dipolar landscape was increased by increasing the strength of the dipole moments, the charges began to make excessively many hops ($> 2 \times 10^6$), making gathering data untenable. This is why the domain for the dipolar system is smaller than for the correlated system.

In Figures 6.12 and 6.13, the dipole disorder is compared to uncorrelated Gaussian disorder. There is a significant increase in ϕ for the dipole case over the strictly random disorder at higher values of σ. This is a strong indicator that energetic disorder in a physical system yields better charge separation than one might expect when using the Gaussian Disorder Model.

6.6 Concluding Thoughts on Disorder

If the discussion up to this point were to be distilled down to a few key ideas, it may be said that

- Disordered organic semiconducting systems of interest have less well-defined

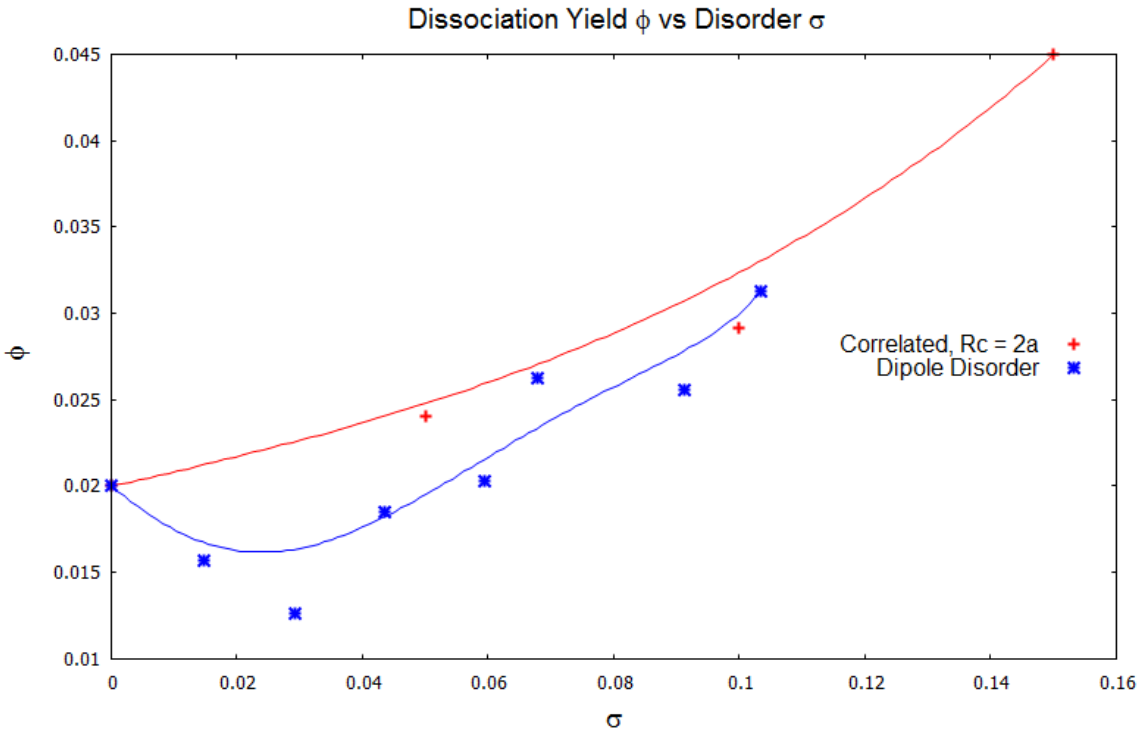

Figure 6.11: The dissociation yield as a function of σ at $T = 300K$ and $|\vec{E}| = 5 \times 10^4 \frac{V}{cm}$. Data for the upper curve was taken on a correlated energy landscape, with $R_c = 2a$. Data for the lower curve was taken from a dipolar landscape. The dipole disorder exhibits a dip similar to the Gaussian disorder case for small values of σ (corresponding to $0.2 - 0.4$ Debyes). At larger values of σ, the dipole disorder trends upward, resembling the artificially correlated case.

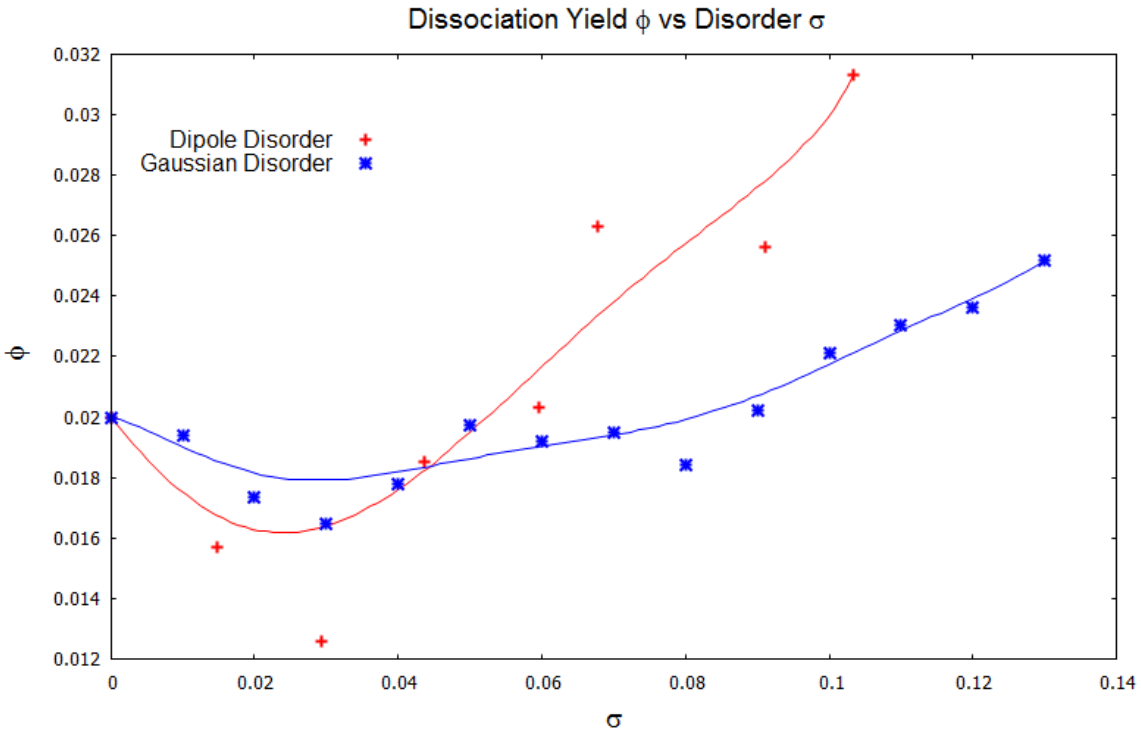

Figure 6.12: The dissociation yield as a function of σ at $T = 250K$ and $|\vec{E}| = 5 \times 10^4 \frac{V}{cm}$. Plotted is dipole disorder versus uncorrelated Gaussian disorder. The dipole disorder appears to dip more strongly for small values of σ, but increases more rapidly as σ grows.

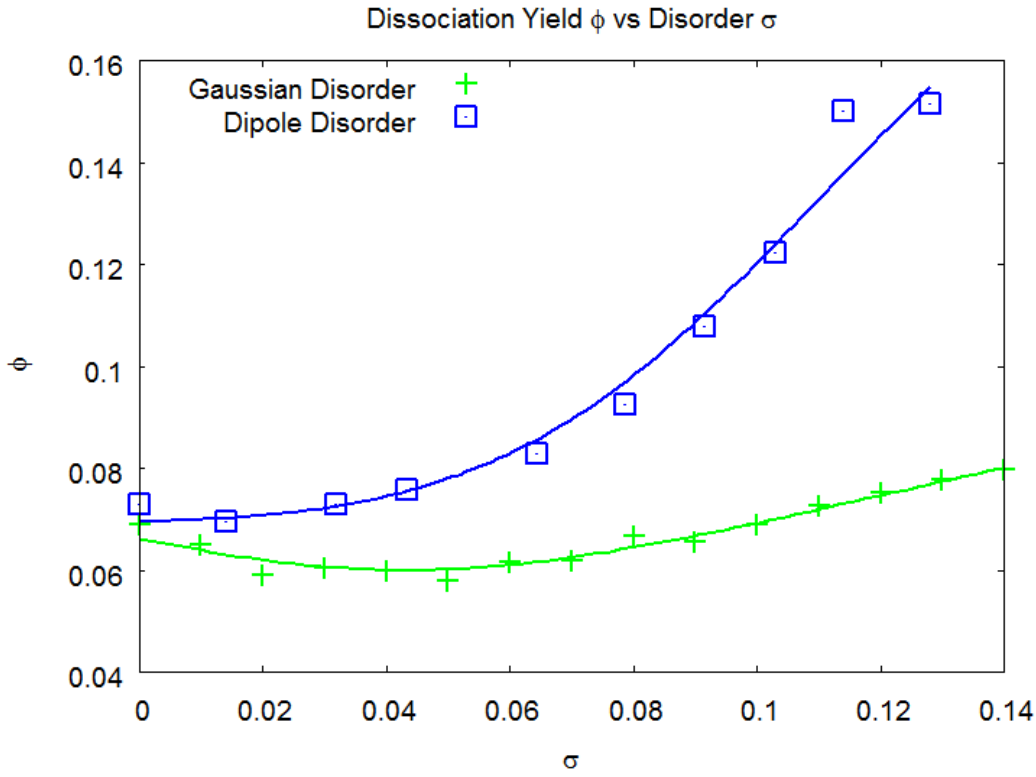

Figure 6.13: The dissociation yield as a function of σ at $T = 300K$ and $|\vec{E}| = 10^5 \frac{V}{cm}$. Plotted is dipole disorder versus uncorrelated Gaussian disorder. At a larger field magnitude, statistics are easier to gather, since the charges tend to dissociate more easily, and the average number of hops a particle makes is reduced. This reduces the noise, and the dipole disorder shows an even more pronounced increase in ϕ over the uncorrelated disorder.

charge transport behavior than their crystalline inorganic and organic counterparts.

- Disorder is not necessarily detrimental to the process of separating and extracting charges.
- Understanding the local properties, correlation, and effects of energetic disorder is important to understanding the macroscopic behavior organic semiconductors.

Now there remain a few last ideas to address.

6.6.1 Scale of Disorder Versus Scale of the System

Many experiments that attempt to characterize organic semiconductors are concerned largely with the macroscopic behavior of the material, e.g. the bulk mobility. These experiments often probe length scales much larger than many of the local features of the system. For example, time-of-flight experiments [71] measure the mobility of charges across samples that are on the order of microns, while an actual organic photovoltaic cell may only be 100nm across. Furthermore, the scales of clusters of molecules or crystallites in a disordered organic semiconductor are even smaller, on the order of a few nanometers. Such experiments tend to average over these local structures. Consider Figure 6.14, in which the blue ellipses represent zones of local energetic correlation (e.g. a crystallite). The charge is forced by the disorder in the system to take a meandering path across the material, resulting in a low bulk mobility. If the size of devices becomes smaller, an occurrence which certainly has precedent, the local order of materials may become more important. An important consequence of correlated disorder, however, is the introduction of long-range order which can supersede the local order of crystallites and other small structure. Consider Figure 6.15, representing a device in which the long-range order due to correlation spans across a device. The path of a charge, the red arrow, travels through an extended correlated zone, rather than the short-range local order presented by the small structures that comprise the organic material. If methods are developed that allow for the level of correlation in energetic disorder to be altered, the scale of the disorder could be tuned to make more effective devices.

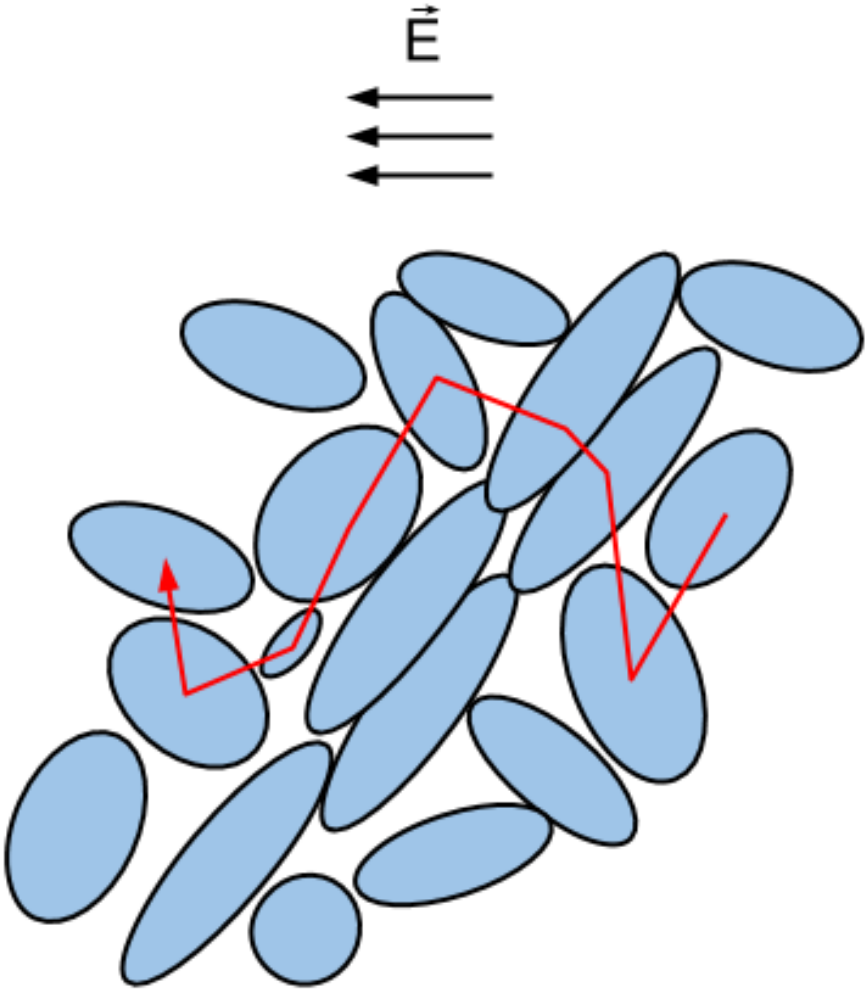

Figure 6.14: A schematic representation of a disordered organic solid, with the blue ellipses representing zones in which the energy is locally correlated. The red path indicates a charge being driven across by an applied electric field. The charge takes an irregular path through the material due to the high disorder over the range of its transit.

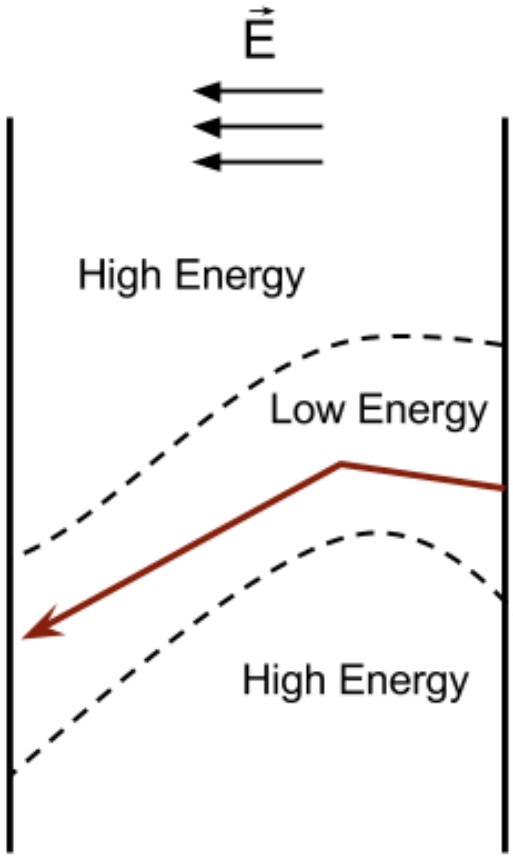

Figure 6.15: A schematic representation of a disordered organic solid that possesses long range order as a result of correlation. The red path indicates a charge being driven across by an applied electric field. The black lines represent the boundaries of a device, for example the terminals of a solar cell. The material may have local disorder, but the long-range correlation allows the charge to cross the device.

6.6.2 Manipulating Disorder

The biggest reason organic semiconductors are a topic of such great interest is the fact that the organic versions of many electronic devices can be fabricated at much less cost and time investment. On the other hand, this reduction in effort means that a sacrifice is made in the control of the microscopic structure of the material. Understanding the mechanisms which give rise to disorder may allow the development of methods to manipulate it. It seems conceivable that one might be able to engineer disorder in a device in such a way as to guide charge transport, forcing charges into desired regions, and disallowing them from others. One example might be strategically doping an organic polymer to change the energetic landscape in such a way that paths of favorable energy appear. To determine what methods might be used to control disorder, the sources and effects of disorder must be understood first.

Understanding this disorder may lead to new uses for organic materials, or improved performance of existing devices. The author hopes that the discussion of energetic disorder presented in this thesis may help to provide a better understanding of charge transport in organic semiconductors.

Part II

The Fragment Hamiltonian

7

Some Preliminary Formalism

7.1 Introduction

The Fragment Hamiltonian (FH) model is currently in development by Valone [4, 72] at Los Alamos National Laboratory. The goal of the FH model can be broadly described as attempting to provide a general model for charge transfer in a material that reduces to the behavior of a metal or an insulator in the corresponding appropriate parameter regimes. Describing charge flow at the microscopic level is a fundamental problem, and has been long studied in physics and chemistry.

There are good descriptions for the very small constituent parts of many systems, such as atoms in a solid. Having a good fine-grained description of the elements of a system does not necessarily mean that one automatically understands the system, however [73]. Certainly one would not attempt to describe a macroscopic system directly in terms of the individual behavior and interaction of its huge number of constituent atoms. The behavior of many macroscopic structures is understood in terms of the collective behavior of its components. For example, the electronic properties of materials with a well-ordered periodic crystal structure can be described in terms of a basis of Bloch states exactly because of their large-scale structure [74].

Systems become difficult to describe when large-scale order is disrupted. The models describing many materials take advantage of some sort of symmetry, e.g. the electronic structure of a crystal being described in terms of Bloch states, as mentioned

above. For example, consider two materials whose individual behavior is understood apart from one another. If two (or more) materials are brought together, however, the interface between them can disrupt the periodicity, causing the previous models to fail. The Fragment Hamiltonian endeavors to describe a system in terms of the charge states of component "fragments", which are a partitioning of the system into new elementary units. For example, the fragments of a system might be defined as clusters of atoms that exhibit an approximately periodic structure, where the individual atoms themselves do not. In this way, it is hoped that systems which previously resisted description can be modeled.

What is meant by a 'fragment' will be explained in more precise detail later, but presently it is important to provide some historical and theoretical context. Many of the approaches of the author and collaborators to the Fragment Hamiltonian have been through a tight-binding-like framework. In order for that work to make sense, it is important that the reader have an understanding of the tight binding method employed by the author. To that end, this chapter will lay a groundwork for the tight binding model to be called upon later. In the next chapter, an extension to the tight-binding model, the Hubbard model, will be introduced. The current-carrying behavior of some simple examples of tight-binding and Hubbard systems will also be examined, for comparison against the FH model later. All of the discussion in the following chapters takes place in 1D. As such, we are not attempting to model any actual physical system, but rather build a frame of reference for the FH model in terms of traditional solid state methods.

7.2 A One-Band 1D Tight-Binding Model

To build context for discussing the Fragment Hamiltonian, let us introduce the tight-binding model. Our discussion here follows treatments that may be found in many textbooks, for example [1, 74, 75]. The tight-binding model derives its name from the fact that it is built on the assumption that one has a lattice of atoms whose individual electronic wavefunctions overlap weakly. As a result, the electrons in the system tend to be tightly bound to the atoms. Since these wavefunctions are weakly interacting with those of their neighbors, each atomic wavefunction approximates that of an isolated atom. The wavefunction for the lattice is approximated as the

following linear combination of atomic orbitals (LCAO)

$$|\Psi(\vec{r},t)\rangle = \sum_m C_m(t)|\phi_m(\vec{r})\rangle, \tag{7.1}$$

where the C_m's are the occupation amplitude at site m, and the ϕ_m's are the local wavefunctions. For simplicity, the ϕ_m's are an orthonormal basis of Wannier functions, and the Hamiltonian includes only nearest neighbor interactions. This is to say

$$\begin{aligned}\langle\phi_m(\vec{r})|\phi'_m(\vec{r})\rangle &= \delta_{m,m'}\\ \langle\phi_m(\vec{r})|H|\phi_m(\vec{r})\rangle &= E_0\\ \langle\phi_m(\vec{r})|H|\phi_{m\pm1}(\vec{r})\rangle &= -V,\end{aligned}$$

where the E_0's are the on-site energies, and the V's represent the wavefunction overlaps between nearest neighbors. Thus, the Hamiltonian matrix in the site basis looks like

$$H \to \begin{pmatrix} E_0 & -V & 0 & 0 & \\ -V & E_0 & -V & 0 & \dots \\ 0 & -V & E_0 & -V & \\ 0 & 0 & -V & E_0 & \\ & & \dots & & \end{pmatrix}, \tag{7.2}$$

To give a picture of the tight-binding model, consider the oft-used simple example a uniform string of N hydrogen atoms. A diagram is presented in Figure 7.1. Consider a large chain of these identical simple atoms with lattice spacing a which present a perfectly periodic potential, and are connected to form a ring. The time-dependent Schrödinger equation is

$$i\hbar\frac{\partial}{\partial t}\sum_m C_m(t)|\phi_m(\vec{r})\rangle = H\sum_m C_m(t)|\phi_m(\vec{r})\rangle. \tag{7.3}$$

Taking an inner product of $\langle\phi_n(\vec{r})|$ with (7.3),

$$i\hbar\frac{\partial}{\partial t}\langle\phi_n(\vec{r})|\sum_m C_m(t)|\phi_m(\vec{r})\rangle = \langle\phi_n(\vec{r})|H\sum_m C_m(t)|\phi_m(\vec{r})\rangle. \tag{7.4}$$

Since H only has nearest neighbor interactions, equation (7.4) vanishes whenever

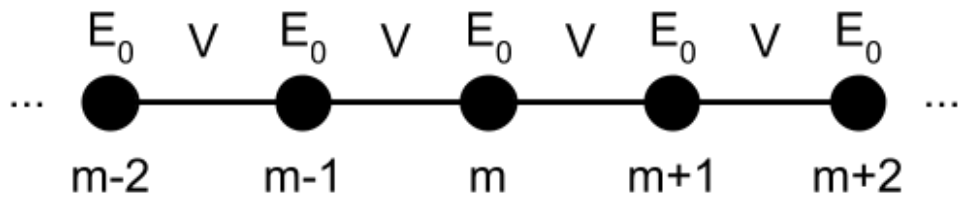

Figure 7.1: A schematic of a monatomic tight binding chain.

$n \neq m, m \pm 1$. As a result, the amplitudes C are represented by

$$i\hbar \dot{C}_m(t) = E_0 C_m - V(C_{m-1} + C_{m+1}). \tag{7.5}$$

At this point, it is useful to perform a discrete Fourier transform on this expression, using the relation

$$C_k = \sum_m C_m e^{ikam}. \tag{7.6}$$

For simplicity, let $ka \to k$, so that k is now a dimensionless quantity. Multiplying both sides of (7.5) by e^{ikm} and summing over m, one gets

$$i\hbar \sum_m \dot{C}_m(t) e^{ikm} = E_0 \sum_m C_m e^{ikm} - V \sum_m (C_{m-1} + C_{m+1}) e^{ikm}. \tag{7.7}$$

Now it is important to note that

$$\sum_m C_{m\pm1} e^{ikm} = e^{\mp ik} \sum_{m\pm1} C_{m\pm1} e^{ik(m\pm1)}. \tag{7.8}$$

This means (7.7) may be expressed as

$$i\hbar\dot{C}_k = E_0 C_k - V(C_{m-1}e^{ikm} + C_{m+1}e^{-ikm}) = (E_0 - 2V\cos k)C_k. \tag{7.9}$$

Taking the ansatz

$$C_k(t) = C_{0k}e^{-\frac{iEt}{\hbar}} \tag{7.10}$$

it follows that the energy for a single band is

$$E(k) = E_0 - 2V\cos k. \tag{7.11}$$

A single period of k is referred to as the first Brillouin zone [1], or more commonly simply the Brillouin zone. The first Brillouin zone is usually defined from $-\pi$ to π as in Figure 7.2, rather than from 0 to 2π, so that the energy minimum corresponds to $k = 0$, as for a free particle.

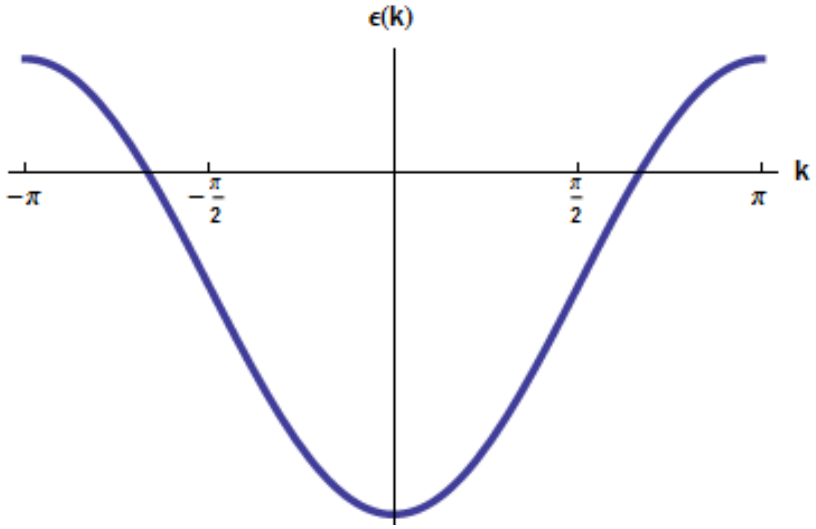

Figure 7.2: A plot of the first Brillouin zone.

The energy eigenvalues $E(k)$ correspond to the Bloch states $\Psi_k(\vec{r}) = e^{i\vec{k}\cdot\vec{r}}u_k(\vec{r})$ with momentum $\vec{k}$, where $u_k(\vec{r})$ is an envelope with the same periodicity as the lattice potential. Note that in more complex systems which possess more than one band, the energies become $E_n(k)$, with n as the band index. The Bloch states arise from the translational symmetry of the system. In spite of the model being called "tight binding", suggesting that individual site wavefunctions are very localized, connections to neighboring atoms result in the electron wavefunctions extending across the lattice.

Treatments of Bloch waves can be found in many textbooks, for example Ashcroft and Mermin [1], and will not be detailed further here.

7.3 The Fermi Surface

As electrons are added to the system, these energy levels are populated from lowest to highest, with alternating spins, according to the *Aufbau* principle. For the simple case of hydrogen atoms, the system will equilibrate to a charge-neutral ground state with N electrons, one for each atom. This is referred to as a half-filled band, since the maximum number of electrons the system may contain (neglecting excited states) is $2N$. The conductivity of a system of electrons obviously depends on the number of electrons; If there are none, the conductivity is identically zero, since there are no charges to carry a current. However, if the band is completely full the conductivity is also zero, as all available states are occupied, and the electrons cannot make transitions. A more detailed discussion of conductivity may be found in Appendix C.

At zero temperature the top of this stack of energy states (the "Fermi sea") is called the Fermi energy, which is the energy one must expend to add another electron to the system. If a band is partially filled, the energy levels at the Fermi energy constitute the Fermi surface [1]. It is near this surface that the excitations in the system take place, as in Figure 7.3. The electrons below the Fermi surface are distributed across all available states within that range of k-values. Ordinary electrical and thermal excitations are on the order of fractions of an electron volt (e.g. $k_bT \approx 0.025eV$ at room temperature). The Fermi energy in a typical metal, however is on the order of a few electron volts. As a result, such excitations cannot boost most of the electrons in the Fermi sea up to an available empty state, restricting the electrons participating in the current to those close to the Fermi surface.

7.4 The Density of States

The density of states (DOS) measures the number of available electronic states per unit energy interval [1]. By the definition of the DOS $g(E)$, the number of states N_s

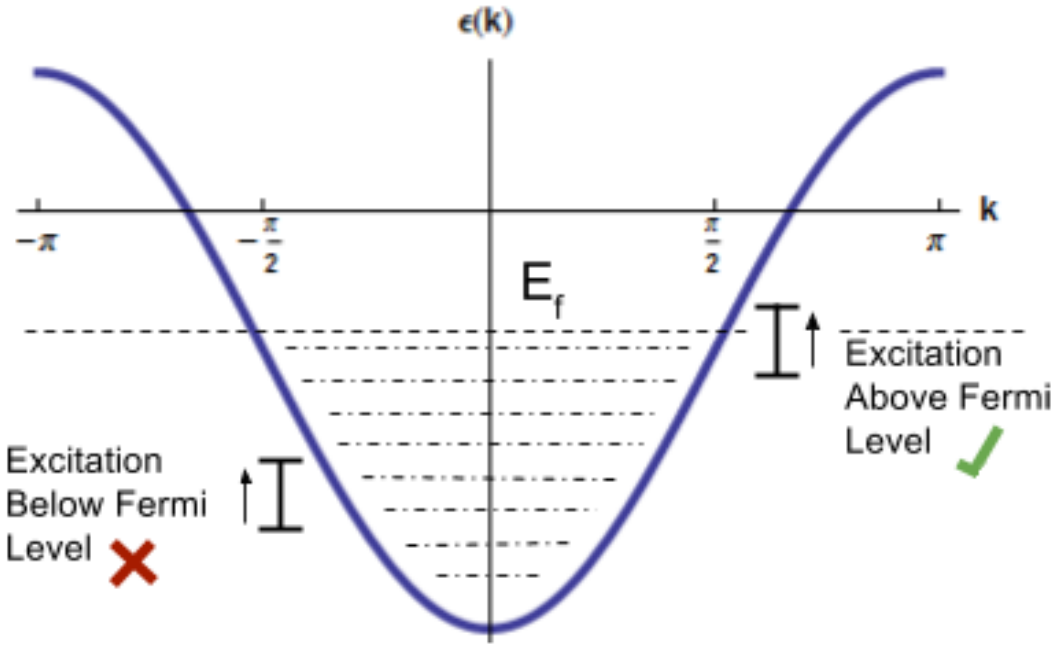

Figure 7.3: The Fermi level within a single band.

occupied in a system is

$$N_s = \int_0^{E_f} g(E)dE, \tag{7.12}$$

where E_f is the Fermi energy. For one dimensional systems, a differential interval in k-space in the Brillouin zone is $\frac{dk}{2\pi}$. The density of energy in that slice of k-space is

$$g(E)dE = \frac{dk}{2\pi}, \tag{7.13}$$

from which it follows that

$$g(E) = \frac{1}{2\pi}\frac{dk}{dE}. \tag{7.14}$$

For example, in the tight-binding system in section 7.2 above,

$$E = E_0 - 2V\cos k \;\;\rightarrow\;\; k = \arccos\frac{E_0 - E}{2V}. \tag{7.15}$$

Differentiating with respect to E, it follows that

$$g(E) = \frac{1}{2\pi}\frac{dk}{dE} = \frac{1}{4\pi V}\frac{1}{\sqrt{1-\left(\frac{E_0-E}{2V}\right)^2}}. \tag{7.16}$$

7.5 A Binary Alloy on a 1D Lattice

The case of a single band is more demonstrative than practical. In this section, the concept of a bandgap will be treated in more detail, using a model of a binary alloy that behaves in a way more typical of many common semiconductors and insulators.

Consider a very long chain of atoms of two different alternating species, with pairs of atoms defining the unit cells. It is these cells that are now enumerated by m, rather than the individual atoms. Using the same procedure as in equations (7.3) through (7.5), the occupation amplitudes obey

$$i\hbar\dot{C}_m^L = -V_b C_{m-1}^R - V_a C_m^R \tag{7.17}$$

$$i\hbar\dot{C}_m^R = -V_a C_m^L - V_b C_{m+1}^L \tag{7.18}$$

where E_0 has been set to zero for convenience, V_a and V_b are the alternating interaction matrix elements between the two different species, and $C_m^{R(L)}$ is the occupation

amplitude for right (left) atom in the mth cell, as in Figure 7.4.

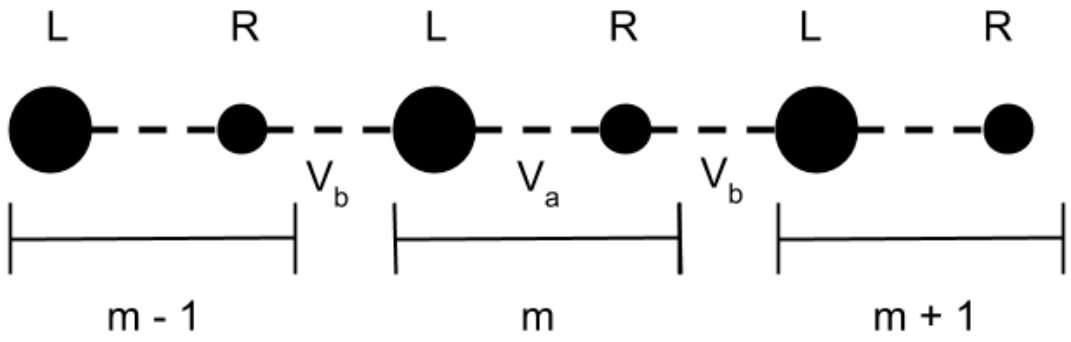

Figure 7.4: A schematic of a diatomic tight binding chain.

By performing a discrete Fourier transform as in equation (7.6),

$$C_k^L = \sum_m C_m^L e^{ikm(2a)}, \tag{7.19}$$

and letting k again be a dimensionless quantity by taking $2ka \to 2k$, (7.17) becomes

$$\begin{aligned} i\dot{C}_k^L &= -V_b \sum_m C_{m-1}^R e^{i2km} - V_a C_k^R = -V_b e^{i2k} \sum_m C_{m-1}^R e^{i2k(m-1)} - V_a C_k^R \\ &= -V_b e^{2ik} C_k^R - V_a C_k^R. \end{aligned} \tag{7.20}$$

The transformation for (7.18) is exactly similar, and equations (7.17) and (7.18) have now become

$$i\dot{C}_k^L = -C_k^R(V_b e^{i2k} + V_a) \tag{7.21}$$

$$i\dot{C}_k^R = -C_k^L(V_a + V_b e^{-i2k}). \tag{7.22}$$

From here, let us take the *ansatz*

$$C_k^{R(L)}(t) = C_k^{R(L)}(0) e^{-iEt}, \tag{7.23}$$

where E is an energy eigenvalue to be determined. Our equations then become

$$EC_k^L = -C_k^R(V_b e^{i2k} + V_a) \tag{7.24}$$

$$EC_k^R = -C_k^L(V_a + V_b e^{-i2k}). \tag{7.25}$$

Expressing these in matrix form, we get

$$\begin{pmatrix} E & -(V_b e^{i2k} + V_a) \\ -(V_a + V_b e^{-i2k}) & E \end{pmatrix} \tag{7.26}$$

Taking the determinant of this matrix yields

$$E(k) = \pm\sqrt{V_a^2 + V_b^2 + 2V_a V_b \cos 2k}, \tag{7.27}$$

the energy of the upper and lower bands with respect to k, plotted in Figure 7.5.

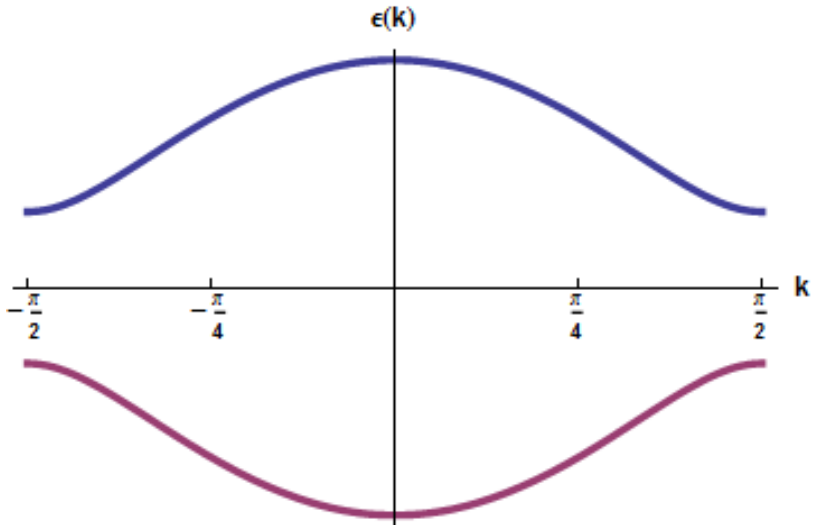

Figure 7.5: A plot of the valence and conduction bands for a 1D binary system.

The disallowed region present between the bands in Figure 7.5 is called the bandgap. The presence of a bandgap results in what are referred to as Bloch-Wilson [76] or band insulators [77], as opposed to Mott insulators which will be discussed later. At $T = 0$, once the states of the lower band (called the valence band) are fully populated, the system cannot support a current.

Consider the band filling, as described for the one-band case. It is still the case

that the system tends toward overall charge neutrality, and that this state corresponds to one electron per site. The magnitude of the Bloch vector, k, is allowed to take values

$$k = \frac{2\pi n}{2N+1}, \tag{7.28}$$

where n is an integer. A proof of this can be found in Appendix B. If the system is half full ($n = N$), then in the ground state the energy levels will be populated for $\frac{2\pi N}{2N+1} \approx \pi$ values of k. Since k is taken to be symmetric about zero, this means that

$$-\frac{\pi}{2} < k < \frac{\pi}{2}. \tag{7.29}$$

Referring to Figure 7.5, one can see that this completely fills the lower band. In this instance the Fermi energy lies halfway between the valence band and the conduction band. Since all the accessible states are occupied in the lower band, and there are zero available states within the band gap, the system is insulating.

Now that some necessary formalism has been introduced, in the next chapter, we will discuss the current carrying behavior of some small systems, against which the behavior of the FH model may be compared later.

8

The Two-Site Hubbard Model

In the previous chapter, the tight-binding model was developed while ignoring electron-electron repulsions. Is this justified? According to Landau's theory of Fermi liquids [78], this may be justified after the fact, as electrons at the Fermi surface can be treated as free particles with a modified effective mass. We expect, however, that this approximation breaks down as the inter-atomic spacing becomes larger, and the coulomb repulsion becomes large compared to the kinetic energy. At some point, the monatomic material should undergo a Mott metal-insulator transition, which will be discussed shortly. The Hubbard Hamiltonian describes a many body system as a tight-binding lattice, and attempts to address this question by including coulomb repulsion between electrons. There is a rich literature on the Hubbard model, as it has few exact solutions, one of the most famous being that of Lieb and Wu on an infinite chain in 1D [79]. Here we look at the Hubbard model for two electrons on two sites.

8.1 The Hubbard Hamiltonian

The next stage in developing a practical Fragment Hamiltonian is to compare it to a model whose behavior is understood. A logical place to start is with the Hubbard model, with the reasons for this being explained shortly. This model is an extension of the tight-binding model which includes electron-electron interactions on the same site. It was introduced in a 1963 paper by Hubbard titled "Electron Correlations in

Narrow Energy Bands" [80]. For a chain of identical hydrogen atoms, the Hubbard Hamiltonian is

$$H_{hub} = -V \sum_{i=j\pm1,\sigma} (a^\dagger_{i,\sigma} a_{j,\sigma} + a^\dagger_{j,\sigma} a_{i,\sigma}) + U_{\text{hub}} \sum_i n_{i\uparrow} n_{i\downarrow} \tag{8.1}$$

It has become convenient to express the Hamiltonian in terms of the second quantized operators $a_{i,\sigma}, a^\dagger_{j,\sigma}$. A discussion of second quantized operators can be found in chapter 2 of the textbook by Atland and Simons [81]. These operators obey the anti-commutation rules for fermions, with the anti-commutator defined as $[A, B]_+ = AB + BA$.

$$[a_{i,\sigma}, a_{i',\sigma'}]_+ = 0 \tag{8.2}$$

$$[a^\dagger_{i,\sigma}, a^\dagger_{i',\sigma'}]_+ = 0 \tag{8.3}$$

$$[a^\dagger_{i,\sigma}, a_{i',\sigma'}]_+ = \delta_{i,i'}\delta_{\sigma,\sigma'} \tag{8.4}$$

The annihilation operator $a_{i,\sigma}$ deletes an electron with spin σ from site i, while the creation operator $a^\dagger_{j,\sigma}$ creates an electron with spin σ on site j. The first term in (8.1) is then simply the nearest neighbor hopping term, as in the tight-binding model. The operators $n_{i\uparrow} = a^\dagger_{i,\uparrow} a_{i,\uparrow}$ and $n_{i\downarrow} = a^\dagger_{i,\downarrow} a_{i,\downarrow}$ are the number operators, and count how many electrons with spin $\sigma = \uparrow, \downarrow$ are one site i. Since electrons obey the Pauli exclusion principle, this number is either 0 or 1. This means the second term in (8.1) represents a coulombic on-site interaction between electrons which happen to occupy the same site. This energy is referred to as the "Hubbard U". The Hubbard U is defined as

$$U_{\text{hub}} = E_I - \mathcal{E} = E(H^-) + E(H^+) - 2E(H). \tag{8.5}$$

E_I is the ionization energy, or the energy required to remove an electron from the atom. $\mathcal{E}$ is the electron affinity, the energy change when an electron is added to a neutral atom to form a negative ion (see Appendix A).

The Hubbard model is an expression of a system known as a Mott insulator (specifically, a Mott-Hubbard insulator) [77]. In 1949 Mott gave an example of a transition between a metal and an insulator now referred to as a Mott transition [82]. There are a few exact solutions to the Hubbard model for some specific cases [83], for example the famous solution to the 1D Hubbard model of Lieb and Wu, using the

Bethe ansatz [79]. In general, however, Mott insulators are not fully understood.

The following is a conceptual explanation of the behavior of Mott-Hubbard insulator (see [77]). Consider a half-filled tight-binding system as described in section 7.2. A site occupied by one electron lies in the center of a half-filled band of width $W = 4V = |2V(\cos\pi - \cos 0)|$. In a Hubbard system as described by (8.1), the band is split in two by the on-site electron-electron interaction. The width of the lower Hubbard band defined as W_2. A singly-occupied site participates in the lower Hubbard band, and therefore has energy $\frac{W_2}{2}$. The upper Hubbard band is formed by the electrons on doubly-occupied sites, and has a bandwidth W_1. The center of the upper band is elevated an amount U_{hub} above the center of the lower band, and so the energy required to boost and electron into the upper band is $U_{\text{hub}} - \frac{W_1}{2}$. Thus, the total chemical potential of a half-filled system is not continuous. Once the lower Hubbard band is full, the energy required to begin populating the upper Hubbard band is $\Delta\mu = U_{\text{hub}} - \frac{W_1}{2} - \frac{W_2}{2} = U_{\text{hub}} - (\frac{W_1+W_2}{2}) > 0$.

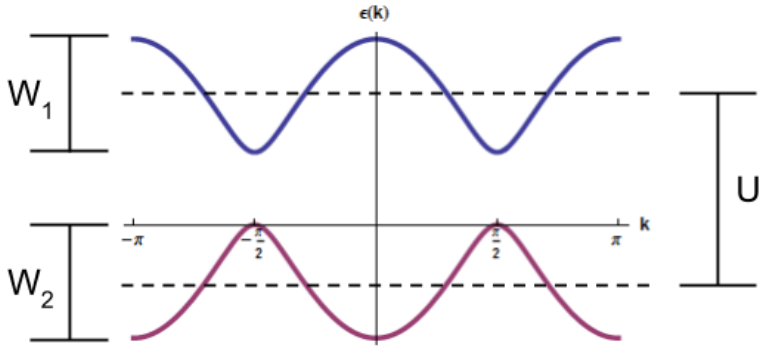

Figure 8.1: The splitting of a single band into two due to the presence of the Hubbard U. Note that at half filling, $-\frac{\pi}{2} < k < \frac{\pi}{2}$, and the lower Hubbard band is full, resulting in an insulating state.

If the sites in the tight-binding model are very far from one another, the overlap V is very small, and thus the bandwidth W is small. Assuming $\frac{W_1+W_2}{2} \approx W$, if $W \ll U_{\text{hub}}$, then a gap is present. This is due to the fact that if $V \ll U_{\text{hub}}$, then it is energetically more favorable for the electrons to remain localized than to try to overcome the Coulomb repulsion encountered when attempting to move about the lattice. As the lattice sites are moved closer to each other, the overlap interaction V becomes larger, along with $W_1 + W_2$. At the point where $U_{\text{hub}} = (\frac{W_1+W_2}{2})$ the

upper and lower Hubbard bands overlap, and the system changes from insulating to metallic, known as the Mott Metal-Insulator Transition.

One of the reasons the Hubbard model is being examined is that it is closely analogous to the descriptions of the FH model we have been exploring. In the present work, the FH model is being studied as a tight-binding-like system, a chain of N fragments which may interact with nearest neighbors, and are each allowed to occupy the charge states $\zeta = 0, -, +$, as in the examples from section 9.1. The Hubbard Hamiltonian also describes a system of nearest-neighbor interacting sites which may host $0, 1$ or 2 electrons, corresponding to charge states $\zeta = +, 0$, and $-$, respectively. Consider equation (9.11). This may be recast as

$$\hat{H}_A = H_{00}^A + \begin{pmatrix} 0 & H_{0-}^A & H_{0+}^A \\ H_{-0}^A & H_{--}^A - H_{00}^A & H_{-+}^A \\ H_{+0}^A & H_{+-}^A & H_{++}^A - H_{00}^A \end{pmatrix}. \tag{8.6}$$

We can make the identifications, $H_{--}^A - H_{00}^A = -\mathcal{E}$ and $H_{++}^A - H_{00}^A = E_I$, taking fragment A to be an atomic site as in the Hubbard model. Then we have an analogous quantity $U_{\mathrm{FH}} = H_{--}^A + H_{++}^A - 2H_{00}^A$. This is an example of why the Hubbard model was chosen to compare against, as it has some features which correspond to the treatment of the FH model presented in the next chapter. The correspondence is not exact, however, as the FH model depends on some variables different to those in the Hubbard model, as we will see.

The place to begin almost any study is with a simple example. In the next sections the dynamics of the smallest nontrivial system available will be examined. A ring geometry is imposed on a two-site system, and a comparison of the current-carrying behavior is made between the tight-binding, Hubbard, and FH models.

8.2 Current on a Two-Site Ring

In this section we will be looking at the current-carrying behavior of (a non-Hubbard) tight-binding chain consisting of two sites as a means of introducing some formalism, and establishing a baseline. One might intuitively suspect that an isolated two-site system cannot support a current. The amount of charge traveling from site 1 to site

2 is the same as that traveling from site 2 to site 1, resulting in zero net current. In order to avoid this, we impose a ring geometry on the system by applying a phase factor to the hopping matrix elements that is sensitive to the direction of travel; $e^{i\phi}$ for clockwise, and $e^{-i\phi}$ for counter-clockwise. These so-called Peierls phase factors arise if the motion is restricted to a ring that is threaded by a magnetic flux, as in Figure 8.2. We then calculate the ground state energy as a function of ϕ. The

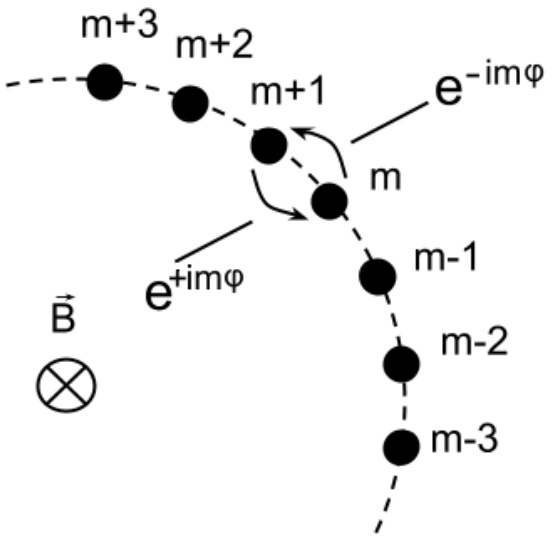

Figure 8.2: A simple visualization of a ring of sites. An imposed magnetic field threads the ring, imparting a phase factor with sign depending on the direction of travel.

(diamagnetic) moment for a magnetic field B can be defined as $\mu = \frac{\partial E(\phi)}{\partial B}$, and since $\mu = IS$ (where S is the area enclosed by the ring), this defines a current $I = \frac{1}{S}\frac{\partial E(\phi)}{\partial B}$.

The idea of using magnetic response as a diagnostic for the onset of a Mott metal/insulator transition dates back to a 1964 paper by Kohn [84]. The idea was to consider the AC electric conductivity in the limit of low frequencies. For a metallic state resembling a free Fermi gas at $T = 0$ K, one anticipates that the imaginary part of the conductivity,

$$\sigma''(\omega) \sim \frac{-ne^2}{m^*\omega},$$

diverges as a simple pole in ω. According to Kohn, the important question is, as the distance between the atoms increases, does the effective mass m^* increase monotonically, or is there a critical value of atomic separation beyond which the residue of the

pole vanishes abruptly, i.e.,

$$\lim_{\omega \to 0} \omega \sigma'' (\omega) = 0.$$

The residue has come to be known as the "charge stiffness" [85]. The AC electric field $\mathcal{E} \exp(i\omega t)$ may be introduced formally via the vector potential A, where the system is imagined to be in the shape of a ring of radius R that is threaded by a time-varying magnetic field, giving

$$\vec{A} = \frac{\hbar}{e} k \ \hat{\phi}$$

where $k = \frac{e\mathcal{E}}{i\hbar\omega} \exp(i\omega t)$. From time-dependent perturbation, Kohn showed that

$$\lim_{\omega \to 0} \omega \sigma'' (\omega) = \left(\frac{-1}{2\pi R} \right) \frac{\partial^2 E}{\partial k^2} \tag{8.7}$$

where E is the ground state energy of the system.

Instead of considering an ac electric field generated by a changing magnetic flux in the limit of low frequency, one could consider the ring to be subjected to a uniform magnetic field B. In such a case, the vector potential will be

$$\vec{A} = \frac{1}{2} B r \hat{\phi}$$

The magnetic moment

$$\mu = -\frac{\partial E(B)}{\partial B} \equiv \pi R^2 I$$

is given by the change in the ground state energy with respect to B, and is formally related to the product of the current I and the area of the ring. The second derivative with respect to B gives the magnetic susceptibility,

$$\chi = \frac{\partial \mu}{\partial B} = -\frac{\partial^2 E(B)}{\partial B^2}. \tag{8.8}$$

Comparing (8.7) and (8.8), noting that $\frac{BR}{2}$ replaces $\frac{e\mathcal{E}}{i\hbar\omega}$, we see that Kohn's "charge stiffness" is equivalent to measuring the diamagnetic susceptibility. Whether or not he was aware of it, at the end of the day, Kohn was suggesting that one use the diamagnetic susceptibility of a ring as a way to characterize the Mott transition.

Consider the Hamiltonian (7.2) for a ring of sites. In Dirac notation with $E_0 = 0$,

it is expressed

$$H = -V \sum_m \left(|m\rangle\langle m+1| + |m+1\rangle\langle m| \right), \tag{8.9}$$

The effect of a magnetic field is incorporated by inserting phase factors so that

$$H = -V \sum_m \left(e^{i\phi}|m\rangle\langle m+1| + e^{-i\phi}|m+1\rangle\langle m| \right). \tag{8.10}$$

Before continuing further, it should be made clear that the Peierls phase factors can be understood by bringing in the magnetic field through a gauge transformation. Recall that the Hamiltonian for a (positive) charge in the presence of a vector potential $\vec{A}$ is,

$$H = \frac{\left(\vec{P} - e\vec{A}\right)^2}{2m_e} + V, \tag{8.11}$$

where $\vec{P} = -i\hbar\vec{\nabla}$ is the momentum, and V is some potential. Consider the Schrödinger equation,

$$H\Psi = E\Psi. \tag{8.12}$$

Making the gauge transformation,

$$\tilde{\Psi} = e^{-i\frac{e}{\hbar}\int \vec{A}\cdot d\vec{l}}\Psi, \tag{8.13}$$

we have

$$He^{i\frac{e}{\hbar}\int \vec{A}\cdot d\vec{l}}\tilde{\Psi} = Ee^{i\frac{e}{\hbar}\int \vec{A}\cdot d\vec{l}}\tilde{\Psi}. \tag{8.14}$$

Note now that

$$\left(\vec{P} - e\vec{A}\right) e^{i\frac{e}{\hbar}\int \vec{A}\cdot d\vec{l}}\tilde{\Psi} = e^{i\frac{e}{\hbar}\int \vec{A}\cdot d\vec{l}}\left(\vec{P}\tilde{\Psi}\right). \tag{8.15}$$

Therefore, it follows that,

$$\begin{aligned} He^{i\frac{e}{\hbar}\int \vec{A}\cdot d\vec{l}}\tilde{\Psi} = e^{i\frac{e}{\hbar}\int \vec{A}\cdot d\vec{l}}\left(\frac{\vec{P}^2}{2m_e} + V\right)\tilde{\Psi} &= Ee^{i\frac{e}{\hbar}\int \vec{A}\cdot d\vec{l}}\tilde{\Psi} \\ \rightarrow \quad \left(\frac{\vec{P}^2}{2m_e} + V\right)\tilde{\Psi} &= E\tilde{\Psi}. \end{aligned} \tag{8.16}$$

This tells us that if $\tilde{\Psi}$ are eigenfunctions of H in the absence of a magnetic field, then $\Psi = e^{i\frac{e}{\hbar}\int \vec{A}\cdot d\vec{l}}\tilde{\Psi}$ are the eigenfunctions in the presence of a magnetic field. In terms of

our tight-binding basis states, this means that,

$$|m\rangle_{\text{with field}} = e^{i\frac{e}{\hbar}\int \vec{A}\cdot d\vec{l}}|m\rangle_{\text{without field}}. \tag{8.17}$$

It follows that

$$\phi_m = \frac{e}{\hbar}\int \vec{A}\cdot d\vec{l} = \frac{e}{\hbar}Ama = \frac{e}{\hbar}\frac{\pi B_0 r^2}{2} = \frac{eB_0 S}{2\hbar}, \tag{8.18}$$

where B_0 is the magnitude of the magnetic field, and a is the spacing between sites, so that ma is the distance along the ring. For two adjacent sites $|m\rangle$ and $|m\pm 1\rangle$, the phase accumulated in a single hop (in units of a) is

$$\langle m|m\pm 1\rangle = e^{-i\frac{e}{\hbar}Am}e^{i\frac{e}{\hbar}A(m\pm 1)} = e^{\pm i\frac{e}{\hbar}A} = e^{\pm i\phi}. \tag{8.19}$$

We return now to the discussion of current on the ring of sites. Using the LCAO representation (7.1)

$$\Psi = \sum_{m'} C_{m'}|m'\rangle, \tag{8.20}$$

the time-independent Schrödinger equation takes the form

$$\begin{aligned} H\Psi &= -V\sum_{m,m'}\left(e^{i\phi}C_{m'}|m\rangle\langle m+1|m'\rangle + e^{-i\phi}C_{m'}|m+1\rangle\langle m|m'\rangle\right) \\ &= -V\sum_{m,m'}\left(e^{i\phi}C_{m'}|m\rangle\delta_{m+1,m'} + e^{-i\phi}C_{m'}|m+1\rangle\delta_{m,m'}\right) \\ E\sum_m C_m|m\rangle &= -V\left(e^{i\phi}C_{m+1}|m\rangle + e^{-i\phi}C_m|m+1\rangle\right). \end{aligned} \tag{8.21}$$

Closing with $\langle n|$ from the left,

$$\begin{aligned} E\sum_m C_m\langle n|m\rangle &= -V\left(e^{i\phi}C_{m+1}\langle n|m\rangle + e^{-i\phi}C_m\langle n|m+1\rangle\right) \\ E\sum_m C_m\delta_{n,m} &= -V\left(e^{i\phi}C_{m+1}\delta_{n,m} + e^{-i\phi}C_m\delta_{n,m+1}\right). \end{aligned} \tag{8.22}$$

Applying the Kronecker δ's and then letting $n\to m$ we have

$$EC_m = -V\left(e^{i\phi}C_{m+1} + e^{-i\phi}C_{m-1}\right). \tag{8.23}$$

Since we are concerned with a two site system, $m+1$ and $m-1$ both correspond to

the same site. This means the above equation reduces to a pair of equations

$$EC_1 = -2V\cos\phi C_2 \tag{8.24}$$

$$EC_2 = -2V\cos\phi C_1, \tag{8.25}$$

with energy eigenvalues

$$E = \pm 2V\cos\phi. \tag{8.26}$$

For the current in the ground state $E_g = -2V\cos\phi$, we have,

$$I = \frac{1}{S}\frac{\partial E_g}{\partial B} = \frac{\partial E_g}{\partial B_0 S} = \frac{e}{2\hbar}\frac{\partial E_g}{\partial \phi} = \frac{eV}{\hbar}\sin\phi, \tag{8.27}$$

a current which varies sinusoidally with ϕ. The expression for the current due to a charge on a ring may also be derived using the Feynman-Hellman theorem, found in Appendix D.

We may alternatively talk about current in terms of the velocity operator for an electron on a chain. First, consider the position operator,

$$\hat{x} = \sum_m |m\rangle\langle m|ma, \tag{8.28}$$

where a is the spacing between sites. The velocity operator is

$$\hat{v} = \frac{d\hat{x}}{dt} = \frac{i}{\hbar}[H, \hat{x}]. \tag{8.29}$$

To evaluate this commutator, we insert (8.10) and (8.28).

$$\begin{aligned} H\hat{x} &= -V\sum_m \left(e^{i\phi}|m\rangle\langle m+1| + e^{-i\phi}|m+1\rangle\langle m|\right)\sum_n |n\rangle\langle n|na \\ &= -V\sum_m \left(e^{i\phi}|m\rangle\langle m+1|(m+1)a + e^{-i\phi}|m+1\rangle\langle m|ma\right) \end{aligned} \tag{8.30}$$

Likewise,

$$\hat{x}H = -V\sum_m \left(e^{i\phi}|m+1\rangle\langle m|(m+1)a + e^{-i\phi}|m\rangle\langle m+1|ma\right). \tag{8.31}$$

Putting this all together, the velocity operator is

$$\hat{v} = -\frac{i}{\hbar} Va \sum_m \left(e^{i\phi} |m\rangle\langle m+1| - e^{-i\phi} |m+1\rangle\langle m| \right). \tag{8.32}$$

For a two site system with periodic boundary conditions, this becomes

$$\begin{aligned} \hat{v} = -\frac{i}{\hbar} Va \Big(& e^{i\phi} |1\rangle\langle 2| - e^{-i\phi} |2\rangle\langle 1| \\ & + e^{i\phi} |2\rangle\langle 1| - e^{-i\phi} |1\rangle\langle 2| \Big), \end{aligned} \tag{8.33}$$

which reduces to

$$\hat{v} = \frac{2Va}{\hbar} \sin\phi \left(|1\rangle\langle 2| + |2\rangle\langle 1| \right). \tag{8.34}$$

The ground state of the system, corresponding to $E = -2V\cos\phi$, is $|GS\rangle = \frac{1}{\sqrt{2}}(|1\rangle + |2\rangle)$. The expectation value of the velocity operator in the ground state is

$$\langle GS|\hat{v}|GS\rangle = \frac{2Va}{\hbar} \sin\phi. \tag{8.35}$$

Since the current is defined to be $I = \frac{ev}{na}$, where n is the number of sites in the ring, we have

$$I = \frac{eV}{\hbar} \sin\phi, \tag{8.36}$$

which is the same as (8.27).

8.3 Current on a Two-Site Hubbard Ring

We now turn our attention back to the Hubbard model. The system in question is the same two-site ring as in the previous section, with the addition of the on-site coulomb interaction mediated by the Hubbard U.

The Hubbard Hamiltonian for an isolated two site system can be represented as

$$\begin{aligned} H_{hub} = & -V(a^\dagger_{1\uparrow} a_{2\uparrow} + a^\dagger_{2\uparrow} a_{1\uparrow} + a^\dagger_{1\downarrow} a_{2\downarrow} + a^\dagger_{2\downarrow} a_{1\downarrow}) \\ & + U_{\text{hub}} (a^\dagger_{1\uparrow} a_{1\uparrow} a^\dagger_{1\downarrow} a_{1\downarrow} + a^\dagger_{2\uparrow} a_{2\uparrow} a^\dagger_{2\downarrow} a_{2\downarrow}). \end{aligned} \tag{8.37}$$

The basis states for this system at half filling are

$$\begin{aligned} a^\dagger_{1\uparrow}a^\dagger_{2\uparrow}|0\rangle &= |s_{\uparrow\uparrow}\rangle \\ a^\dagger_{1\downarrow}a^\dagger_{2\downarrow}|0\rangle &= |s_{\downarrow\downarrow}\rangle \\ a^\dagger_{1\uparrow}a^\dagger_{2\downarrow}|0\rangle &= |s_1\rangle \\ a^\dagger_{1\downarrow}a^\dagger_{2\uparrow}|0\rangle &= |s_2\rangle \\ a^\dagger_{1\uparrow}a^\dagger_{1\downarrow}|0\rangle &= |d_1\rangle \\ a^\dagger_{2\uparrow}a^\dagger_{2\downarrow}|0\rangle &= |d_2\rangle \end{aligned} \tag{8.38}$$

The first two states are referred to as "spin polarized", and are eigenstates of the Hamiltonian with eigenvalue zero, meaning they don't couple to any other states and can be ignored [81]. The remaining states are the singly occupied states ($|s_1\rangle$ and $|s_2\rangle$) and the doubly occupied states ($|d_1\rangle$ and $|d_2\rangle$). Using the (s_1, s_2, d_1, d_2) basis, the Hamiltonian has the form

$$H = \begin{pmatrix} 0 & 0 & -V & -V \\ 0 & 0 & -V & -V \\ -V & -V & U_{\text{hub}} & 0 \\ -V & -V & 0 & U_{\text{hub}} \end{pmatrix}. \tag{8.39}$$

The analysis can be simplified by introducing the linear combinations,

$$|s_\pm\rangle = \frac{1}{\sqrt{2}}\left(|s_1\rangle \pm |s_2\rangle\right), \tag{8.40}$$

$$|d_\pm\rangle = \frac{1}{\sqrt{2}}\left(|d_1\rangle \pm |d_2\rangle\right). \tag{8.41}$$

In the (s_+, s_-, d_+, d_-) basis, the Hamiltonian matrix elements are

$$H = \begin{pmatrix} 0 & 0 & -2V & 0 \\ 0 & 0 & 0 & 0 \\ -2V & 0 & U_{\text{hub}} & 0 \\ 0 & 0 & 0 & U_{\text{hub}} \end{pmatrix}. \tag{8.42}$$

Conveniently, the states s_- and d_- completely decouple from the others, with eigenvalues 0 and U_{hub} respectively. Neither corresponds to the ground state, as we will see. Writing the remaining Hamiltonian in terms of the coupled states s_+ and d_+, we

have a 2×2 operator,

$$H = \begin{pmatrix} 0 & -2V \\ -2V & U_{\text{hub}} \end{pmatrix}, \tag{8.43}$$

with eigenvalues

$$E = \frac{1}{2}\left(U_{\text{hub}} \pm \sqrt{U_{\text{hub}}^2 + 16V^2}\right). \tag{8.44}$$

The normalized ground state $|GS\rangle$, corresponding to $E_g = \frac{1}{2}\left(U_{\text{hub}} - \sqrt{U_{\text{hub}}^2 + 16V^2}\right)$, is

$$|GS\rangle = \frac{-2V}{\sqrt{4V^2 + E_g^2}}|s_+\rangle + \frac{E_g}{\sqrt{4V^2 + E_g^2}}|d_+\rangle. \tag{8.45}$$

The next step is to put the two-site system on a ring, and introduce a magnetic field. For the specific case of a two-site ring, something interesting occurs. On a ring larger than two sites, a charge may traverse one direction and acquire a phase, or it may traverse the opposite direction and acquire the opposite phase. On a two-site ring, the charge has the possibility to reach the other site by traveling *either direction* around the ring, as pictured in Figure 8.3. As a result, both of the transitions described in equation (8.9) have a sum of the phases corresponding to moving either direction attached to them,

$$\begin{aligned} |m\rangle\langle m+1| \quad &\rightarrow \quad |m\rangle\langle m+1|\left(e^{i\phi} + e^{-i\phi}\right), \\ |m+1\rangle\langle m| \quad &\rightarrow \quad |m+1\rangle\langle m|\left(e^{i\phi} + e^{-i\phi}\right). \end{aligned}$$

This is equivalent to,

$$V \quad \rightarrow \quad \left(Ve^{i\phi} + Ve^{-i\phi}\right) = 2V\cos\phi. \tag{8.46}$$

Consequently, equation (8.43) now takes the form

$$H = \begin{pmatrix} 0 & -4V\cos\phi \\ -4V\cos\phi & U_{\text{hub}} \end{pmatrix}, \tag{8.47}$$

with energy eigenvalues

$$E = \frac{1}{2}\left(U_{\text{hub}} \pm \sqrt{U_{\text{hub}}^2 + 64V^2\cos^2\phi}\right). \tag{8.48}$$

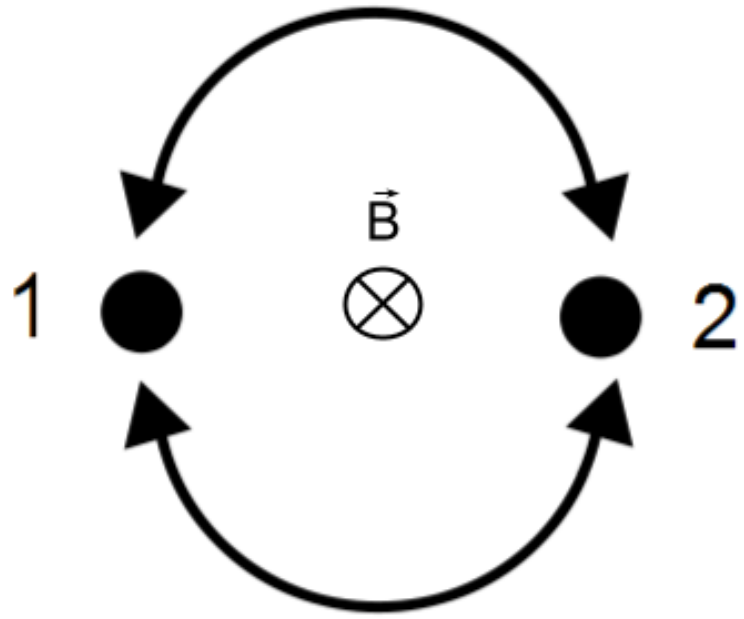

Figure 8.3: A diagram of a two-site ring, in which a charge may move to the opposite site by traveling either direction around the ring.

The ground state energy corresponds to

$$E_g = \frac{1}{2}\left(U_{\text{hub}} - \sqrt{U_{\text{hub}}^2 + 64V^2\cos^2\phi}\right). \tag{8.49}$$

For an energy eigenvalue E, the current is $I = -\frac{\partial E}{\partial \phi}$,

$$I = -\frac{\partial E_g}{\partial \phi} = \left(\frac{16V^2\sin\phi\cos\phi}{\sqrt{U_{\text{hub}}^2 + 64V^2\cos^2\phi}}\right). \tag{8.50}$$

Note that in the limit $U_{\text{hub}} \to 0$, equation (8.50) reduces to $I = 2V\sin\phi$, verifying equation (8.35). The current as a function of ϕ is plotted in Figure 8.4. The current

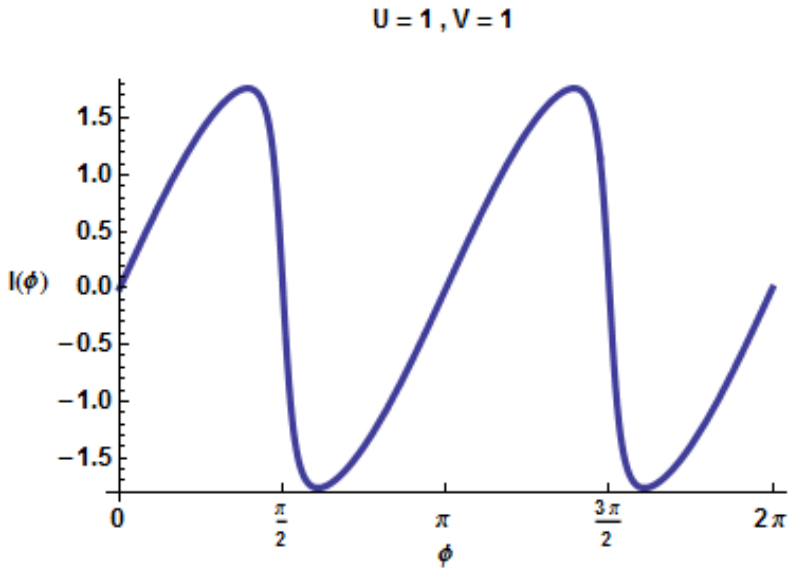

Figure 8.4: The current I on a two site ring as a function of ϕ at $U_{\text{hub}} = V = 1$. It exhibits a rapid reversal near $\phi = \frac{2n+1}{2}\pi$.

is oscillatory, with a rapid change of sign near $\phi = \frac{2n+1}{2}\pi$.

An important question to ask is, "Does the limiting behavior of this current make sense?" In particular, we expect the current to fall off for small values of the ratio $\frac{V}{U_{\text{hub}}}$. As U_{hub} gets large relative to V, we expect the system to look something like a Mott-Hubbard insulator. The two-site Hubbard ring does not correspond to a system which would exhibit a sudden Mott transition, however. The current $I(U)$ in (8.50) tends to zero continuously as $U_{\text{hub}} \to \infty$.

In the interest of examining the behavior of the current as a function of U_{hub} and

V, let ϕ be fixed at $\phi = \frac{\pi}{4}$. For the case that $V = 1$, the dimensionless current $I(U)$ appears in Figure 8.5. This exhibits the behavior that one would expect, specifically

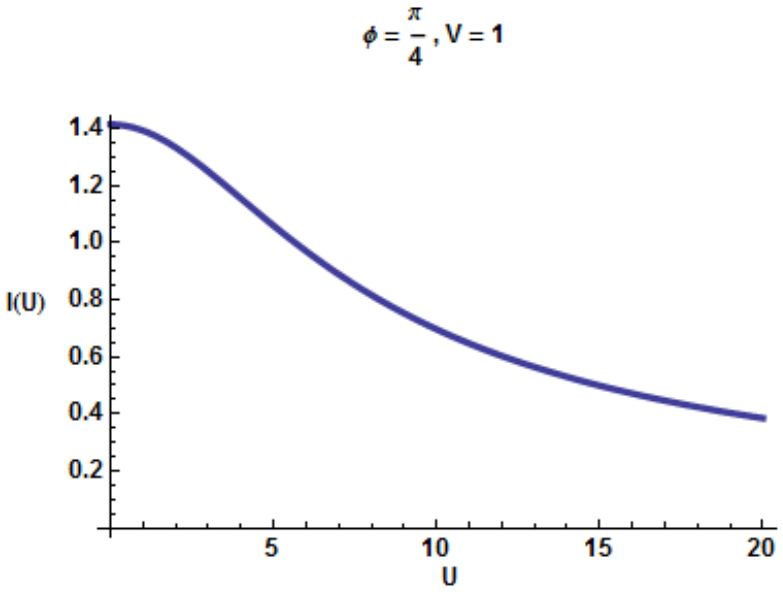

Figure 8.5: The current I on a two site ring as a function of the Hubbard U for $\phi = \frac{\pi}{4}$ and $V = 1$. As one would expect, the current falls off as U_{hub} is increased.

that the magnitude of the current decreases as U_{hub} grows. In addition, the current should diminish as the interaction V decreases, all else being equal. To check for this behavior, $I(U)$ is plotted for $V = 0.5$ in Figure 8.6. As one would expect, the current is smaller for a smaller value of V at corresponding values of U_{hub}. This result is interesting due to the fact that it does not share the behavior of the infinite 1D chain solution found by Lieb and Wu [79]. On an infinite chain, they predict that the system is insulating for any nonzero value of U_{hub}, whereas the solution for a two-site ring predicts that the system will always conduct.

In the next chapter, we will discuss the Fragment Hamiltonian. After making some definitions and constructing a bit of formalism, the current carrying behavior of the FH model on a ring will be examined, for two sites, and for larger rings. Having these results for the Hubbard model, we can compare the behavior of the FH model against them.

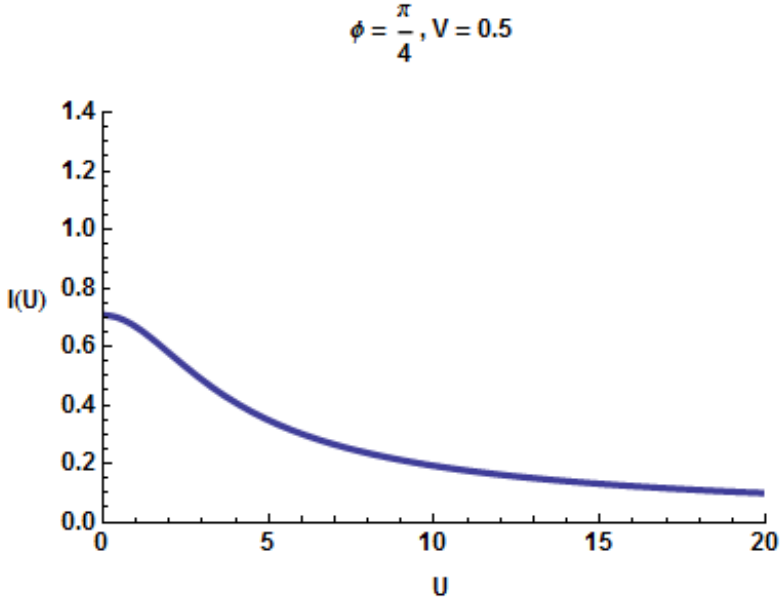

Figure 8.6: The current I on a two site ring as a function of the Hubbard U for $\phi = \frac{\pi}{4}$ and $V = 0.5$. The current is smaller than the case of a larger $V = 1$ for corresponding values of U_{hub}.

9

Exploring the Fragment Hamiltonian

In this chapter, we will begin by giving a definition of the Fragment Hamiltonian. Following that is a discussion of the behavior of the FH model on a ring of sites, analogous to the tight-binding and Hubbard systems described in chapters 7 and 8. By exercising the FH model in this way, comparing the behavior to traditional solid state methods can serve as a diagnostic.

9.1 Defining the Fragment Hamiltonian

Modern materials science relies heavily on families of electronic structure and "atomistic" methods to describe systems [86–89]. Electronic structure methods include Density Functional Theory (DFT) [90], configuration interaction (CI) [91], and tight-binding (TB). These approaches are concerned with extracting the states of the electrons in a system. Broadly speaking, an atomistic model is one in which a large molecule or bulk structure is represented by a set of atomic sites connected by chemical bonds. The interaction between sites due to the electrons and the interaction between sites and electrons is described by a potential, often referred to as a "force field", which is built from contributions due variously to inter-atomic bond stretching, bending, torsion, and other effects. These force fields are largely empirically determined. The goal at present is the development of a description in terms of fragments, in an effort to theoretically construct a force field. In this section, the basic definition of FH model will be presented.

In electronic structure methods the building blocks are single electrons and their states. In a system constructed from fragments, however, the granularity is more coarse. The fundamental quantities may be the charge states of whole atoms, or even molecules [4]. Consider the wavefunction for an entire system,

$$\psi(N_e) = \sum_i c_i \psi_i(N_e). \tag{9.1}$$

N_e is the number of electrons in the system, the c_i's are the state amplitudes, and the states i represent possible configurations of the electrons (as opposed to indexing sites on a lattice). For example, in the case of $N_e = 1$ on a tight-binding chain of size N, the wavefunction is a superposition of the electron being located at site 1, site 2, and so forth all the way up to site N, viz.,

$$\begin{aligned} |\psi(1)\rangle &= \sum_i c_i |1, 2, \ldots, N-1, N\rangle \\ &= c_1|1, 0, 0, \ldots\rangle + c_2|0, 1, 0, \ldots\rangle + \ldots \end{aligned} \tag{9.2}$$

Next, let us define a fragment A. The wavefunction describing a fragment is

$$\psi_A(N_e) \equiv \sum_\zeta C_{A^\zeta} \psi_{A^\zeta}(N_e). \tag{9.3}$$

The index ζ represents a possible charge state for a fragment. To clarify the term "charge state", suppose that fragment A is an atom which is allowed to be neutral, be missing an electron (cation), or be host to one extra electron (anion). There are then three allowed charge states, A^0, A^-, and A^+. This means the allowed values of ζ are $\zeta = 0, -, +$ (cf. Figure 6.1).

The wavefunction for a specific charge state of a fragment, $\psi_{A^\zeta}(N_e)$, is defined as

$$\psi_{A^\zeta}(N_e) \equiv \frac{1}{C_{A^\zeta}} \sum_i \delta_{\zeta, \zeta_i^A} c_i \psi_i(N_e). \tag{9.4}$$

This wavefunction is a superposition of all of the configurations i which leave the fragment A in charge state ζ. Consider for example, a system consisting of three species of atoms, A, B, and C which are allowed to take on the neutral, cation, or anion states as above, and let them share charge with one another. If the half-filling

constraint that there be an average of one electron per atom in the system is imposed, then there are three configurations which leave fragment A in the A^0 state. In the $(A^\zeta, B^\zeta, C^\zeta)$ basis they are

$$|\psi_1\rangle \equiv (A^0, B^0, C^0)$$
$$|\psi_2\rangle \equiv (A^0, B^-, C^+)$$
$$|\psi_3\rangle \equiv (A^0, B^+, C^-)$$

Therefore, the wavefunction for the fragment state A^0 is

$$\psi_{A^0}(N_e) = \frac{1}{C_{A^0}} \left(c_1\psi_1(N_e) + c_2\psi_2(N_e) + c_3\psi_3(N_e)\right). \tag{9.5}$$

It is now that we finally arrive at the Hamiltonian part of the Fragment Hamiltonian formalism. The total electronic Hamiltonian for some fragment A is given by,

$$\hat{H}_A = \hat{T}_A + \hat{V}_A + \hat{V}_A^{ee}. \tag{9.6}$$

The operator $\hat{T}_A$ is the kinetic energy of the electrons associated with fragment A; $\hat{V}_A$ is the electron interaction with the nucleus of the fragment; $\hat{V}_A^{ee}$ is the electron-electron interaction on fragment A. In the general case, following the reasoning of Moffitt [92], the total electronic Hamiltonian may be rewritten as the *Fragment Hamiltonian*

$$\hat{H} = \sum_A \hat{H}_A + \frac{1}{2}\sum_{A\neq B} \hat{V}_{AB}, \tag{9.7}$$

where A and B index the different fragments, and $\hat{V}_{AB}$ is the interaction between fragments. The expectation value of the energy for a fragment is

$$\bar{E}_A = \sum_{\zeta,\zeta'} C_{A^\zeta} C_{A^{\zeta'}} H^A_{\zeta\zeta'}. \tag{9.8}$$

The term $H^A_{\zeta\zeta'}$ is defined as

$$H^A_{\zeta\zeta'} \equiv \langle\psi_{A^\zeta}|\hat{H}^A_{\zeta\zeta'}|\psi_{A^{\zeta'}}\rangle, \tag{9.9}$$

where

$$\hat{H}^A_{\zeta\zeta'} \equiv \frac{\hat{H}^A_\zeta + \hat{H}^A_{\zeta'}}{2}. \tag{9.10}$$

On the right side of equation (9.10), the $\hat{H}^A_\zeta$ terms represent the on-fragment energy of fragment A while in charge state ζ. As such, $\hat{H}^A_{\zeta\zeta'}$ on the left side of (9.10) represents the change in energy when transitioning from charge state ζ to ζ'. The decision for $\hat{H}^A_{\zeta\zeta'}$ to be the average of the operators for the two different charge states was somewhat arbitrary, and is currently a working definition. However, the form makes intuitive sense, and also preserves Hermiticity [4].

As a simple example, consider again a fragment A which is allowed to take on charge states $\zeta = 0, -, +$ (neutral, anion, cation, as before). Given the above definitions, the matrix for $\hat{H}_A$ looks like

$$\hat{H}_A = \begin{pmatrix} H^A_{00} & H^A_{0-} & H^A_{0+} \\ H^A_{-0} & H^A_{--} & H^A_{-+} \\ H^A_{+0} & H^A_{+-} & H^A_{++} \end{pmatrix}, \tag{9.11}$$

Note that for the diagonal terms, $H^A_{\zeta\zeta} = H^A_\zeta$.

The interaction energy between fragments, $\bar{V}_{AB}$, is defined similarly;

$$\bar{V}_{AB} = \sum_{\zeta,\zeta'} C_{A^\zeta} C_{B^{\zeta'}} V^{AB}_{\zeta\zeta'}. \tag{9.12}$$

The factor $V^{AB}_{\zeta\zeta'}$ represents the energy from the coulomb interaction between fragment A in charge state ζ with fragment B in charge state ζ'.

The total energy of the system is

$$\bar{E} = \sum_A \left(\bar{E}_A + \frac{1}{2} \sum_{A \neq B} V_{AB} \right). \tag{9.13}$$

At this level, the Fragment Hamiltonian model is still very general in its formulation. The Fragment Hamiltonian describes a system in terms of fragment quantities, but the model itself does not place constraints on how large or small a fragment is. That is a choice which must be made dependent on the type of system being described. For example, the sites in the hopping system illustrated in Figure 6.1 could readily be defined as fragments. In the context of charge hopping in Part 1, the focus is on the presence of an electron or hole in a molecular orbital at a site. In the context of fragments, however, the focus is on the charge states of the fragments,

which change as the charge shifts from site to site, and how the energy of the system changes as the charge configuration changes.

This may make the FH model something of a double-edged sword. The ability to describe systems which are not highly regular or completely periodic is very powerful, but the success of the model depends on carefully defining what the fragments are which compose the system.

9.2 A Tight-Binding-Like Description of the Fragment Hamiltonian Model

In this section the Fragment Hamiltonian will be written to describe a chain of identical fragments, in the spirit of tight-binding. Consider a 1D chain of identical atoms, each of which can occupy three possible charge states, labeled +, 0, and − (Cation, neutral, and anion, respectively). These atoms, labeled as sites m, will serve as the fragments in our system. We are working in a basis of fragment charge states, i.e.,

$$|\psi_{A^\zeta}\rangle \quad \rightarrow \quad |m^\zeta\rangle, \tag{9.14}$$

where $|\psi_{A^\zeta}\rangle$ corresponds to equation (9.4). It then follows that equation (9.3) takes the form,

$$|m\rangle = C_m^+|m^+\rangle + C_m^0|m^0\rangle + C_m^-|m^-\rangle. \tag{9.15}$$

For an interaction between fragments V_{AB} that is restricted to nearest neighbors, the time-independent Schrödinger equation is

$$E\sum_m |m\rangle = H\sum_m |m\rangle = \sum_m \left(\sum_{m'} \hat{H}_{m'} + \frac{1}{2}\sum_{m'=m\pm1} \hat{V}_{m,m'}\right)|m\rangle. \tag{9.16}$$

Closing with $\langle m'|$ from the left,

$$E\sum_m \langle m'|m\rangle = \sum_m \left(\sum_{m'} \langle m'|\hat{H}_{m'} + \frac{1}{2}\sum_{m'=m\pm1} \langle m'|\hat{V}_{m,m'}\right)|m\rangle. \tag{9.17}$$

At this point, it is helpful to write out the explicit forms of $\hat{H}_{m'}$ and $\hat{V}_{m,m'}$. The on-fragment term $\hat{H}_{m'}$ is

$$\hat{H}_{m'} = \begin{pmatrix} H_{00}^{m'} & H_{0-}^{m'} & H_{0+}^{m'} \\ H_{-0}^{m'} & H_{--}^{m'} & H_{-+}^{m'} \\ H_{+0}^{m'} & H_{+-}^{m'} & H_{++}^{m'} \end{pmatrix} = \begin{pmatrix} \epsilon_0 & 0 & 0 \\ 0 & \epsilon_- & 0 \\ 0 & 0 & \epsilon_+ \end{pmatrix}, \tag{9.18}$$

with on-fragment energies ϵ_ζ, and the vanishing off-diagonal terms indicating that fragments are not allowed to change their charge state independently of their neighbors in this description. The fragment-fragment interaction term $\hat{V}_{m,m'}$ is,

$$\hat{V}_{m,m'} = \begin{pmatrix} -V_{00} & -V_{0-} & -V_{0+} \\ -V_{-0} & -V_{--} & -V_{-+} \\ -V_{+0} & -V_{+-} & -V_{++} \end{pmatrix}, \tag{9.19}$$

where the matrix elements $V_{\zeta,\zeta'}$ are the interaction between a fragment in charge state ζ and its neighbor in charge state ζ'.

Inserting equations (9.18) and (9.19) into (9.17) yields a system of three equations for the charge state amplitudes C_m^ζ,

$$\begin{aligned} EC_m^0 = &- V_{0+}C_{m-1}^+ - V_{00}C_{m-1}^0 - V_{0-}C_{m-1}^- \\ &- V_{0+}C_{m+1}^+ - V_{00}C_{m+1}^0 - V_{0-}C_{m+1}^- + \epsilon_0 C_m^0, \end{aligned} \tag{9.20}$$

$$\begin{aligned} EC_m^- = &- V_{-+}C_{m-1}^+ - V_{-0}C_{m-1}^0 - V_{--}C_{m-1}^- \\ &- V_{-+}C_{m+1}^+ - V_{-0}C_{m+1}^0 - V_{--}C_{m+1}^- + \epsilon_- C_m^-, \end{aligned} \tag{9.21}$$

$$\begin{aligned} EC_m^+ = &- V_{++}C_{m-1}^+ - V_{+0}C_{m-1}^0 - V_{+-}C_{m-1}^- \\ &- V_{++}C_{m+1}^+ - V_{+0}C_{m+1}^0 - V_{+-}C_{m+1}^- + \epsilon_+ C_m^+. \end{aligned} \tag{9.22}$$

Equations (9.20), (9.21), and (9.22) should be compared with equation (7.5) for the one-electron Schrödinger equation for the tight-binding Hamiltonian. The structure describes the evolution of a state amplitude, formerly C_m giving the amplitude for an electron on the mth site, and now C_m^ζ gives the amplitude that the mth site

carries a charge ζ. Formerly, there were N possible states for the system, describing the number of ways an electron can occupy the N sites. Now there are $3N$ possible states, corresponding to the $3N$ ways to excite the system by charging one of the sites. The Hilbert space is greatly contracted from the 2^N possible states of the Hubbard, and at best represents the Hubbard model in a mean-field approximation. How to express such a mean-field theory remains to be seen, and is the subject of current research. Leaving that issue aside, let us move onward to address several observables,

- Energy eigenvalues
- Current on a ring
- Net charge of the system

9.2.1 Energy Eigenvalues

Having reached the limit of what can be gleaned in site space, let us make a discrete Fourier transform (cf. section 7.5),

$$\begin{aligned} i\hbar\dot{C}_k^0 = &-(V_{0+}C_k^+ + V_{00}C_k^0 + V_{0-}C_k^-)e^{ik} \\ &-(V_{0+}C_k^+ + V_{00}C_k^0 + V_{0-}C_k^-)e^{-ik} + \epsilon_0 C_k^0, \end{aligned} \tag{9.23}$$

$$\begin{aligned} i\hbar\dot{C}_k^- = &-(V_{-+}C_k^+ + V_{-0}C_k^0 + V_{--}C_k^-)e^{ik} \\ &-(V_{-+}C_k^+ + V_{-0}C_k^0 + V_{--}C_k^-)e^{-ik} + \epsilon_- C_k^-, \end{aligned} \tag{9.24}$$

$$\begin{aligned} i\hbar\dot{C}_k^+ = &-(V_{++}C_k^+ + V_{+0}C_k^0 + V_{+-}C_k^-)e^{ik} \\ &-(V_{++}C_k^+ + V_{+0}C_k^0 + V_{+-}C_k^-)e^{-ik} + \epsilon_+ C_k^+, \end{aligned} \tag{9.25}$$

where k has once again been taken to be dimensionless by letting $ka \to k$. Taking the familar ansatz, $C_k^\zeta(t) = C_{0k}^\zeta e^{-\frac{iEt}{\hbar}}$, the three equations above become,

$$(\epsilon_0 - E)C_k^0 - 2\cos k(V_{0+}C_k^+ + V_{00}C_k^0 + V_{0-}C_k^-) = 0, \tag{9.26}$$

$$(\epsilon_- - E)C_k^- - 2\cos k(V_{-+}C_k^+ + V_{-0}C_k^0 + V_{--}C_k^-) = 0, \tag{9.27}$$

$$(\epsilon_+ - E)C_k^+ - 2\cos k(V_{++}C_k^+ + V_{+0}C_k^0 + V_{+-}C_k^-) = 0, \tag{9.28}$$

which may be expressed in matrix form as,

$$\begin{pmatrix} (\epsilon_0 - E) - 2V_{00}\cos k & -2V_{0-}\cos k & -2V_{0+}\cos k \\ -2V_{-0}\cos k & (\epsilon_- - E) - 2V_{--}\cos k & -2V_{-+}\cos k \\ -2V_{+0}\cos k & -2V_{+-}\cos k & (\epsilon_+ - E) - 2V_{++}\cos k \end{pmatrix} = 0. \tag{9.29}$$

Taking the determinant of (9.29) equal to zero gives the following characteristic equation,

$$\begin{aligned} &(E - \epsilon_- + 2V_{--}\cos k)\times \\ &\left[(E - \epsilon_0 + 2V_{00}\cos k)(E - \epsilon_+ + 2V_{++}\cos k) - 4V_{0+}V_{+0}\cos^2 k\right] + \\ &(4V_{-+}\cos^2 k)\left[V_{+-}(\epsilon_0 - E) + 2(V_{0-}V_{+0} - V_{00}V_{+-})\cos k\right] + \\ &(4V_{-0}\cos^2 k)\left[V_{0-}(\epsilon_+ - E) + 2(V_{0+}V_{+-} - V_{0-}V_{++})\cos k\right] = 0. \end{aligned} \tag{9.30}$$

While unwieldy, this expression is easily solved using computer algebra software. In this case, Mathematica was used.

9.2.2 Matrix Elements of the Fragment Hamiltonian

Before examining the solutions of equation (9.30), an aside on the components of the Fragment Hamiltonian. The Hamiltonian matrix in k-space $\tilde{H}$ may be extracted from equation (9.29) as,

$$\tilde{H} = \begin{pmatrix} \epsilon_0 & 0 & 0 \\ 0 & \epsilon_- & 0 \\ 0 & 0 & \epsilon_+ \end{pmatrix} + -2\begin{pmatrix} V_{00} & V_{0-} & V_{0+} \\ V_{-0} & V_{--} & V_{-+} \\ V_{+0} & V_{+-} & V_{++} \end{pmatrix}\cos k. \tag{9.31}$$

As mentioned previously, this formulation of the Fragment Hamiltonian has some features in common with the Hubbard Hamiltonian. For example, the on-site repulsion term in the Hubbard model, $U_{\text{hub}} = E_I - \mathcal{E} = E(\text{anion}) + E(\text{cation}) - 2E(\text{neutral})$ has an analog in the Fragment Hamiltonian, where $U_{\text{FH}} = \epsilon_- + \epsilon_+ - 2\epsilon_0$. We also believe that the matrix elements $V_{\zeta\zeta'}$ correspond to transitions between bands, these bands being analogous to the upper and lower Hubbard bands.

9.2.3 The Fragment Hamiltonian Band Structure

Samples of the numerical solutions to equation (9.30) for some different sets of parameters will now be presented. In Figure 9.1, a plot of the dispersion and the corresponding DOS appears for some baseline parameter values which are listed. Since

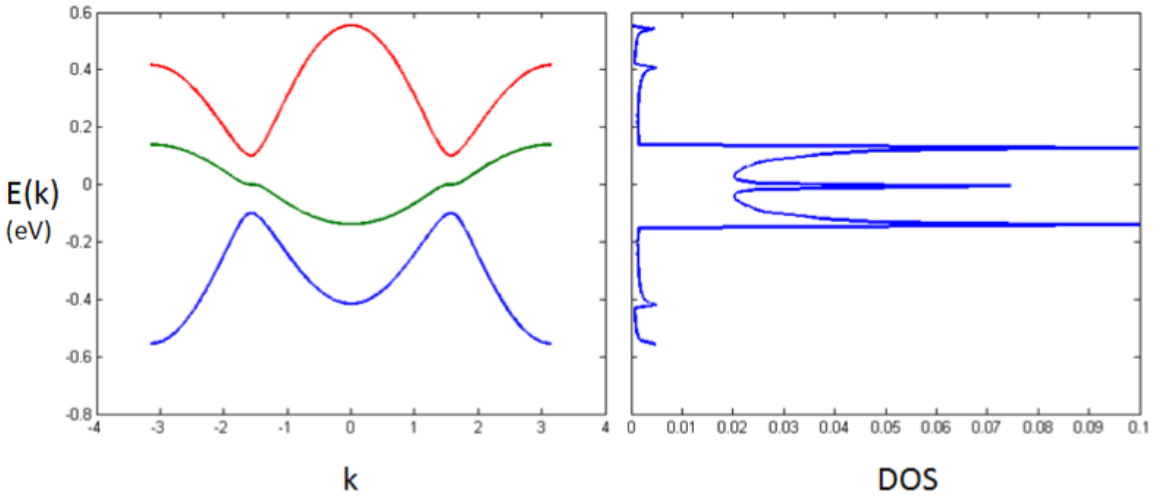

$$\epsilon_+ = 0.1 \qquad V_{00} = V_{++} = V_{--} = 0$$
$$\epsilon_0 = 0 \qquad V_{0+} = V_{+0} = V_{0-} = V_{-0} = 0.1$$
$$\epsilon_- = -0.1 \qquad V_{+-} = V_{-+} = -0.2$$

Figure 9.1: A sample of the dispersion curves and DOS for the Fragment Hamiltonian modeled on a 1D chain. For this choice of parameters, the bands do not cross.

(9.30) is cubic in $E(k)$, three bands appear. For this particular choice of parameters, the bands never actually cross, but there is a small amount of energetic overlap.

A second example is presented in Figure 9.2. The values of the parameters represented in these plots were chosen more aggressively, such that the bandgaps have closed.

The important question to ask is, "What is the meaning of these bands?" Are they analogous to bands for non-interacting electrons in the tight-binding model, the bands that arise when there is a lattice with a basis (such as in section 7.5)? If so, do we think of the charge on a site as being a fermion? How many charged sites are there at $0K$? Presumably, at $T = 0$, everything is neutral on average, but these

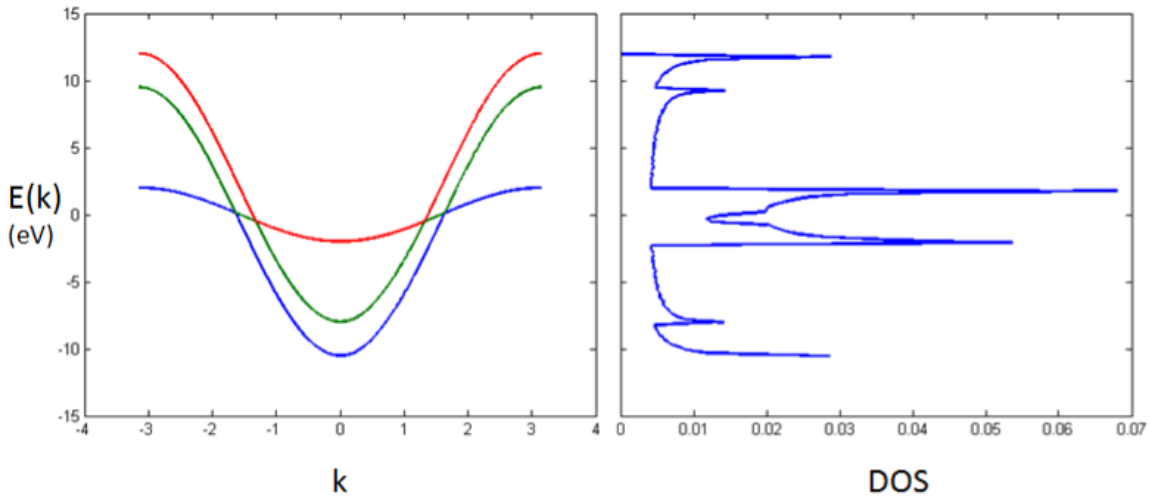

$$\epsilon_+ = 2.0 \qquad V_{00} = 1.0$$

$$\epsilon_0 = 0 \qquad V_{++} = V_{--} = 5.0$$

$$\epsilon_- = -0.5 \qquad V_{0+} = V_{+0} = V_{0-} = V_{-0} = 0.05$$

$$V_{+-} = V_{-+} = -0.1$$

Figure 9.2: A sample of the dispersion curves and DOS for the Fragment Hamiltonian modeled on a 1D chain. The choice of parameters was made for this case such that the bandgaps close.

changes represent quantum fluctuations which allow the system to lower its energy. The ground state is thus the lowest possible state formed in the three-band manifold, and occurs at $k = 0$ in the lowest band.

Another issue has to do with the overall charge in the system. An eigenvalue $E(k)$ corresponds to a state amplitude C_k composed of a linear combination of C_k^+, C_k^0, and C_k^-, which in turn correspond to the amplitudes for charging the sites m. The charge in the system can be calculated by introducing the (dimensionless) charge operator,

$$\hat{Q} = \sum_m \left(|m^+\rangle\langle m^+| - |m^-\rangle\langle m^-| \right). \tag{9.32}$$

The expectation value of this operator in a state,

$$|\psi\rangle = C_k^+|\psi_k^+\rangle + C_k^0|\psi_k^0\rangle + C_k^-|\psi_k^-\rangle \tag{9.33}$$

is exactly what one would anticipate,

$$Q_k = \langle\psi|\hat{Q}|\psi\rangle = |C_k^+|^2 - |C_k^-|^2. \tag{9.34}$$

If this is not zero, one can always make the system neutral overall by introducing a uniform background of compensating charge $-Q_k$. The difficulty comes when we look at the response of the system to an external perturbation. We will find it necessary to bring in different amounts of compensatory charge for different magnetic fields, which requires bringing in the chemical potential and looking at the free energy.

9.3 Chemical Potential and Variational Methods

The FH set of basis states does not in general maintain a constant charge. That is, if you assume a trial wavefunction,

$$|\psi\rangle = \sum_m \left(C_m^+|\psi_m^+\rangle + C_m^0|\psi_m^0\rangle + C_m^-|\psi_m^-\rangle \right), \tag{9.35}$$

then, as you vary the coefficients to find the lowest value for $\langle H\rangle$, one finds that $\langle Q\rangle$ changes. While this is an annoyance if our intent is to describe a system at constant Q, it is not without precedent to encounter this type of thing in a variational scheme.

For example, in Schrieffer's variational approach to the problem of superconductivity (BCS theory) [93], he took a trial wavefunction that did not conserve the number of electrons as its parameters were varied. Rather than search for an alternate method of solution, he chose to minimize the auxiliary quantity,

$$F = \langle H - \mu N \rangle. \tag{9.36}$$

This "Lagrange multiplier scheme" may be used to enforce charge conservation. To this end, we will minimize the free energy,

$$\langle F \rangle = \frac{\langle H - \mu Q \rangle}{\langle \psi | \psi \rangle}. \tag{9.37}$$

The normalization $\langle \psi | \psi \rangle$ can be imposed by introducing an additional Lagrange multiplier E to the auxiliary function,

$$\langle \tilde{F} \rangle = \langle F \rangle - E_F \langle \psi | \psi \rangle = \langle \psi | H - \mu Q - E_F | \psi \rangle. \tag{9.38}$$

Varying $\langle \tilde{F} \rangle$ with respect to the expansion coefficients C_m^ζ leads to the same set of coupled equations as (9.20)-(9.22), with the addition of the chemical potential to preserve charge, as we will see.

9.4 Current on a Ring in the Fragment Hamiltonian Model

In order to make contact with the results from Chapter 8, we will now examine the current carrying behavior of the FH model on a ring.

Consider a large ring of m identical fragments. In the presence of a magnetic field, the charges pick up phase ϕm corresponding to how far around the ring they have traveled (see Figure 8.2). The wavefunctions acquire a phase,

$$\begin{aligned} \Psi_m^+ &\to \Psi_m^+ e^{2i\phi m}, \\ \Psi_m^0 &\to \Psi_m^0 e^{i\phi m}, \\ \Psi_m^- &\to \Psi_m^-. \end{aligned}$$

In k-space, these amplitudes become

$$\Psi^+_{k+2\phi} = \sum_m e^{i(k+2\phi)m}\Psi^+_m,$$
$$\Psi^0_{k+\phi} = \sum_m e^{i(k+\phi)m}\Psi^0_m,$$
$$\Psi^-_k = \sum_m e^{ikm}\Psi^-_m.$$

The Hermitian charge operator $\hat{Q}$ defined in equation (9.32) has an expectation value in the state

$$|\psi\rangle = C^+_{k+2\phi}|\psi^+_{k+2\phi}\rangle + C^0_{k+\phi}|\psi^0_{k+\phi}\rangle + C^-_k|\psi^-_k\rangle \tag{9.39}$$

that is what one would expect it to be, namely,

$$\langle\psi|\hat{Q}|\psi\rangle = |C^+_{k+2\phi}|^2 - |C^-_k|^2. \tag{9.40}$$

Setting the variation $\delta\langle\tilde{F}\rangle = 0$ gives the following set of equations,

$$\begin{pmatrix} (\epsilon_+ - \mu - E_F) & 0 & 0 \\ 0 & (\epsilon_0 - E_F) & 0 \\ 0 & 0 & (\epsilon_- + \mu - E_F) \end{pmatrix} \begin{pmatrix} C^+_{k+2\phi} \\ C^0_{k+\phi} \\ C^-_k \end{pmatrix} + 2\cos(k+\phi) \begin{pmatrix} -V_{++} & -V_{+0} & -V_{+-} \\ -V_{0+} & -V_{00} & -V_{0-} \\ -V_{-+} & -V_{-0} & -V_{--} \end{pmatrix} \begin{pmatrix} C^+_{k+2\phi} \\ C^0_{k+\phi} \\ C^-_k \end{pmatrix} = 0. \tag{9.41}$$

We set the determinant of this matrix to zero and look for the lowest eigenvalues $E(k,\phi)$. This eigenvalue is the lowest value of the free energy, $F = H - \mu Q$.

The current response of the system is what we are after. Define the current at constant charge Q as,

$$I_Q = \left(\frac{\partial\langle H\rangle}{\partial\phi}\right)_Q = \left(\frac{\partial E_H}{\partial\phi}\right)_Q, \tag{9.42}$$

where E_H are the eigenvalues of H (as opposed to E_F, which are the eigenvalues of the auxiliary quantity F). Also define the current at constant chemical potential μ

as,

$$I_\mu = \left(\frac{\partial\langle F\rangle}{\partial\phi}\right)_\mu = \left(\frac{\partial E_F}{\partial\phi}\right)_\mu . \tag{9.43}$$

We would like to know the value of I_Q, but in order to constrain the charge in the system to be constant, we are forced to work with the eigenvalues E_F. Given knowledge of the values E_F, how does one find I_Q? First, note that the charge Q is given by,

$$Q = \left(\frac{\partial F}{\partial\mu}\right)_\phi , \tag{9.44}$$

which gives us a relation between Q, μ, and ϕ. This allows us to find,

$$\mu = \mu(Q,\phi), \tag{9.45}$$

as a function of Q and ϕ. Making a formal Legendre transformation to H,

$$H(Q,\phi) = F(\mu(Q,\phi),\phi) + Q\mu(Q,\phi). \tag{9.46}$$

Finally, let us take a derivative with respect to ϕ at constant Q, which gives,

$$\begin{aligned} I_Q = \left(\frac{\partial\langle H\rangle}{\partial\phi}\right)_Q &= \left(\frac{\partial\langle F\rangle}{\partial\phi}\right)_\mu + \left(\frac{\partial\langle F\rangle}{\partial\mu}\right)_\phi \left(\frac{\partial\mu}{\partial\phi}\right)_Q + Q\left(\frac{\partial\mu}{\partial\phi}\right)_Q \\ &= I_\mu + \left(\frac{\partial\mu}{\partial\phi}\right)_Q \left[\left(\frac{\partial\langle F\rangle}{\partial\mu}\right)_\phi + Q\right] = I_\mu, \end{aligned} \tag{9.47}$$

since the term in square brackets is zero.

With the result $I_Q = I_\mu$ in hand, the next step is to seek a numerical solution to $I_\mu = \left(\frac{\partial E_F}{\partial\phi}\right)_\mu$. To that end, we tabulate values of $E_F(\mu,\phi)$, choosing the lowest value of E_F at each step to be the ground state. In addition, for a given value of ϕ, μ is found such that Q remains constant. We then calculate an accompanying list $E_F(\mu,\phi+\delta\phi)$ while not changing the values of μ. Finally, a numerical derivative is taken,

$$I_\mu(\mu,\phi) = \frac{E_F(\mu,\phi+\delta\phi) - E_F(\mu,\phi)}{\delta\phi}. \tag{9.48}$$

At each value of ϕ, the value of k must be chosen corresponding to the lowest energy eigenvalue. Since these eigenvalues are a function of $\cos(k+\phi)$, as ϕ is increased, the value of k will change periodically to keep the system in the ground state. For

the case of a two-site ring, the only allowed values of k are 0 and π, since $k = \frac{2\pi n}{N}$, where N is the number of sites. At $\phi = \frac{\pi}{2}$, the value of k changes, resulting in a step as pictured in Figure 9.3. The oscillatory behavior of the current in Figure 9.3 resem-

$$\epsilon_+ = U_{\mathrm{FH}}$$
$$\epsilon_0 = 0$$
$$\epsilon_- = \frac{U_{\mathrm{FH}}}{2}$$
$$V_{00} = 0.5$$
$$V_{++} = V_{--} = 0.8$$
$$V_{0+} = V_{+0} = V_{0-} = V_{-0} = 0.1$$
$$V_{+-} = V_{-+} = 0.1$$

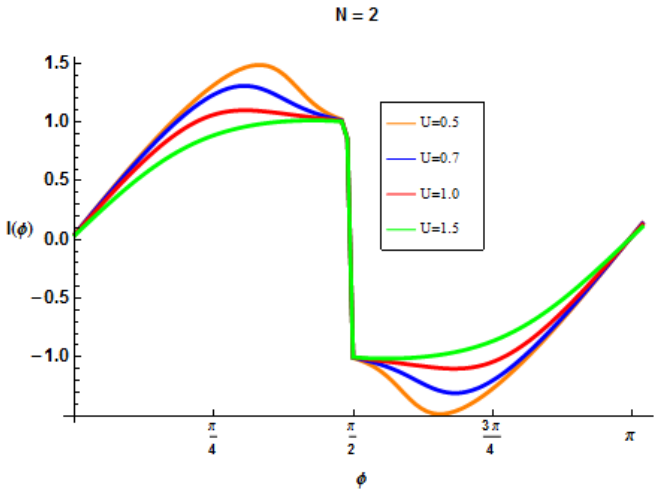

Figure 9.3: The current on a two-site FH ring for the parameters listed. As ϕ is increased, the value of k which corresponds to the lowest energy eigenvalue changes, resulting in a step in the current. This plot displays several curves, parametrized by values of U_{FH} given in the legend. As U_{FH} increases, the maximum value of the current decreases.

bles that of Hubbard ring in Figure 8.4. Note that the behavior as a function of U_{FH} also resembles that of the Hubbard ring, in that the current falls off as U_{FH} increases relative the the fixed parameters $V_{\zeta,\zeta'}$. The current appears to tend asymptotically toward a nonzero maximum value as U_{FH} gets larger, however, unlike the Hubbard case. It is unclear as to why this happens, as the relationship between U_{FH} and the interaction terms $V_{\zeta,\zeta'}$ is not completely understood.

An interesting behavior arises when the size of the ring is increased. As more sites are added to the ring, the shape of the current $I(\phi)$ approaches a sawtooth, pictured in Figure 9.4. When there are a larger number of sites in the ring, there are a larger number of available k-values. This causes the current to step more frequently. The maximum magnitude of the current is also lower than in the two-site case, as the amount the current is allowed to rise between steps decreases as the steps become more frequent.

$$\epsilon_+ = U_{\mathrm{FH}}$$
$$\epsilon_0 = 0$$
$$\epsilon_- = \frac{U_{\mathrm{FH}}}{2}$$
$$V_{00} = 0.5$$
$$V_{++} = V_{--} = 0.8$$
$$V_{0+} = V_{+0} = V_{0-} = V_{-0} = 0.1$$
$$V_{+-} = V_{-+} = 0.1$$

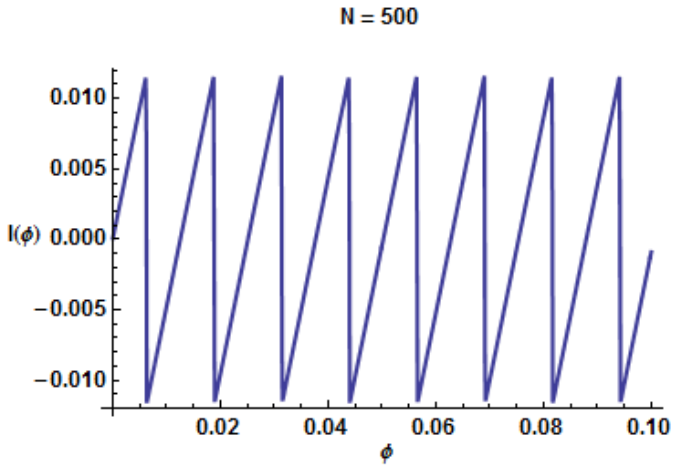

Figure 9.4: The current on an FH ring of 500 sites for the parameters listed. As more sites are added, there are more allowed values of k, which in turn causes the current to step more frequently. Note that the range of ϕ is only 0.1 in this plot, indicating that the current is highly oscillatory.

9.5 Discussion of the Fragment Hamiltonian and Hubbard Results

The behavior exhibited by the two-site ring in both the Hubbard and FH cases is interesting in light of the solution found by Lieb and Wu for an infinite 1D chain [79]. They concluded that, for an infinite chain, any nonzero value of U_{hub} results in an insulating stated. However, the two site ring in both the Hubbard and FH cases carries a current for nonzero U_{hub} and U_{FH}, respectively. When the FH chain is extended to a large number of sites, as in Figure 9.4, the maximum magnitude of the current at constant U_{FH} decreases, as $I(\phi)$ is highly oscillatory. Extrapolating from this trend, the current will vanish as the number of sites becomes infinite, and it seems that fragment-chain description agrees with the Lieb and Wu solution as the size of the chain becomes very large. Due to limitations in the numerical method, determining the current on a large chain at $U_{\mathrm{FH}} = 0$ to check the agreement with Lieb and Wu has not yet been done. Such a result remains a topic of near-term research.

In this thesis, the FH model was employed in a tight-binding-like fashion, and displayed some similarities to analogous tight-binding systems, although there is still much to be developed about the FH model. It was demonstrated that, once the issue

charge conservation is addressed, the FH model exhibits a current-carrying behavior similar to that of the Hubbard model for small systems. Something which remains elusive, however, is a description of a metal-insulator transition. On the two-site ring, the Hubbard model lacks an abrupt, discontinuous phase transition that Mott submitted was a possibility [47]. For the FH model on two sites, no metal-insulator transition was found for the parameter ranges that were examined. That being said, the parameter space is large, and the exact meanings behind the matrix elements in the tight-binding-like formulation of the Fragment Hamiltonian are not completely understood.

Something interesting which may bear investigating is the relationship between the current calculated in this chapter for the FH model, and the "charge stiffness" presented by Kohn [84] [85]. The slope of the current $\frac{\partial I(\phi)}{\partial \phi}$ in Figures 9.3 and 9.4 corresponds to the diamagnetic susceptibility $\frac{\partial^2 E(B)}{\partial B^2}$ in equation (8.8). It may very well be that there is a particular configuration of the system for which this value vanishes, indicating a metal-insulator transition.

It may turn out in the future that a tight-binding approach is not the most appropriate way to employ the Fragment Hamiltonian. The generality of the formalism leaves it flexible to be used by more than one description. It has demonstrated some interesting behavior in a tight-binding-like system, however, and the author hopes that this thesis may inform the further development of the model.

10

Concluding Thoughts

The overarching theme of this dissertation has been charge transport, discussed in two rather different contexts. Another theme running through this thesis is that of correlation. The difference in transport mechanisms being emphasized in Parts 1 and 2 serves to underscore how considering different types and ranges of correlation reveals interesting behavior within a system. Electron-electron correlations occur between electrons on the same atom, between electrons on different nearby atoms, and between electrons far from one another within a system. In this thesis systems that were discussed include correlations spanning this gamut.

In Part 1, the discussion was focused on hopping charge transport in disordered organic solids. Such a system is described in terms of the local molecular orbitals of sites which an electron may occupy. The energies of these orbitals are in large part a result of a long-range classical charge-dipole interaction. In a real system there are certainly electron correlations within the molecular wavefunction, e.g. exchange and Coulomb correlation between electrons in different orbitals below the HOMO of the site. These do not appear explicitly in such a hopping treatment, but rather the net effect of these correlations is represented by site occupation energies which correspond to some statistical distribution. It is important to note that the word 'correlation' can have different meanings in different contexts. Unfortunately, we use the term "correlation" to mean two different things in this thesis, which can be confusing. In the case of spatially correlated energetic disorder, the energies of the occupation sites are correlated to those of nearby sites as a result of a charge's interaction with the

field arising from the contributions of the fixed net dipole moments of all the other sites. This spatial correlation of site energies uses the word in a different context.

The problem we solve is one of electron-hole dissociation, where the electron and hole are both able to move about under the influence of the field of the the other. Because this is a two-body problem, there is a temptation to rewrite the problem from the center of mass frame of reference, so that it looks as though one body is moving in the field of the other. While this is possible in the absence of disorder (and is what Onsager did, and what we did for the non-disordered case on a lattice), once the disorder is introduced, such that the charges see opposite energy landscapes, it is no longer possible to reduce it to a one-body problem. We must track both moving charges. Defining a "strongly-correlated" electron system as one that cannot be reduced to a one-body problem [94], such a system of an electron and hole might be thought of as strongly-correlated, even though it is a classical diffusive hopping problem, and not a quantum mechanical one.

In Part 2, we turned aside from classical calculations, and looked at fully quantum systems of more than one electron moving on a lattice. We focused on the 1D problem, which amounts to a description of electrons moving on a chain of atoms. Here we were interested in the current-carrying behavior of several tight-binding type systems where Coulomb interactions could not be described by a mean-field approach. In a system described using a basis of Bloch states, the electrons are noninteracting, and much of the electronic correlation is neglected. The simplest case which accounts for electron-electron correlations that was introduced in Part 2 is the Hubbard model. In the Hubbard model the Coulomb correlation between electrons which share the same site is mediated by the Hubbard U. This correlation is as local as possible, only appearing as an on-site interaction. Such a local interaction is already enough to give rise to a global effect, in this case the splitting of a single energy band into an upper and lower Hubbard band, and the appearance of an insulating state. Accounting for this type of electron-electron is important to the dynamics of the system. If one were to consider the two-site ring in terms of a mean field description, i.e. each electron sees the average field of the other, one would have a degenerate dimer, and the effect of U would be lost. Allowing both electrons to occupy the same site, which is energetically unfavorable, allows for nontrivial transport. This requires that we keep track of both electrons relative to one another, rather than merely considering one electron at a

time.

The crux of Part 2 was the treatment of the Fragment Hamiltonian cast in a tight-binding-like way. The FH model does the most accounting for electron correlations of the models examined in this thesis. It represents on-site correlations in terms of the charge state energies of a fragment, ϵ_ζ, which we have demonstrated are analogous to the on-site Coulomb interaction in the Hubbard model. The FH formalism is distinct from the other models studied in this thesis in that it has an inter-fragment correlation, represented by the terms $V_{\zeta,\zeta'}$. In the Hubbard model there are transition terms V take an electron between adjacent sites. In the FH model, the terms $V_{\zeta,\zeta'}$ are dependent on the relative charge states of interacting fragments (taken to be nearest neighbors in this thesis, but does not have to be the case in general). This Coulomb correlation between different charge states gives rise to behavior similar to, but richer than, that in the Hubbard model. Rather than tracking the correlation between electrons, a fragment-fragment correlation arises due to the Coulomb interaction between fragments in various charge states. Exploring these charge state interactions is an exciting prospect for research in the near future.

The models examined in this dissertation were simple approximations of complicated physical systems, but some essential behavior was deduced nonetheless. The author hopes that a better fundamental understanding of charge transport in these systems will be useful to their future development.

11

Appendices

Appendix A

Electronegativity

A cornerstone concept in the study of charge transfer is that of electronegativity, which represents the tendency of an atom or molecule to attract electrons. The concept of electronegativity was first proposed in 1932 by Linus Pauling [95] as an explanation of the fact that given two atomic species A and B, the bond $(A-B)$ is stronger than expected if one simply takes the average of the strengths of the $(A-A)$ and $(B-B)$ bonds. The Pauling electronegativity $\chi_{Pauling}$ is a dimensionless relative quantity defined by the difference

$$\chi_{Pauling} = \chi_A - \chi_B = \frac{1}{\sqrt{eV}}\sqrt{E_d(AB) - \frac{E_d(AA) + E_d(BB)}{2}}, \tag{A.1}$$

where E_d is the energy required to dissociate the pair indicated. Since this is a relative quantity, a reference point must be set before a scale can be constructed. Pauling used hydrogen, since it is common and involved in many chemical reactions. Once this reference point was set, the electronegativity of the rest of the elements could be expressed in terms of their difference from hydrogen. Bromine, for example, has a Pauling electronegativity of 0.73, since $E_d(H,Br) = 3.79$ eV, $E_d(H,H) = 4.52$ eV, and $E_d(Br,Br) = 2.00$ eV. This definition is semi-empirical, and requires one to apply a bit of physical intuition to things such as the selection of signs. For example, hydrogen bromide dissolves in water to form H^+ and Br^-, indicating that bromine is more electronegative than hydrogen and that a positive sign should be chosen accordingly.

In 1934 Robert Mulliken published a paper [96] presenting a definition which has been called "absolute electronegativity" [97]. Consider a molecule formed from two atomic species A and B. Mulliken expressed the wavefunction of the molecule in terms of a superposition of the charge states of A and B,

$$\psi_{AB} = \gamma\psi(A^0B^0) + \alpha\psi(A^+B^-) + \beta\psi(A^-B^+), \tag{A.2}$$

where γ, α, and β are unknown coefficients. Quoting Pauling [95], Mulliken states "if the two atoms have the same degree of electrongativity... the terms corresponding to A^+B^- and A^-B^+ will occur with the same coefficient", which is to say that $\alpha = \beta$. He then submits that in the event

$$E_{IA} - \mathcal{E}_B = E_{IB} - \mathcal{E}_A, \tag{A.3}$$

one expects that $\alpha = \beta$, and thus that $\chi_A = \chi_B$. E_I is the ionization energy, or the energy required to remove an electron from the atom. $\mathcal{E}$ is the electron affinity, the energy change when an electron is added to a neutral atom to form a negative ion. In the case that (A.3) is true, then it is also true that

$$E_{IA} + \mathcal{E}_A = E_{IB} + \mathcal{E}_B. \tag{A.4}$$

Mulliken suggests that this allows one to define the absolute electronegativity as

$$\chi = \frac{E_I + \mathcal{E}}{2}, \tag{A.5}$$

where both sides of equation (A.4) were divided by 2 for practical convenience. It seems intuitive that the electronegativity would be the average of two quantities, but there is no analytical reason to believe that factor in particular is correct. Mulliken validates the form of (A.5) by instead comparing to empirical data, which agrees well with the choice. The Pauling and Mulliken definitions of electronegativity are the two most commonly used.

Appendix B

Proof for the Allowed Values of the Bloch Vector $\vec{k}$

Consider the discrete Fourier transform of the occupation amplitudes C_m on a 1D tight-binding lattice with N sites.

$$C_k = \sum_m C_m e^{ikm} \tag{B.1}$$

Its inverse transform is

$$C_m = \frac{1}{2N+1} \sum_{k=-N}^{N} C_k e^{-ikm}. \tag{B.2}$$

Inserting (B.1) into (B.2), we have

$$\begin{aligned} C_m &= \frac{1}{2N+1} \sum_k e^{-ikm} \sum_{n'} e^{ikn'} C_{n'}. \\ &= \sum_{n'} C_{n'} \left(\frac{1}{2N+1} \sum_k e^{-ik(m-n')} \right) \end{aligned} \tag{B.3}$$

It must be true that the quantity in parenthesis is a Kronecker delta $\delta_{m,n'}$. To satisfy this, let

$$k = \frac{2\pi n}{2N+1}, \tag{B.4}$$

and define the quantity in parenthesis in equation (B.3) to be

$$S = \frac{1}{2N+1} \sum_{n=-N}^{N} e^{-i\frac{2\pi n}{2N+1}(m-n')} \tag{B.5}$$

Note that

$$\begin{aligned} Se^{-i\frac{2\pi}{2N+1}(m-n')} &= \frac{1}{2N+1} \sum_{n=-N}^{N} e^{-i\frac{2\pi(n+1)}{2N+1}(m-n')} = \frac{1}{2N+1} \sum_{n''=-N+1}^{N+1} e^{-i\frac{2\pi(n'')}{2N+1}(m-n')} \\ &= S - \frac{1}{2N+1} e^{i\frac{2\pi N}{2N+1}(m-n')} + \frac{1}{2N+1} e^{-i\frac{2\pi(N+1)}{2N+1}(m-n')}, \end{aligned} \tag{B.6}$$

which leads to

$$S\left(e^{-i\frac{2\pi}{2N+1}(m-n')} - 1\right) = \frac{1}{2N+1}\left(e^{-i\frac{2\pi(N+1)}{2N+1}(m-n')} - e^{i\frac{2\pi N}{2N+1}(m-n')}\right). \tag{B.7}$$

From this point, we get

$$\begin{aligned} &Se^{-i\frac{\pi(m-n')}{2N+1}}\left(2i\sin\left(\frac{\pi(m-n')}{2N+1}\right)\right) \\ &= \frac{1}{2N+1} e^{-i\frac{\pi(m-n')}{2N+1}} 2i\sin\left(\frac{2\pi(N+\frac{1}{2})(m-n')}{2N+1}\right). \end{aligned} \tag{B.8}$$

Cancelling several terms across both sides, we get an expression for S

$$S = \frac{\sin\left(\pi(m-n')\right)}{(2N+1)\sin\left(\frac{\pi(m-n')}{2N+1}\right)}. \tag{B.9}$$

For $m - n' \neq 0$, S vanishes. If $m - n'$ is any integer multiple of $2N+1$, $S = 1$. Thus, the Kronecker delta requirement is satisfied, and in addition

$$S = \sum_{n=-\infty}^{\infty} \delta_{(m-n'),n(2N+1)}. \tag{B.10}$$

Appendix C

The Kubo-Greenwood Conductivity

For most systems in condensed matter physics, the electrical conductivity is an important quantity. The following is a derivation for the Kubo-Greenwood formulae, which follows closely that found in Madelung's *Introduction to Solid State Theory*, section 8.3.4 [75].

C.1 Kubo Linear Response

First, define the expectation value $\langle f \rangle$ of an operator f as

$$\langle f \rangle = Tr[f\rho], \tag{C.1}$$

where ρ is the Boltzmann distribution normalized by the partition function Z, called the statistical operator

$$\rho = \frac{1}{Z} e^{\frac{H}{k_b T}} \quad , \quad Z = Tr[e^{\frac{H}{k_b T}}]. \tag{C.2}$$

The time derivative of ρ is the commutator

$$i\hbar\dot{\rho} = [H, \rho] \tag{C.3}$$

Let H be a sum of a zero-field Hamiltonian H_0 and a perturbation δH. For an electric field $\vec{E}$ applied to the system at time $t = -\infty$ and increased adiabatically to

some value at $t = 0$, we have

$$H = H_0 + \delta H = H_0 + \lim_{\alpha \to 0} \left(e\vec{E} \cdot \vec{r} e^{-i\omega t + \alpha t} \right) \quad , \quad \rho = \rho_0 + \delta\rho. \tag{C.4}$$

It is the perturbation $\delta\rho$ to the probability distribution which gives rise to a current. To linearize the equations of motion for ρ, we take

$$\begin{aligned} i\hbar\dot{\rho} = i\hbar(\dot{\rho}_0 + \delta\dot{\rho}) = i\hbar\delta\dot{\rho} &= [H_0 + \delta H, \rho_0 + \delta\rho] \\ &= [H_0, \rho_0] + [\delta H, \rho_0] + [H_0, \delta\rho] + [\delta H, \delta\rho]. \end{aligned} \tag{C.5}$$

Neglecting the quadratic terms of order $\delta H \delta\rho$, we get

$$i\hbar\delta\dot{\rho} = [\delta H, \rho_0] + [H_0, \delta\rho]. \tag{C.6}$$

To find $\delta\rho$, we define $\Delta\rho$ by shifting to the interaction picture

$$\delta\rho = e^{-\frac{i}{\hbar}H_0 t} \Delta\rho e^{\frac{i}{\hbar}H_0 t}. \tag{C.7}$$

Continuing to neglect quadratic perturbation terms, it follows that

$$\begin{aligned} i\hbar\Delta\dot{\rho} &= e^{\frac{i}{\hbar}H_0 t}[\delta H, \rho_0] e^{-\frac{i}{\hbar}H_0 t} \\ &= \lim_{\alpha \to 0} \left(e^{-i\omega t + \alpha t} e^{\frac{i}{\hbar}H_0 t} [e\vec{r}, \rho_0] e^{-\frac{i}{\hbar}H_0 t} \cdot \vec{E} \right). \end{aligned} \tag{C.8}$$

At $t = 0$, $\delta\rho$ and $\Delta\rho$ are the same, and at $t = -\infty$ they are both zero. Therefore, $\delta\rho$ is defined by the following integration

$$\delta\rho(t = 0) = -\frac{i}{\hbar} \lim_{\alpha \to 0} \left(\int_{-\infty}^{0} e^{-i\omega t + \alpha t} e^{\frac{i}{\hbar}H_0 t} [e\vec{r}, \rho_0] e^{-\frac{i}{\hbar}H_0 t} \cdot \vec{E} dt \right). \tag{C.9}$$

Using equation (C.9) to find the current density j, we have

$$\langle \vec{j} \rangle = Tr[\vec{j}\delta\rho] = -\frac{i}{\hbar} \lim_{\alpha \to 0} \left(\int_{-\infty}^{0} e^{-i\omega t + \alpha t} Tr \left[\vec{j} e^{\frac{i}{\hbar}H_0 t} [e\vec{r} \cdot \vec{E}, \rho_0] e^{-\frac{i}{\hbar}H_0 t} \right] dt \right). \tag{C.10}$$

Since the conductivity tensor $\sigma_{\mu\nu}$ is given by

$$j_\mu = \sigma_{\mu\nu} E_\nu, \tag{C.11}$$

equation (C.10) tells us

$$\sigma_{\mu\nu} = \lim_{\alpha\to 0} \int_{-\infty}^{0} e^{-i\omega t + \alpha t} K_{\mu\nu} dt, \tag{C.12}$$

with

$$K_{\mu\nu} = -\frac{i}{\hbar} Tr\left[j_\mu e^{\frac{i}{\hbar}H_0 t} [e r_\nu, \rho_0] e^{-\frac{i}{\hbar}H_0 t} \right]. \tag{C.13}$$

We are nearly at the Kubo formula. Next, note that

$$\begin{aligned}
[r_\nu, \rho_0] &= \rho_0(\rho_0^{-1} r_\nu \rho_0 - r_\nu) = \rho_0 \left(e^{\frac{H_0}{k_b T}} r_\nu e^{-\frac{H_0}{k_b T}} - r_\nu \right) \\
&= \rho_0 \int_0^{\frac{1}{k_b T}} \frac{d}{d\lambda} \left(e^{\lambda H_0} r_\nu e^{-\lambda H_0} \right) d\lambda \\
&= \rho_0 \int_0^{\frac{1}{k_b T}} \frac{d}{d\lambda} \left(e^{\lambda H_0} [H_0, r_\nu] e^{-\lambda H_0} \right) d\lambda.
\end{aligned} \tag{C.14}$$

The commutator $[H_0, r_\nu]$ is the time derivative $-i\hbar\dot{r}_\nu$. Also note that $-e\dot{r}_\nu = j_\nu$. Then we have

$$[e r_\nu, \rho_0] = i\hbar\rho_0 \int_0^{\frac{1}{k_b T}} e^{\lambda H_0} j_\nu e^{-\lambda H_0} d\lambda, \tag{C.15}$$

and consequently

$$K_{\mu\nu} = \int_0^{\frac{1}{k_b T}} Tr\left[\rho_0 j_{mu} e^{\frac{i}{\hbar}H_0(t - i\hbar\lambda)} j_{nu} e^{-\frac{i}{\hbar}H_0(t - i\hbar\lambda)} \right] d\lambda. \tag{C.16}$$

The final step is to shift back from the interaction picture to the time-dependent current in the Heisenberg picture

$$j(t) = e^{\frac{i}{\hbar}Ht} \vec{j} e^{-\frac{i}{\hbar}Ht}. \tag{C.17}$$

Writing $\langle f \rangle = Tr[\rho_0 f]$ we arrive at

$$K_{\mu\nu} = \int_0^{\frac{1}{k_b T}} \langle j_{mu}(0) j_{nu}(t - i\hbar\lambda) \rangle d\lambda. \tag{C.18}$$

Equation (C.18) taken with equation (C.12) is the customary form of the Kubo formula.

C.2 The Kubo-Greenwood Formula

The Kubo Formula for conductivity is extremely general. The Kubo-Greenwood formula is a simplified form which is more relevant for the 1D tight-binding model. Let the current density $\langle j \rangle$ be defined by the current operator j_{op} as

$$\langle j \rangle = Tr[\rho j_{op}], \tag{C.19}$$

with

$$j_{op} = Re\left[-\frac{e\hbar}{iV_g m_e}\vec{\nabla}\right]. \tag{C.20}$$

V_g is the volume of the system (length in the 1D case). For a vector potential $\vec{A}$, the electric field is $\vec{E} = -\dot{\vec{A}}$, and H is

$$H = \frac{e}{m_e}\vec{A}\cdot\vec{p} = \frac{e\hbar}{im_e}\vec{A}\cdot\vec{\nabla} = -\frac{e\hbar}{m_e\omega}\vec{E}\cdot\vec{\nabla}, \tag{C.21}$$

assuming an electric field of the form $E = \lim_{\alpha\to 0} e^{-i\omega t+\alpha t}$. It was shown earlier in the text (Madelung [75], equation 3.53) that $\delta\rho$ has the form

$$\langle \Psi_{\epsilon'}|\delta\rho|\Psi_\epsilon\rangle = \frac{f(\epsilon') - f(\epsilon)}{\epsilon' - \epsilon - \hbar\omega - i\hbar\alpha}\langle \Psi_{\epsilon'}|H|\Psi_\epsilon\rangle, \tag{C.22}$$

where Ψ_ϵ is the electronic wavefunction for energy ϵ, and f is the Fermi-Dirac distribution function

$$f = \frac{1}{e^{(\epsilon-\mu)/k_bT}+1}. \tag{C.23}$$

The current density may be written explicitly as

$$\langle j \rangle = V_g^2 \int\int g(\epsilon)g(\epsilon')\langle \Psi_{\epsilon'}|\delta\rho|\Psi_\epsilon\rangle\langle \Psi_{\epsilon'}|j_{op}|\Psi_\epsilon\rangle d\epsilon d\epsilon'. \tag{C.24}$$

$g(\epsilon)$ is the density of states. Inserting equations (C.20), (C.21), and (C.22) into equation (C.19), we get for the ij-th component of the conductivity tensor

$$\sigma_{ij}(\omega) = Re\left[\lim_{\alpha\to 0}\frac{e^2\hbar^2 V_g}{i\omega m_e^2}\int\int g(\epsilon)g(\epsilon')\langle \Psi_{\epsilon'}|\frac{\partial}{\partial x_i}|\Psi_\epsilon\rangle\langle \Psi_\epsilon|\frac{\partial}{\partial x_j}|\Psi_{\epsilon'}\rangle\frac{f(\epsilon') - f(\epsilon)}{\epsilon' - \epsilon - \hbar\omega - i\hbar\alpha}d\epsilon d\epsilon'\right]. \tag{C.25}$$

Noting that

$$Re\left[\lim_{\alpha\to 0}\frac{1}{i}\frac{1}{\epsilon'-\epsilon-\hbar\omega-i\hbar\alpha}\right]=\pi\delta(\epsilon'-\epsilon-\hbar\omega), \tag{C.26}$$

it follows that

$$\sigma_{ij}(\omega)=\frac{e^2\hbar^2\pi V_g}{\omega m_e^2}\int g(\epsilon)g(\epsilon+\hbar\omega)\langle\Psi_{\epsilon+\hbar\omega}|\frac{\partial}{\partial x_i}|\Psi_\epsilon\rangle\langle\Psi_\epsilon|\frac{\partial}{\partial x_j}|\Psi_{\epsilon+\hbar\omega}\rangle(f(\epsilon+\hbar\omega)-f(\epsilon))d\epsilon. \tag{C.27}$$

In the limit that $omega \to 0$, we get the Kubo-Greenwood expression for the DC conductivity

$$\sigma=-\int\frac{e^2\hbar^2\pi V_g}{m_e^2}g(\epsilon)^2\left|\langle\Psi_\epsilon|\frac{\partial}{\partial x}|\Psi_\epsilon\rangle\right|^2\frac{\partial f}{\partial\epsilon}d\epsilon \tag{C.28}$$

C.3 Application to the Tight-Binding Model

For the 1D tight-binding model, we have

$$\epsilon=-2V\cos k\ \ \rightarrow\ \ k=\arccos\frac{-\epsilon}{2V} \tag{C.29}$$

and

$$g(\epsilon)=\frac{1}{2\pi}\frac{dk}{d\epsilon}=\frac{1}{2\pi V}\frac{1}{\sqrt{1-(\frac{-\epsilon}{2V})^2}} \tag{C.30}$$

Before continuing, note that the phase velocity $\vec{v}(k)$ is

$$\vec{v}(k)=\frac{1}{\hbar}\vec{\nabla}_k\epsilon_k=\frac{1}{\hbar}\frac{d}{dk}(-2V\cos k)=2V\sin k. \tag{C.31}$$

With that in hand, the factor $\langle\Psi_\epsilon|\frac{\partial}{\partial x}|\Psi_\epsilon\rangle$ becomes

$$\langle\Psi_\epsilon|\frac{\partial}{\partial x}|\Psi_\epsilon\rangle=\langle\Psi_\epsilon|\frac{-p}{i\hbar}|\Psi_\epsilon\rangle=\langle\Psi_\epsilon|\frac{-mv}{i\hbar}|\Psi_\epsilon\rangle=\frac{-m}{i\hbar}\sum_k\langle k|\frac{1}{\hbar}2V\sin k|k\rangle\langle k|k\rangle. \tag{C.32}$$

Finally, let's consider the term $\frac{\partial f}{\partial\epsilon}$. When referring to conductivity, the two broad categories a material may fall into are metal and insulator. These classifications are made at zero temperature, with a material being defined as a metal if it possesses a non-zero conductivity at $T=0K$, and an insulator otherwise. As such, let $T=0$. In

that case,

$$\frac{\partial f}{\partial \epsilon} = \delta(\epsilon - \epsilon_f) \tag{C.33}$$

where ϵ_f is the fermi energy. Putting all of these factors together, and making a change of variables to an integral over dk

$$\sigma = \frac{e^2\hbar^2\pi V_g}{m^2} \int \frac{1}{16\pi^2 V^2} \frac{1}{|\sin k|^2} \frac{4m^2V^2}{\hbar^4} |\sin k|^2 \delta(k - k_f) 2V \sin k dk \tag{C.34}$$

Quite a few things cancel, and the Dirac delta collapses the integral, leaving the final result

$$\sigma = \frac{V_g e^2 V}{2\pi\hbar^2} \sin k_f \tag{C.35}$$

The conductivity varies sinusoidally with the filling of the band. When the band is empty ($k_f = 0$), the conductivity vanishes. The conductivity peaks for a half filled band ($k_f = \frac{\pi}{2}$), and vanishes again when the band is full ($k_f = \pi$).

Appendix D

Current and the Feynman-Hellman Theorem

In this appendix, an expression for the current due to a charge undergoing circular motion in a magnetic field will be derived using the Feynman-Hellman theorem. The Feynman-Hellman theorem states

$$\frac{dE}{d\lambda} = \langle \Psi(\lambda) | \frac{dH}{d\lambda} | \Psi(\lambda) \rangle, \tag{D.1}$$

where E is the energy eigenvalue for state Ψ, H is the Hamiltonian, and λ is a parameter of interest.

Consider a charge in a magnetic field defined by a vector potential $\vec{A}$. For a uniform magnetic field in cylindrical coordinates,

$$\vec{A} = \frac{1}{2} r B_0 \hat{\phi}, \tag{D.2}$$

and the momentum $\vec{P}$ is

$$\vec{P} = -\frac{i\hbar}{r} \frac{\partial}{\partial \phi}. \tag{D.3}$$

The Hamiltonian is

$$H = \frac{\left(\vec{P} - e\vec{A}\right)^2}{2m_e}. \tag{D.4}$$

The time independent Schrödinger equation is

$$\frac{\left(\vec{P} - e\vec{A}\right)^2}{2m_e}|\Psi\rangle = E|\Psi\rangle. \tag{D.5}$$

Taking the ansatz $\Psi = e^{-im\phi}$ with m an integer due to obey periodicity, the energy eigenvalues for this system are

$$E_m = \frac{\hbar^2}{2m_e r^2}\left(m - \frac{eB_0 r^2}{2\hbar}\right)^2. \tag{D.6}$$

Note that as B_0 increases, one must choose m appropriately to remain in the ground state.

Next, we need a velocity operator. Note that

$$m_e v = |\vec{P} - e\vec{A}|. \tag{D.7}$$

Also note that

$$m_e v r = |\vec{L} - e\vec{r} \times \vec{A}|. \tag{D.8}$$

Therefore,

$$v = \frac{L - eAr}{m_e r} = \omega r. \tag{D.9}$$

Now note that the current through some point on the ring is

$$I = e\nu = e\frac{\omega}{2\pi}, \tag{D.10}$$

where ν is the frequency in Hz. The current then becomes

$$I = \frac{e}{2\pi}\frac{(L - eAr)}{m_e r^2}. \tag{D.11}$$

We will use this momentarily. Note that our Hamiltonian has the form

$$H = \frac{(L - eAr)^2}{2m_e r^2}. \tag{D.12}$$

Recalling that $A = \frac{1}{2}B_0 r$,

$$\frac{\partial H}{\partial B_0} = -\frac{1}{2}\frac{e(L - eAr)}{m_e} = -\pi r^2 I. \tag{D.13}$$

This can also be expressed as

$$-I = \frac{\partial H}{\partial(B_0 \pi r^2)} = \frac{\partial H}{\partial \phi}. \tag{D.14}$$

Thus, according to the Feynman-Hellman theorem (D.1), we arrive at

$$I_m = -\frac{\partial E_m}{\partial \phi}. \tag{D.15}$$

References

[1] N.W. Ashcroft and N.D. Mermin. *Solid State Physics*. Harcourt Inc., 1976. 2, 8, 9, 80, 83, 84

[2] W. Heywang and K.H. Zaininger. **Silicon: The Semiconductor Material**. In P. Siffert and E.F. Krimmel, editors, *Silicon: Evolution and Future of a Technology*. Springer Verlag, 2004. 2

[3] L. Onsager. **Initial Recombination of Ions**. *Phys. Rev.*, **54**:554–57, 1938. 2, 23, 25, 27, 28, 57

[4] S.M. Valone. **Quantum Mechanical Origins of the Iczkowski-Margrave Model of Chemical Potential**. *J. Chem. Theory and Comp.*, **7**:2253–61, 2011. 3, 79, 107, 109

[5] P. Würfel and U. Würfel. *Physics of Solar Cells: From Basic Principles to Advanced Concepts*. Wiley-VCH, 2009. 6, 7, 9, 11

[6] A. McEvoy, T. Markvart, and L. Casta ner. *Practical Handbook of Photovoltaics: Fundamentals and Applications*. Elsevier Ltd., 2012. 6

[7] C. Deibel and V. Dyakonov. **Polymer-Fullerene Bulk Heterojunction Solar Cells**. *Rep. Prog. Phys.*, **73**, 2010. 9, 12, 13, 15, 30, 36, 41, 44, 63

[8] C.B. Duke and L.B. Schein. **Organic Solids: Is Energy-Band Theory Enough?** *Physics Today*, **33**:42–48, 1980. 11

[9] W.P. Su, J.R. Schrieffer, and A.J. Heeger. **Solitons in Polyacetylene**. *Phys. Rev. Lett.*, **42**:1698–1701, 1979. 11

[10] C.W. Tang. **Two-Layer Organic Photocell**. *Appl. Phys. Lett.*, **48**:183–85, 1986. 11, 15

[11] S.L.M. van Mensfoort. *Effects of Disorder on the Charge Transport and Recombination in Organic Light-Emitting Diodes*. PhD thesis, Eindhoven University of Technology, 2009. 12

[12] A. Klein et. al. **Transparent Conducting Oxides for Photovoltaics: Manipulation of Fermi Level, Work Function and Energy Band Alignment**. *Materials*, **3**:4892–4914, 2010. 14

[13] D. Kearns and M. Calvin. **Photovoltaic Effect and Photoconductivity in Laminated Organic Systems**. *J. Chem. Phys.*, **29**:950–51, 1958. 14

[14] Eds. A.D. McNaught and A. Wilkinson. *Compendium of Chemical Terminology*. International Union of Pure and Applied Chemistry, 1997. 15

[15] G. Yu, J. Gao, J.C. Hummelen, F. Wudl, and A.J. Heeger. **Polymer Photovoltaic Cells: Enhanced Efficiencies Via a Network of Internal Donor-Acceptor Heterojunctions**. *Science*, **270**:1789, 1995. 16

[16] M.A. Green, K. Emery, Y. Hishikawa, W. Warta, and E.D. Dunlop. **Solar Cell Efficiency Tables (Version 39)**. *Prog. Photovolt.*, **20**:12–20, 2012. 17

[17] A. Fick. **Ueber Diffusion**. *Ann. der Physik*, **170**:59–86, 1855. 18

[18] A. Einstein. **Über die von der molekularkinetischen Theorie der Wärme geforderte Bewegung von in ruhenden Flüssigkeiten suspendierten Teilchen**. *Annalen der Physik*, **17**:549–60, 1905. 19

[19] M. Smoluchowski. **Zur kinetischen Theorie der Brownschen Molekularbewegung und der Suspensionen**. *Annalen der Physik*, **21**:756–80, 1906. 19

[20] S. Chandrasekhar. **Stochastic Problems in Physics and Astronomy**. *Rev. Mod. Phys.*, **15**:1–89, 1943. 22

[21] R.F. Probstein. *Physiochemical Hydrodynamics: An Introduction*. John Wiley and Sons, Inc., 1994. 22

[22] E. Rutherford. *Radioactivity*. Courier Dover Publications (2004), 1904. 22

[23] K.M. Downey. **The Variation of the Residual Ionization in Air with Pressure, for a Range of 57 Atmospheres**. *Phys. Rev.*, **20**:186–93, 1922. 22

[24] H.F. Fruth. **Variation with Pressure of the Residual Ionization of Gases**. *Phys. Rev.*, **22**:109–21, 1923. 23

[25] J.W. Broxon. **Natural Ionization in Gases**. *Phys. Rev.*, **27**:542–54, 1926.

[26] W.F.G. Swann. **The Variation of the Residual Ionization with Pressure at Different Altitudes, and Its Relation to the Cosmic Radiation**. *J. Frank. Inst.*, **209**:151–200, 1930. 22, 23

[27] R.A. Millikan and I.S. Bowen. **Similarity Between Cosmic Rays and Gamma Rays**. *Nature*, **128**:58–83, 1931. 23

[28] A.H. Compton, R.D. Bennett, and J.C. Stearns. **The Constancy of Cosmic Rays**. *Phys. Rev.*, **38**:1865, 1931. 23

[29] A.H. Compton, R.D. Bennett, and J.C. Stearns. **Ionization by Penetrating Radiation as a Function of Pressure and Temperature**. *Phys. Rev.*, **39**:873–82, 1932. 23

[30] J.W. Broxon and G.T. Merideth. **Measurements of Gamma-Ray Ionization Currents in Air at High Pressures and High Gradients**. *Phys. Rev.*, **54**:1–9, 1938. 25

[31] L. Onsager. **Deviations From Ohm's Law in Weak Electrolytes**. *J. Chem. Phys.*, **2**:599–615, 1934. 25, 27, 29

[32] Eds. A. Mozumder and Y. Hatano. *Charged Particle and Photon Interactions with Matter: Chemical, Physiochemical, and Biological Consequences with Applications*. Marcel Dekker, Inc., 2004. 27

[33] R. Courant and D. Hilbert. *Methods of Mathematical Physics*. Interscience, New York, 1953. 28

[34] C.L. Braun. **Electric Field Assisted Dissociation of Charge Transfer States as a Mechanism of Photocarrier Production**. *J. Chem. Phys.*, **80**:4157–61, 1983. 30, 36

[35] A. Devižis, A. Serbenta, K. Meerholz, D. Hertel, and V. Gulbinas. **Ultrafast dynamics of carrier mobility in a conjugated polymer probed at molecular and microscopic length scales**. *Phys. Rev. Lett.*, **103**, 2009. 31

[36] A. Miller and E. Abrahams. **Impurity Conduction at Low Concentrations**. *Phys. Rev.*, **120**:745–55, 1960. 33

[37] R.A. Marcus. **On the Theory of Oxidation-Reduction Reactions Involving Electron Transfer**. *J. Chem. Phys.*, **24**:966–78, 1965. 34

[38] G. Schönherr, R. Eiermann, and H. Bässler. **Dispersive Exciton Transport in a Hopping System with Gaussian Energy Distribution**. *Chem. Phys.*, **52**:287–98, 1980. 35, 44

[39] B. Ries and H. Bässler. **Monte Carlo Study of Dispersive Charge-Carrier Transport in Spatially Random Systems with and without Energetic Disorder**. *Phys. Rev. B*, **35**:2295–2302, 1986. 37

[40] H. Bässler. **Charge Transport in Disordered Organic Photoconductors: A Monte Carlo Simulation Study**. *Phys. Stat. Solidi*, **175**:15–56, 1993. 37, 53

[41] U. Albrecht and H. Bässler. **Yield of Geminate Pair Dissociation in an Energetically Random Hopping System**. *Chem. Phys. Let.*, **235**:389–93, 1995. 36, 37, 39, 44, 61, 63, 65

[42] S. Barth and H. Bässler. **Intrinsic Photoconduction in PPV-Type Conjugated Polymers**. *Phys. Rev. Let.*, **79**:4445–48, 1997.

[43] S. Barth, H. Bässler, H. Rost, and H.H. Hörhold. **Extrinsic and Intrinsic DC Photoconductivity in a Conjugated Polymer**. *Phys. Rev. B*, **56**:3844–51, 1997.

[44] S. Barth, D. Hertel, Y.H. Tak, H. Bässler, and H.H. Horhold. **Geminate Pair Dissociation in Random Organic Systems**. *Chem. Phys. Let.*, **274**:165–70, 1997. 65

[45] V.I. Arkhipov, E.V. Emelianova, and H. Bässler. **Temperature-Independent Quantum Yield of Carrier Photogeneration in Weakly Disordered Conjugated Polymers**. *Chem. Phys. Let.*, **296**:452–58, 1998.

[46] V.I. Arkhipov, E.V. Emelianova, Y.H. Tak, and H. Bässler. **Charge Injection Into Light-Emitting Diodes: Theory and Experiment**. *J. App. Phys.*, **84**:848–56, 1998. 35

[47] N.F. Mott. **Conduction in Non-Crystalline Materials**. *Phil. Mag.*, **19**:835–52, 1968. 37, 122

[48] P.E. Parris. **Low-Field Hopping Among Randomly Distributed Sites with Uncorrelated Energetic Disorder**. *J. Chem. Phys.*, **108**:218–26, 1998.

[49] J.M. Sin and Z.G. Soos. **Hopping Transport in Molecularly Doped Polymers: Joint Modelling of Positional and Energetic Disorder**. *Phil. Mag.*, **83**:901–28, 2002. 37

[50] H. Scher and S. Rackovsky. **Theory of Geminate Recombination on a Lattice**. *J. Chem. Phys.*, **81**:1994–2009, 1984. 43

[51] Y.N. Gartstein and E.M. Conwell. **High-Field Hopping Mobility in Disordered Molecular Solids: A Monte Carlo Study of Off-Diagonal Disorder Effects**. *J. Chem. Phys.*, **100**:9175–80, 1994. 44, 54, 65

[52] D.H. Dunlap. **Explanation for the $\sqrt{E}$-Dependant Mobilities of Charge Transport in Molecularly Doped Polymers**. *Phys. Rev. B*, **52**:939–54, 1995.

[53] S.V. Novikov and A.V. Vannikov. **Cluster Structure in the Distribution of the Electrostatic Potential in a Lattice of Randomly Oriented Dipoles**. *J. Phys. Chem.*, **99**:14573–76, 1995. 44, 45, 65, 66

[54] D.H. Dunlap, P.E. Parris, and V.M. Kenkre. **Charge-Dipole Model for the Universal Field Dependence of Mobilities in Molecularly Doped Polymers**. *Phys. Rev. Let.*, **77**:542–45, 1996. 44, 65

[55] S.V. Novikov, D.H. Dunlap, V.M. Kenkre, P.E. Parris, and A.V. Vannikov. **Essential Role of Correlations in Governing Charge Transport in Disordered Organic Materials**. *Phys. Rev. Let.*, **81**:4472–75, 1998. 44

[56] D.H. Dunlap, V.M. Kenkre, and P.E. Parris. **What is Behind the $\sqrt{E}$?** *J. Imaging Sci.*, **43**:437–42, 1999. 47, 48

[57] D. Abramavicius and L. Valkunas. **Geminate Pair Recombination in Molecular Systems with Correlated Disorder**. *Phys. Rev. B*, **68**, 2003. 44, 64, 65

[58] P.M. Borsenberger and D.S. Weiss. *Organic Photoreceptors for Imaging Systems*. Marcel Dekker, Inc., 1993. 45

[59] D.M. Pai. **Transient Photoconductivity in Poly(N-vinylcarbazole)**. *J. Chem. Phys.*, **52**:2285, 1970. 48

[60] Y.N. Gartstein and E.M. Conwell. **High-Field Hopping Mobility in Molecular Systems with Spatially Correlated Energetic Disorder**. *Chem. Phys. Lett.*, **245**:351, 1995. 48, 49

[61] J.Y. Pan and D. Haarer. **Numeric Modeling of the Photogeneration of Free Charge Carriers**. *Chem. Phys. Let.*, **324**:411–15, 2000. 48

[62] M.D. McGehee and M.A. Topinka. **Solar Cells: Pictures From the Blended Zone**. *Nat. Mat.*, **5**:675–76, 2006.

[63] R.A. Marsh, C. Groves, and N.C. Greenham. **A Microscopic Model for the Behavior of Nanostructured Organic Photovoltaic Devices**. *J. App. Phys.*, **101**, 2007.

[64] C. Groves, R.A. Marsh, and N.C. Greenham. **Monte Carlo Modeling of Geminate Recombination in Polymer-Polymer Photovoltaic Devices**. *J. Chem. Phys.*, **129**, 2008. 48

[65] C. Groves, L.J.A. Koster, and N.C. Greenham. **The Effect of Morphology Upon Mobility: Implications for Bulk Heterojunction Solar Cells with Nonuniform Blend Morphology**. *J. App. Phys.*, **105**, 2009. 48

[66] C. Lee, J.W. Oh, C.S. Choi, N.S. Lee, and N. Kim. **New Calculation of Charge Generation Efficiency and Photocurrent in Organic Photoconducting Device**. *Korean Chem. Soc.*, **30**:97–101, 2009.

[67] J.A. Anta. **Random Walk Numerical Simulation for Solar Cell Application**. *Energy Environ. Sci.*, **2**:387–92, 2009.

[68] C. Groves, R.G.E. Kimber, and A.B. Walker. **Simulation of Loss Mechanisms in Organic Solar Cells: A Description of the Mesoscopic Monte Carlo Technique and an Evaluation of the First Reaction Method**. *J. Chem. Phys.*, **133**, 2010. 48, 53

[69] C. Groves, J.C. Blakesley, and N.C. Greenham. **Effect of Charge Trapping on Geminate Recombination and Polymer Solar Cell Performance**. *Nano Lett.*, **10**:1063–69, 2010. 48, 49

[70] Y. Frenkel. **On the Transformation of Light into Heat in Solids**. *Phys. Rev.*, **37**:17, 1931. 56

[71] M. Pope and C.E. Swenberg. *Electronic Processes in Organic Crystals and Polymers*. Oxford University Press, 1999. 74

[72] S.M. Valone. Personal Correspondence, July 2013. 79

[73] P.W. Anderson. **More is Different: Broken Symmetry and the Nature of the Hierarchical Structure of Science**. *Science*, **177**:393–96, 1972. 79

[74] C. Kittel. *Introduction to Solid State Physics*. Wiley, 1995. 79, 80

[75] O. Madelung. *Introduction to Solid State Theory*. Springer, 1978. 80, 131, 134

[76] A. H. Wilson. **The Theory of Electronic Semi-Conductors**. *Proc. R. Soc. Lond. A*, **133**:458–91, 1931. 88

[77] F. Gebhard. *The Mott Metal-Insulator Transition*. Springer, 2000. 88, 91, 92

[78] L. Landau. **The Theory of a Fermi Liquid**. *Soviet Physics JETP*, **3**:920–25, 1957. 90

[79] E.H. Lieb and F.Y. Wu. **Absence of Mott Transition in an Exact Solution of the Short-Range, One-Band Model in One Dimension**. *Phys. Rev. Lett.*, **20**:1445–48, 1968. 90, 92, 104, 121

[80] J. Hubbard. **Electron Correlations in Narrow Energy Bands**. *Proc. R. Soc. London*, **276**:238–57, 1963. 91

[81] A. Atland and B. Simons. *Condensed Matter Field Theory*. Cambridge University Press, 2010. 91, 100

[82] N.F. Mott. **The Basis of the Electron Theory of Metals, with Special Reference to the Transition Metals**. *Proc. Phys. Soc. London*, **A26**:416, 1949. 91

[83] H. Tasaki. **The Hubbard Model - An Introduction and Selected Rigorous Results**. *J. Phys.: Cond. Mat.*, **10**:4353–78, 1998. 91

[84] W. Kohn. **Theory of the Insulating State**. *Phys. Rev.*, **133**:A171–A81, 1964. 94, 122

[85] B.S. Shastry and B. Sutherland. **Twisted Boundary Conditions and Effective Mass in Heisenberg-Ising and Hubbard Rings**. *Phys. Rev. Lett.*, **65**:243, 1990. 95, 122

[86] R.G. Parr, P.W. Ayers, and R.F. Nalewajski. **What is an Atom in a Molecule?** *J. Phys. Chem.*, **109**:3957–59, 2005. 106

[87] M. Elstner, D. Porezag, G. Jungnickel, J. Elsner, M. Haugk, T. Frauenheim, S. Suhai, and G. Seifert. **Self-Consistent-Charge Density-Functional Tight-Binding Method for Simulations of Complex Materials Properties**. *Phys. Rev. B*, **58**:7260–68, 1998.

[88] M.S. Daw and M.I. Baskes. **Embedded-Atom Method: Derivation and Application to Impurities, Surfaces, and Other Defects in Metals**. *Phys. Rev. B*, **29**:6443–53, 1984.

[89] R.F. Nalewajski and R.G. Parr. **Information Theory, Atoms in Molecules, and Molecular Similarity**. *Proc. Nat. Acad. Sci.*, **97**:8879–82, 2000. 106

[90] R.G. Parr and W. Yang. *Density-Functional Theory of Atoms and Molecules*. Oxford University Press, 1989. 106

[91] C.D. Sherrill and H.F. Schaefer III. **The Configuration Interaction Method: Advances in Highly Correlated Approaches**. *Advances in Quantum Chemistry*, **34**:146–269, 1999. 106

[92] W. Moffitt. **Atoms in Molecules and Crystals**. *Proc. R. Soc. London*, **210**:245–68, 1951. 108

[93] J.R. Schrieffer. *Theory of Superconductivity*. Westview Press, 1964. 117

[94] J. Quintanilla and C. Hooley. **The Strong-Correlations Puzzle**. *Physics World*, **22**:32–37, 2009. 124

[95] L. Pauling. **The Nature of the Chemical Bond IV; The Energy of Single Bonds and the Relative Electronegativity of Atoms**. *J. Am. Chem. Soc.*, **54**:3570–82, 1932. 127, 128

[96] R.S. Mulliken. **A New Electroaffinity Scale; Together with Data on Valence States and on Valence Ionization Potentials and Electron Affinities**. *J. Chem. Phys.*, **2**:782–93, 1934. 128

[97] R.G. Pearson. **Absolute Electronegativity and Absolute Hardness of Lewis Acids and Bases**. *J. Am. Chem. Soc.*, **107**:6801, 1985. 128